BIOCHEMICAL AND STRUCTURAL CHARACTERIZATION OF *Lactobacillus johnsonii* FERULOYL ESTERASES

By

KIN-KWAN LAI

A DISSERTATION PRESENTED TO THE GRADUATE SCHOOL
OF THE UNIVERSITY OF FLORIDA IN PARTIAL FULFILLMENT
OF THE REQUIREMENTS FOR THE DEGREE OF
DOCTOR OF PHILOSOPHY

UNIVERSITY OF FLORIDA

2011

To my parents, Hon-Yuen Lai and Lai-Yin Kong, and to my brothers, Ping-Kwan Lai and King-Kwan Lai, for their unlimited love and support.

ACKNOWLEDGMENTS

I express my highest gratitude to my primary advisor, Dr. Claudio Gonzalez, for his unwavering guidance throughout my entire graduate school experience. His support and constant push for improvement has made my experience as a graduate student successful and more rewarding. I also thank Dr. Graciela Lorca for her indispensable insight as well as my other committee members Dr. Julie Maupin-Furlow, Dr. Joseph Larkin III, Dr. Nicole Horenstein, and Dr. Veronika Butterweck for their advice and the faculty of the Microbiology and Cell Science Department for their support.

I would like to express my appreciation for the help and support provided by my fellow members of the Gonzalez and Lorca labs: graduate students Santosh Pande, Ricardo Valladares, Algevis Wrench; undergraduate students Sara Molloy and Clara Vu; scientist Fernando Pagliai; and lab technician Beverly Driver. I would also like to thank the members of Banting and Best Department of Medical Research in the University of Toronto, especially Peter Stogios and Xiaohui Xu for their invaluable contribution with the protein crystal structures.

Finally, I would like to thank my family and close friends especially Anastasia Potts for their kind encouragement that helped motivate me throughout my graduate school career.

TABLE OF CONTENTS

page

LIST OF TABLES

LIST OF FIGURES

LIST OF ABBREVIATIONS

Amp	ampicillin
Amp^r	ampicillin resistance
ATCC	American type culture collection
BB-DP	bio-breeding diabetes-prone
BB-DR	bio-breeding diabetes-resistant
BES	N,N-bis(2-hydroxyethyl)-2-aminoethanesulfonic acid
BLAST	Basic Local Alignment Search Tool
bp	base pair
BRENDA	BRaunschweig ENzyme Database
C	carbon
CHES	2-(n-cyclohexylamino)ethane Sulfonic Acid
cm	centimeter
c.n.d.	could not determine
DNA	deoxyribonucleic acid
dNTPs	deoxyribonucleotide triphosphates
DTT	dithiothreitol
ε	extinction coefficient
EC	Enzyme Commission number
EF	ethyl ferulate
FAE	ferulic acid esterase
FAE-A	type-A ferulic acid esterase
FAE-B	type-B ferulic acid esterase
FAE-C	type-C ferulic acid esterase
FAE-D	type-D ferulic acid esterase

FAE-E	type-E ferulic acid esterase
FPLC	fast protein liquid chromatography
F_o-F_c	Fourier refinement
g	gravitational force
GRAS	Generally Recognized As Safe
HEPES	4-(2-hydroxyethyl)-1-piperazineethanesulfonic acid
His	histidine
HPLC	high performance liquid chromatography
IPTG	isopropyl β-D-1-thiogalactopyranoside
kb	kilobase pair
K_{cat}	catalytic rate constant
K_{cat} / K_m	catalytic efficiency
kDa	kilodalton
K_m	Michaelis constant
L	liter
LAB	lactic acid bacteria
LB	Lysogeny broth / Luria-Bertani
LIC	ligation-independent cloning
M	molarity
MCT	monocarboxylic acid transporter
MES	2-(n-morpholino)ethanesulfonic acid
mAbs	milliabsorbance
MCT	monocarboxylic acid transporter
mg	milligram
min	minutes

mL	milliliter
mM	millimolar
mm	millimeter
MR	molecular replacement
MRS	de Man Rogosa Sharpe
NaCl	sodium chloride
NCBI	National Center for Biotechnology Information
Ni-NTA	nickel-nitriloacetic acid
nmol	nanomole
NOD	non-obese diabetic
^{o}C	degree celsius
OD_{600}	optical density at 600nm
ORFs	open reading frames
PCR	polymerase chain reaction
PDB	Protein Data Bank
PMSF	phenylmethanesulphonylfluoride
PSI-BLAST	Position-Specific Iterated Basic Local Alignment Search Tool
R	residual factor
R_{free}	free residual factor
R_{work}	a residual factor
RNA	ribonucleic acid
rpm	revolutions per minute
s	second
SDS-PAGE	sodium dodecyl sulfate polyacrylamide gel electrophoresis
SEC	size exclusion chromatography

sp.	Species (singular)
spp.	species (plural)
TEV	tobacco etch virus
TID	type 1 diabetes
µg	microgram
µL	microliter
µm	micrometer
UV	ultraviolet
V_{max}	maximum rate of reaction
v / v	volume to volume
w / v	weight to volume
w / w	weight to weight

Abstract of Dissertation Presented to the Graduate School
of the University of Florida in Partial Fulfillment of the
Requirements for the Degree of Doctor of Philosophy

BIOCHEMICAL AND STRUCTURAL CHARACTERIZATION OF *Lactobacillus johnsonii* FERULOYL ESTERASES

By

Kin-Kwan Lai

August 2011

Chair: Claudio F Gonzalez
Major: Microbiology and Cell Science

Phytophenols are natural phenolic compounds with widespread distribution throughout the plant kingdom. These phytophenols participate in the formation of macromolecular structures in plant cell walls via ester linkages. Phenolic acids, chemicals that possess beneficial properties to human health, are released during hydrolysis of phytophenols. The hydrolysis is catalyzed by enzymes (ferulic acid esterases, FAEs) of the gut microbiota. Before this work, no enzymes produced by human gastrointestinal commensals displaying FAE activity were described. FAE activity was observed from several *Lactobacillus* spp. isolated from stool samples collected from bio-breeding diabetes-resistant rats. The isolated *Lactobacillus johnsonii* N6.2 displayed the highest FAE activity among the isolated strains. Potential FAEs were identified by *in silico* prediction, cloned, and purified from *Escherichia coli* as recombinant proteins. By utilizing a variety of enzyme activity assays, two enzymes (LJ0536 and LJ1228) showed high substrate preference for aromatic esters, including chlorogenic acid and rosmarinic acid, which are commonly found in human diets. Site directed mutagenesis and x-ray crystallization of LJ0536 identified critical amino acids

involved in ester hydrolysis. The catalytic triad is composed of serine, histidine, and aspartic acid. A classical oxyanion hole, formed by phenylalanine and glutamine, also contributes to substrate binding. The substrate binding mechanism consists of a specific hydrophobic cavity in addition to an inserted domain located on top of the binding cavity. The inserted domain protects the small hydrophobic region and forms hydrogen bond(s) with the aromatic ring of the substrate to stabilize the binding interaction. Bioinformatic and structural analyses indicate bacterial FAEs are well conserved within the Lactobacillaceae family. The features of inserted domain distinguish the substrate binding mechanism of different types of proteins. The current FAE classification scheme is primarily based on enzyme activity and primary sequence identity of fungal FAEs. The unique structural and functional features of the inserted domain could contribute to refine the classification of FAEs. Taken together, this work describes the identification, purification, characterization, and crystallization of FAEs from probiotic bacteria. This study will provide insight for further exploration of FAEs in other species, and potentially will enhance the path for future applications of FAEs.

CHAPTER 1
INTRODUCTION

Phytophenols

Phenolic compounds are naturally available chemicals that contain one or more phenolic rings with or without substituents, such as hydroxyl or methoxy group(s). The term phytophenol, or phytochemical, is also used due to their high abundance in plants (Huang *et al.*, 2007). Phytophenols are secondary metabolites of plants, which are primarily used as defences against ultraviolet radiation and pathogens (Beckman, 2000). They are widely distributed and highly abundant in plant cell walls. Ferulic and *p*-coumaric acids reinforce the cell wall structure by crosslinking the hemicellulose fraction. In general, phytophenols are divided into four major groups: flavonoids, phenolic acids, stilbenes, and lignans (Spencer *et al.*, 2008). The classification of phytophenols is based on their characteristic chemical structures (Figure 1-1). All chemicals classified as phytophenols have at least one phenolic ring in their structure. The characteristic structure of flavonoids is a flavone, which contains two benzene rings connected by three carbons to form an oxygenated heterocycle. The phenolic acids contain a benzene ring attached to a carboxylic acid. The stilbenes have a backbone structure of 1,2-diarylethene, with two benzene rings bonded to each end of a carbon-carbon double bond. Lignans have a backbone structure of 1,4-dibenzybutane, with two benzene rings bonded to each end of a four-carbon chain. These major groups can be further divided into small subgroups depending on the position and number of hydroxyl substituents or other derivatives present in the backbone structure. Among these four major groups, the flavonoids are the largest group and contain six subgroups: flavonols, flavanones, flavanols, flavones, anthocyanins, and isoflavones. Phenolic acids can be

further divided into two groups: hydroxycinnamic acids and hydroxybenzoic acids. The hydroxycinnamic acids have a cinnamic acid as a backbone structure, while the hydroxybenzoic acids have a backbone structure of benzoic acid. Even though hydroxycinnamic acids and hydroxybenzoic acids have similar chemical structures, hydroxycinnamic acids are more common in nature than hydroxybenzoic acids.

Phenolic acids with a single phenolic ring, such as caffeic, ferulic, and coumaric acids, are the simplest derivatives of hydroxycinnamic acids (Crozier *et al.*, 2009). Caffeic acid has hydroxyl substituents at carbon 3 and carbon 4 (C3 and C4) of the cinnamic acid backbone. Ferulic acid has a hydroxyl substituent at C4 and a methoxy substituent at C3 of the cinnamic acid backbone. Coumaric acid has one hydroxyl substituent at C4 of the cinnamic acid backbone. Salicylic acid, syingic acid, and gallic acid are examples of hydroxybenzoic acid derivatives (Figure 1-2). Salicylic acid has a hydroxyl substituent on C2 of the benzoic acid backbone. Syingic acid has methoxy substituents on C3 and C5 and a hydroxyl substituent on C4 of the benzoic acid backbone. Gallic acid has hydroxyl substituents on C3, C4, and C5 of the benzoic acid backbone.

Depending on the type of storage or the location in the plants, phenolic acids can be either soluble or insoluble. The phenolic acids are soluble when they are stored within plant cell vacuoles. They are insoluble when they are acting as components of the plant cell wall structure. However, in reality, phenolic acids exist in much more complex forms.

The carboxylic acid moiety is usually esterified (Figure 1-3A and B), which generates a variety of phenolic compounds. Usually more than one phenolic moiety can

be found in these chemical structures. Consequently, phenolic compounds are also called polyphenols. For example, chlorogenic acid (5-*O*-caffeoylquinic acid) is composed of two phenolic acids; it is an ester of caffeic acid and quinic acid. Chlorogenic acid is a soluble phenolic compound found in a variety of plants. For instance, *Catharanthus roseus* produces terpenoid-indole alkaloids utilized for anti-cancer drug synthesis (Ferreres *et al.*, 2011). Rosmarinic acid is another soluble phenolic compound, which is found in the extract of Labiatae herbs (Tada *et al.*, 1996). It is an ester of caffeic acid and 3,4-dihydroxyphenyl lactic acid. In contrast, ferulic acid and coumaric acid are found in the cell walls of barley and malt. These acids are ester linked to arabinoxylan, and are part of the insoluble fractions (Figure 1-3C) (Maillard & Berset, 1995).

The hydrolysis of the ester bond releases the phenolic acids from macromolecular structures and from the respective polyphenols. Although the chemical structures of phenolic acids are similar, they have different biochemical properties. In the past decade, the studies on phenolic acids increased dramatically due to its beneficial properties demonstrated *in vitro* as well as *in vivo* (Srinivasan *et al.*, 2007).

Health Beneficial Properties of Phenolic Acids

It is generally accepted that the beneficial properties shown by phenolic acids are related to their high level of anti-oxidative and anti-inflammatory properties (Maurya & Devasagayam, 2010; Sato *et al.*, 2011). They have strong scavenging activity for free radicals such as hydrogen peroxide, superoxide, hydroxyl radical, and nitrogen dioxide (Srinivasan *et al*., 2007; Graf, 1992). In addition, it is accepted that phenolic acids are able to stimulate insulin secretion to maintain normal blood glucose levels

(Adisakwattana *et al.*, 2008; Huang *et al.*, 2009), reduce carcinogenesis (Murakami *et al.*, 2002; Yi *et al.*, 2005), and diminish cardiovascular disease (Chao *et al.*, 2009).

It has been demonstrated that ferulic acid has neuroprotective effect in rats (Cheng *et al.*, 2008) and protects against liver injury in mice (Kim *et al.*, 2011). Caffeic acid shows inhibitory effects against cancer cell proliferation in human cell lines (Rajendra Prasad *et al.*, 2011). Besides these common derivatives of hydroxycinnamic acids, the importance of other diverse phenolic acids and polyphenols such as hydroxytyrosol, 3,4-dihydroxyphenyl lactic acid, and resveratrol were recently discovered and studied (Yu *et al.*, 2010). Hydroxytyrosol showed anti-atherogenic, cardioprotective, anti-inflammatory, anti-platelet aggregation, anti-tumor, and anti-microbial activities (Granados-Principal *et al.*, 2010). 3,4-dihydroxyphenyl lactic acid has been found to have protective effects against brain and liver injuries (Lam *et al.*, 2003; Xing *et al.*, 2005). Resveratrol, a compound found in red wines, is one of the most studied and commercially exploited phenolics by the nutraceutical industry. It has been demonstrated that resveratrol is an excellent dietary anti-oxidant and can prevent uncontrolled cell proliferation and cancer (Athar *et al.*, 2009; Pervaiz & Holme, 2009). Antiviral and antimicrobial properties of diverse phenolic acids are also well documented (Puupponen-Pimiä *et al.*, 2005).

In general, *in vitro* assays have been used to demonstrate the beneficial properties of phenolic acids. A few works carried out with animal models indicate that a diet rich in phytophenols could be beneficial for humans. However, the evidence is still indirect. The assays using animal models described in the scientific literature utilized purified phytophenols delivered directly into the blood stream (Kim *et al*., 2011). In order to

strongly support that the inclusion of dietary food components rich in phytophenols is beneficial to humans, several aspects such as toxicity and absorbability of phytophenols should be deeply investigated.

Common Phytophenols Present in Human Diets

Phytophenols are highly abundant in the plant kingdom and can be easily found in dietary fiber. However, the distribution of phenolic acids is highly variable among different species of plants. Wheat bran and rice bran oil contain gamma-oryzanol. Gamma-oryzanol is a phytosteryl ferulate mixture. It is composed of 12 ferulate esters (Akihisa *et al.*, 2000), which can release ferulic acid upon hydrolysis. The total amount of ferulic acid varies from 0.5%, 0.9%, and 5% dry weight in wheat bran, suger-beet pulp, and corn kernel respectively (Ou & Kwok, 2004) The rice bran contains 0.19% to 0.42% dry weight of gamma-oryzanol (Lilitchan *et al.*, 2008; Chen & Bergman, 2005). Rosmarinic acid is an ester of caffeic acid and 3,4-dihydroxyphenyl lactic acid. It is naturally present in high amounts in herbs such as rosemary and lemon balm, which are frequently used in food preparations. The content of rosmarinic acid in herbs varies from 0.2% to 3% dry weight of herbs (Wang *et al.*, 2004a). Chlorogenic acid is abundant in coffee and green tea. It is an ester of caffeic acid and quinic acid. A cup of coffee potentially contains 15 mg to 325 mg chlorogenic acid (Richelle *et al.*, 2001). Oleuropein is found in olive trees and in olive oil. It is an ester of elenoic acid and 3,4-dihydroxyphenylethanol (hydroxytyrosol). Olive tree leaves typically contain 9% dry weight of oleuropein (Omar, 2010). Salvianolic acid is found in *Salvia miltiorrhiza* which is also known as danshen, a Chinese herbal medicine. Up to 82.52 mg of salvianolic acid B can be found in one gram of danshen (Li *et al.*, 2008). Hydrolysis of salvianolic acid B forms 3,4-dihydroxyphenyl lactic acid and lithospermic acid.

Many studies have shown that the consumption of dietary fiber can lead to better health (Sansbury *et al.*, 2009; Slavin, 2008). The beneficial properties of dietary fibers are directly linked with detoxification by stimulating intestinal peristalsis. The actual scientific discussion, regarding to the importance of dietary fibers, is focused on the importance of the phytophenols absorbed at the intestinal level. However, the absorption and metabolism of phenolic acids by humans are not completely understood. It is well known that the dietary phytophenols are poorly absorbed at the intestinal level. In order to be absorbed, enzymatic hydrolysis of the ester bond is required to release the bioactive phenolic acids from the phytophenols. The free carboxylic monophenols are then specificly and efficiently assimilated by cells of the intestinal tract (Kroon *et al.*, 1997).

Limitation on Phenolic Acid Absorption

The knowledge of phenolic acids absorption by humans is limited. It is accepted that two pathways are being utilized for cellular transport of phenolics (Konishi & Kobayashi, 2005): a passive paracellular diffusion and an active monocarboxylic acid transporter (Figure 1-4). Passive paracellular diffusion is a low efficiency system that allows some phytophenols and phenolic acids to slowly pass through the intestinal epithelial cells into the blood plasma for absorption. The active monocarboxylic acid transporter allows small, simple chemicals with a monocarboxylic acid motif (monophenolic acids such as ferulic acid and gallic acid) to pass through the layer with high efficiency.

Monocarboxylic acid transporter does not have affinity towards complex phytophenols or phenolic acid esters. Since the majority of monophenolic acids are esterified to other molecules, an enzymatic step is required prior to absorption. Once

the ester linkage is hydrolyzed, monophenolic acids are released and absorbed in the intestines with high efficiency by the monocarboxylic acid transporter. The enzymes catalyzing the phenolic acid ester hydrolysis are called cinnamoyl or feruloyl esterases (FAEs). To the best of today's knowledge, humans do not produce enzymes that can hydrolyze the ester linkages of polyphenols. However, the metabolites of phenolic acids are detected in the blood stream immediately after the ingestion of phytophenols (Baba *et al.*, 2004). These results indicate that FAE activity is present in the intestines. It has also been demonstrated that FAE activity is present in the lumen of the human gut as well as in the fecal samples (Kroon *et al*., 1997; Gonthier *et al.*, 2006).

The human colon harbors 10^{12} microorganisms per gram of feces (Hooper & Gordon, 2001). It is not surprising that some of these microorganisms encode FAEs (Andreasen *et al.*, 2001). Several bacterial species such as *Escherichia coli*, *Bifidobacterium lactis*, and *Lactobacillus gasseri* isolated from human intestine display FAE activity (Couteau *et al.*, 2001). It has also been found that lactic acid bacteria such as *L. fermentum*, *L. reuteri*, *L. leichmanni*, and *L. farciminis* are able to produce FAEs (Donaghy *et al.*, 1998). However, the genes encoding these enzymes have not yet been identified. Consequently, the presence of FAE activity in the intestines indicates that phenolic acids can be released from the dietary fiber, and that FAE activity is produced exclusively by some members of the gut microbiota.

Microbial Interaction with Food Components

Functional food is denoted as food that provides beneficial effects in addition to dietary nutritional value. Bioactive food components, such as phenolic acids in functional foods, are usually tightly bound to the non-digestible fraction. The activity of microbial enzymes is required to release these bioactive components. The intestinal

tract is an active site not only for absorption and excretion but also for food modification by microorganisms. It has been demonstrated by Kroon that ferulic acid is released from fiber sources such as wheat bran and sugar beet pulp by bacterial FAE activity in the human colon (Kroon *et al*., 1997). The bioavailability and function of phenolic acids depend on the specific FAE activity present in the gut microbiota. Not all released phenolics are intestinally absorbed. The non-absorbed portion can exert an action *in situ* (i.e., anti-oxidative) or be subsequently converted into other metabolites by the gut microbiota. Microbial metabolism and other activities from enzymes such as dehydrogenases, reductases, and decarboxylases play a critical role in the phenolics modifications (Landete *et al.*, 2010; Rodríguez *et al.*, 2010; Rodríguez *et al.*, 2009). It has been demonstrated that a change in the composition of gut microbiota affects intestinal permeability, energy homeostasis, and the inflammatory response (Musso *et al.*, 2011). It is also clearly associated with obesity (Cani *et al.*, 2009; Cani *et al.*, 2008). Thus, bioactive food components can alter the health of the host by regulating the metabolism and composition of gut microbiota or by directly altering the host metabolism and immune response (Musso *et al*., 2011).

An additional and very important function of bioactive phenolic acids and their metabolites is related to the regulation of the gut microbiota composition. A number of phytophenols can affect the growth and metabolic activity of several members of the gut microbiota (Selma *et al.*, 2009). Consequently, since the gut microbiota plays an important role in shaping the host metabolic and immune network, the phenolics will have an important impact on the health of the host.

The Increase in consumption of functional foods (i.e., fibers) usually leads to an increase not only in the number of probiotic bacteria (bifidobacteria and lactobacilli) in the intestine but also in the amount of phenolic acids in the blood (Costabile *et al.*, 2008). Altogether, functional foods, the gut microbiota, and human health are related to each other. A change on any one of these components will introduce a significant change in the other components. In order to take advantage of the phenolic contents of dietary fiber, researchers are focused on developing efficient ways to improve the bioavailability and assimilation of phenolic acids. The use of FAEs produced by the gut microbiota is one of the potential ways to improve the bioavailability of phenolic acids in human diet.

Esterases

There are a large variety of esterases described in the literature. Esterases are sub-divided into 31 subgroups on the basis of ester bond specificity (Figure 1-5). For example, carboxylic ester hydrolases (EC 3.1.1.-) target carboxylic esters; thiolester hydrolases (EC 3.1.2.-) target thiolester bonds.

Ferulic acid esterases (FAEs) are classified in the group of carboxylic ester hydrolases (EC 3.1.1.-). This group is further divided into 84 specific types of esterases based on the functional groups attached to the ester bond (Figure 1-5). Consequently, acetylesterases (EC 3.1.1.6) hydrolyze acetyl esters. For example, they can hydrolyze ethyl acetate into ethanol and acetate. Arylesterases (EC 3.1.1.2) hydrolyze esters that contain a phenyl group attached to the oxygen atom of the ester bond. They can hydrolyze, for example, phenyl acetate into phenol and acetate. Feruloyl esterases (EC. 3.1.1.73) hydrolyze esters that contain a phenolic acid derivative esterified to another molecule. For example, they can hydrolyze feruloyl-polysaccharide to release ferulic

acid and polysaccharide. In the past decade, researchers have focused their attention on FAEs because these enzymes release bioactive phenolic acids from prebiotics.

Ferulic Acid Esterases (FAEs)

FAEs (EC 3.1.1.73) are classified as a subclass of carboxylic acid esterases (EC 3.1.1.1). Alternative names such as cinnamoyl ester hydrolases, feruloyl esterases, and hydroxycinnamoyl esterases are generally used in the literature to describe the same group. They are also called hemicellulase accessory enzymes because they can act synergistically with xylanases, cellulases, and pectinases to break down the hemicellulose of plant cell walls. In the presence of water, FAEs hydrolyze phenolic esters into respective alcohols and phenolic acids.

These enzymes have higher substrate preference when the carboxylic ester is in the phenolic / aromatic form, such that an aromatic hydrocarbon is attached to the carbon atom of the carbonyl group of the ester. The carbohydrate of the hemicellulose is ester linked to phenolics and this aromatic ester linkage protects against hemicellulose degradation by masking the potential substrates for cellulolytic and hemicellulolytic enzymes (Akin, 2008). FAEs are important enzymes in the rumen ecosystem due to their ability to increase the absorption of energy sources in ruminant animals. In recent years, several FAEs from fungi were partially characterized, but little is known about bacterial or plant FAEs.

A specific short amino acid sequence, glycine-X-serine-X-glycine, associated with esterases can be easily identified on primary sequences using bioinformatics analysis. Thus, a large number of proteins are annotated as hypothetical or putative esterases in several databases. However, most of them remain biochemically uncharacterized. Brenda database (http://www.brenda-enzymes.info/) described more than 140 enzymes

from 52 organisms with known amino acid sequences (Scheer *et al.*, 2011). Only 8 structures of FAEs are described in the Protein Data Bank (PDB) (http://www.pdb.org/). All the structures (apo-enzymes or co-crystallized with a substrate) deposited in PDB belong to two enzymes purified from only two species, *Aspergillus niger* and *Butyrivibrio proteoclasticus*.

In 2004, Wang and his co-worker (Wang *et al.*, 2004b) claimed that a feruloyl esterase was successfully purified and characterized from the intestinal bacterium *L. acidophilus*. The molecular weight of the purified enzyme was determined as 36 kDa using sodium dodecyl sulfate polyacrylamide gel electrophoresis (SDS-PAGE). The N-terminal amino acid sequence of this enzyme was identified as ARVEKPRKVILVGDGAVGST. However, the N-terminal amino acid sequence matches 100% with LA2_01145, a L-lactate dehydrogenase (35.1kDa) from *Lactobacillus amylovorus GRL 1112* and LBA_0271, a L-lactate dehydrogenase (35.0kDa) from *L. acidophilus NCFM*. L-lactate dehydrogenases are enzymes that catalyze the conversion of pyruvate to lactate. They do not possess esterase activity. Thus, there is no evidence in the scientific literature regarding the purification and characterization of a FAE cloned from lactobacilli.

General Characteristic of FAEs

FAEs are serine esterases that utilize serine as a catalytic residue for hydrolysis. They have a classically conserved pentapeptide esterase motif with a consensus sequence glycine-X-serine-X-glycine (GXSXG), with X represents any amino acids. They belong to a structural group described as α / β fold hydrolases (Ollis *et al.*, 1992). The secondary structure of this group is composed of a minimum of eight β-strands in the center core surrounded by α-helices. The term α / β barrel is also used to describe

the structure. The β-strands in the central core and α-helices are mostly parallel. The α-helices and β-strands tend to alternate along the chain of the polypeptide.

The fungal FAEs do not display high sequence homology with bacterial FAEs. Since only 2 FAEs structures were solved by crystallization studies, the substrate binding mechanism of most FAEs is still not fully understood. However, the X-ray structures of these two FAEs display important differences. These differences suggest that the catalytic and the substrate binding mechanisms of bacterial and fungal enzymes could be substantially different.

Reaction Mechanism of FAEs

FAEs can hydrolyze a wide range of substrate including both aliphatic and aromatic esters. Enzymes that hydrolyze a broad range of substrates are generally described as “promiscuous enzymes”. Some of the most optimal FAE substrates are chlorogenic acid, rosmarinic acid, bran, oleuropein, and salvianolic acid. These compounds are naturally present in a variety of dietary foods (Figure 1-6).

The active site of these enzymes is formed by a catalytic triad. The triad is formed by serine, histidine, and aspartic acid residues, where serine is the nucleophilic residue. Thus, the catalytic mechanism of FAEs is very similar to that of serine proteases, lipases, and other esterases, which involves the formation of a covalent acylenzyme intermediate (Ding *et al*., 1994).

Two basic steps are involved during carboxylesterase catalysis: acylation and deacylation (Figure 1-7). During acylation, the hydroxyl oxygen of the catalytic serine carries out a nucleophilic attack on the carbonyl carbon of the ester substrate (step 1-8a). After the attack, a general base (the histidine of the catalytic triad) deprotonates the catalytic serine and the first tetrahedral intermediate is formed (step 1-8b). The

hydrogen bonding of the third member of the triad, aspartic acid, plays a critical role in the stabilization of the protonated histidine. The oxyanion of the resulting tetrahedral intermediate is positioned towards the oxyanion hole. The oxyanion hole is created by hydrogen bonding between the substrate carbonyl oxygen anion and the backbone of two nitrogen atoms from other residues of the catalytic pocket. The general base, histidine, transfers the proton to the leaving group. The deprotonation of histidine leads to the protonation of an ester oxygen to release the first product (for example: methanol with methyl ferulate as substrate). As a consequence, the tetrahedral intermediate collapses and the characteristic acylenzyme intermediate is formed. Thus, the residual half of the substrate remains attached to the catalytic serine (step 1-8c).

The second step of the reaction, deacylation, takes place in the presence of water. A molecule of water performs a nucleophilic attack on the carbonyl carbon of the remaining substrate in the acylenzyme intermediate (step 1-8d). The general base (histidine) immediately deprotonates a molecule of water, leading to the formation of a second tetrahedral intermediate. The catalysis follows a similar pattern described for the acylation. The second tetrahedral intermediate is stabilized by the formation of the oxyanion hole (step 1-8e). The proton of the general base moves to the nucleophilic serine. Consequently, the ester oxygen is protonated and the tetrahedral intermediate collapses. The protonation of ester oxygen at the expense of histidine deprotonation releases the final product (for example: ferulic acid with methyl ferulate as substrate) and reconstitutes the native serine residue and the original state of the enzyme (step 1-8f). The reaction mechanism is summarized in Figure 1-7.

Structural Binding Mechanism of FAEs

The PDB database displays only two FAE structures co-crystallized with ligands (AnFaeA: type-A feruloyl esterase from *A. niger*; Est1E: feruloyl esterase from *B. proteoclasticus*). Although all the enzymes present in the α / β fold group follow the same structural pattern, they do not display a conserved substrate binding mechanism.

The analysis of the two models co-crystallized with substrates indicates that AnFaeA displays the α / β hydrolase fold, which is similar to fungal lipases. The entry into the binding cavity is restricted by a lid structure composed of 13 amino acid residues similar to the lipolytic enzymes. Two different conformations are the characteristics of lipolytic enzymes: the inactive, open conformation and the active, closed conformation. In the open conformation, the binding cavity is open and in contact with the solvent. The open conformation facilitates the binding of substrate. In the closed conformation, a helical flap structure covers the binding cavity and restricts access of the substrate to the cavity. A conformational change in the main protein scaffold facilitates the movement of the helical flap to control the substrate binding (Grochulski *et al*., 1994). The helical flap structure of the lipases has remarkable similarity with the lid structure of the AnFaeA. The main difference with the lipases flap structure is that the AnFaeA lid has a higher percentage of polar residues plus an N-glycosylation site. These features suggests that the AnFaeA's lid structure is rigid and the enzyme is always in the open conformation (Hermoso *et al*., 2004). The structure of AnFaeA is discussed in depth in Chapter 5.

In regards to Est1E, it also displays an α / β hydrolase fold with a loop insertion on top of the catalytic groove. The loop insertion participates in the conformation of the catalytic pocket and contributes to the substrate binding. The insertion is composed of

51 amino acids with four small β-sheets (two hairpins) and three α-helices. A flapping of one amino acid (tryptophan) from the loop insertion is the only modification in the configuration between the open and closed conformations. Several residues in the inserted loop participate in the substrate binding by forming hydrogen bonds with the phenolic moiety of the substrate (Goldstone *et al*., 2010). These characteristics suggest that the lid structures / loop insertions in lipases, fungal FAEs, and bacterial FAEs are important for substrate binding.

Classification of FAEs

A comprehensive classification scheme was proposed in 2004 (Crepin *et al*., 2004). The classification system uses three main characteristics to group proteins into four different types: 1) the substrate specificity of enzyme on four substrates (methyl ferulate, methyl sinapate, methyl *p*-coumarate, methyl caffeate), 2) the ability to release diferulic acid from plant cell walls, and 3) the primary amino acid sequence similarity. The scheme divides the FAEs into subtypes A, B, C, and D.

Type-A FAEs (FAE-A) display activity on methyl *p*-coumarate but not methyl caffeate. The enzymes in this group are able to release 5,5'-diferulic acid from plant cell walls and the primary amino acid sequence shows similarity with lipases.

Type-B FAEs (FAE-B) display activity on methyl caffeate but not methyl *p*-coumarate. They are not able to release 5,5'-diferulic acid from plant cell walls. The primary amino acid sequence shows similarity to cinnamoyl esterases family 1 and acetyl xylan esterases.

Type-C FAEs (FAE-C) display activity on methyl caffeate and methyl *p*-coumarate. They are not able to release 5,5'-diferulic acid from plant cell walls and the primary amino acid sequence shows similarity to chlorogenate esterases and tannases.

Type-D FAEs (FAE-D) display activity on methyl caffeate and methyl *p*-coumarate. These enzymes are able to release 5,5'-diferulic acid from plant cell walls and the primary amino acid sequence shows similarity to xylanases.

The full classification scheme (Crepin *et al*., 2004) is summarized in Table 1-1. This classification scheme was built based on the data collected from fungal FAEs. Consequently, this classification system may not be valid for classifying FAEs from all kingdoms (primarily bacteria, and plantae). A second limitation of the system is related to the number of substrates used for the classification. The esterases display tremendous catalytic flexibility, being active with a large variety of substrates. The use of only four substrates may not be enough to measure the catalytic potential of each group. Even though FAEs display impressive catalytic flexibility and are able to hydrolyze a broad range of substrates, they are very sensitive with any substitutions of the aromatic ring (Vafiadi *et al*., 2006). Altering the substitutions of the aromatic rings on *meta* and / or *para* position drastically affects the enzyme activity. These characteristics were not used in the classification, perhaps because there is only fragmentary knowledge regarding the mechanisms of substrate binding.

A second classification model was proposed in 2008 (Benoit *et al*., 2008). The new classification scheme is based on the phylogenetic analysis of identified and putative fungal FAEs. The Benoit scheme proposes the division of FAEs into seven subfamilies, based on the phylogenetic relationships. The classification does not include biochemical characteristics. A phylogenetic clustering usually does not correlate with enzymological characteristics. Since the classification was done *in silico* using the amino acid sequences, the scheme represents only the phylogenetic diversity of fungal FAEs.

A new classification scheme was also proposed in 2011. This system includes FAEs from three important kingdoms: bacteria, fungi, and plantae (Udatha *et al*., 2011). The main goal of this classification system is to cluster the FAEs that display similar characteristics into the same group. The template sequences of FAEs were retrieved from three different sources: NCBI database (http://www.ncbi.nlm.nih.gov/), biochemically characterized FAEs, and BROAD Institute database (http://www.broadinstitute.org/) / DOE Joint Genome Institute Database (http://www.jgi.doe.gov/). The sequences were analyzed with a sequence-derived descriptor software. Sequence-derived descriptor works with a mathematical algorithm that can cluster proteins with similar function based on the distribution pattern of critical amino acids. The amino acids are identified directly from the primary sequence independently of the full sequence identity (Han *et al*., 2004). The authors claim that the pattern of those residues is critical for organizing the catalytic pocket and for substrate binding. Consequently, the proteins clustered in the same group should display similar biochemical properties. The complete classification consists of 12 groups and 31 subgroups. The main characteristics of each group are summarized in Table 1-2.

Applications of FAEs

FAEs have a wide application including paper, biofuel, medical, food, and cosmetic industries. FAEs are used in the pulp and paper industry (Record *et al.*, 2003; Sigoillot *et al.*, 2005) to remove fine particles from pulp, which reduces the use of chlorine based chemicals during the bleaching process. It is also important for biofuel industry, especially as the demand for ethanol increase dramatically. Thus, hemicellulosic by-products from fermentation become one of the target sources to produce ethanol. By using FAEs, it is possible to increase the efficiency of

hemicellulosic degradation (Fazary & Ju, 2008). Bi-functional enzymes synthesized by fusing a FAE and an endoxylanase are also used to improve the degradation of agricultural by-products (Levasseur *et al.*, 2005). An important agricultural by-product, ferulic acid, is the precursor of vanillin, a flavoring food additive (Priefert *et al.*, 2001). It can be used as food preservatives because it can inhibit the growth of microorganisms (Ou & Kwok, 2004). Due to its anti-oxidative property, ferulic acid is a common ingredients in cosmetics which contributes to skin protection against the UV damage (Srinivasan *et al*., 2007).

Another important aspect of FAEs is the stereoselective organic synthesis. Carboxylesterases are known to catalyze the hydrolysis of ester substrates as well as the reverse reaction, the acylation of alcohols. Transesterification of secondary alcohols in low water condition generates synthetic substrates that have no structural similarity to the natural substrates (Panda & Gowrishankar, 2005). It has been demonstrated that FAEs from *Humicola insolens* are able to catalyze the transesterification of secondary alcohols (Hatzakis *et al.*, 2003; Hatzakis & Smonou, 2005). Pentylferulate ester, an aromatic precursor used in cosmetics and food processing, is synthesized in high yield using ferulic acid and acidified *n*-pentanol by *A. niger* FAEs (Giuliani *et al.*, 2001). Sugar phenolic esters have anti-microbial and anti-tumor activities (Fazary & Ju, 2008). A FAE produced by *Fusarium oxysporum* is able to esterify several phenolic acids such as hydroxyphenylacetic acid and cinnamic acid with 1-propanol working in a mixture of *n*-hexane / 1-propanol / water condition (Topakas *et al.*, 2003). The ability to perform catalysis in organic systems with low water content indicates that FAEs could be important for synthesizing phenolic chemicals with specific scaffolds. This is an

important enzyme characteristic required for the synthesis of prodrugs and chiral compounds. A deep knowledge regarding the enzyme biochemistry, estereospecificity, and the molecular mechanisms involved in substrate selection are critical to evaluate the potential of the enzymes to be used in these kinds of applications.

Project Rationale and Design

The objectives of this study were to identify the coding sequences, elucidate the biochemical properties, reveal the enzyme structure, and determine the substrate binding mechanism of a bacterial FAE found in the intestinal tract. *Lactobacillus johnsonii*, a bacterium isolated from animal models that display high FAE activity, was selected as an enzyme donor to clone recombinant FAEs. *L. johnsonii* was selected because it is also a human commensal that could be used as a probiotic. It is expected that the FAE activity displayed by *L. johnsonii* will contribute to: 1) the dietary importance of phenolic acids and 2) the importance of microbial gut esterases on the improvement of carboxylic phenols absorption at the intestinal level.

Although several bacterial species isolated from mammal intestines display FAE activity, the genes encoding FAEs were not identified before this work. A genomic approach was used to identify the genes encoding hypothetical enzymes with potential FAE activity. Once the FAE coding sequences were located, the genes were cloned, expressed in *E. coli* and purified by nickel affinity chromatography as recombinant His_6-tagged proteins. The substrate preference of the selected enzymes was verified using multiple assays with a large array of substrates.

The major challenge of the experimental design was the elucidation of the substrate binding mechanism. To accomplish this challenge, the nucleophile of the

enzyme was mutated using site-directed mutagenesis. This strategy was used to perform further co-crystallization assays with substrates of interest.

The majority of FAEs characterized and described in the publicly available databases were purified from fungal species. The amount of data concerning the biochemistry or even structural information of bacterial FAEs is limited. This work has contributed to the knowledge of phytophenol esters catalysis by a bacterial FAE.

Table 1-1. Functional classification of FAEs based on substrate specificity and primary sequence similarity.

Type	Hydrolyzable Substrates	Ability to release diferulic acid from plant cell wall	Primary sequence similarity
A	methyl ferulate, methyl sinapate, methyl *p*-coumarate	yes	lipase
B	methyl ferulate, methyl sinapate, methyl caffeate	no	cinnamoyl esterase family 1, acetyl xylan esterase
C	methyl ferulate, methyl sinapate, methyl *p*-coumarate, methyl caffeate	no	chlorogenate esterase, tannase
D	methyl ferulate, methyl sinapate, methyl *p*-coumarate, methyl caffeate	yes	xylanase

Table 1-2. Descriptor-based classification of FAE proposed by Udatha (Udatha *et al*., 2011).

FAE family	Sub-family	Orientation and distance (number of amino acids) between catalytic residues				
FEF1	1A	D	.....54 – 81.....	S	.....79 – 111.....	H
	1B	S	.....51 – 183.....	D	.....29 – 178.....	H
FEF2	-	S	.....53.....	D	.....71.....	H
FEF3	3A	S	.....192 – 269.....	D	.....36 – 50.....	H
	3B	S	.....18.....	D	.....265 – 270.....	H
	3C	H	.....50.....	S	.....79.....	D
FEF4	4A	S	.....194 – 248.....	D	.....36 – 46.....	H
	4B	S	.....18.....	D	.....154 – 241.....	H
	4C	S	.....64 – 69.....	D	.....30 – 182.....	H
	4D	H	.....54.....	D	.....28.....	S
				or		
		H	.....27.....	S	.....211.....	D
FEF5	5A	S	.....236 – 255.....	D	.....37 – 39.....	H
	5B	S	.....18 – 89.....	D	.....47 – 62.....	H
	5C	H	.....71 – 81.....	S	.....84 – 176.....	D
FEF6	6A	S	.....81 – 247.....	D	.....38 – 59.....	H
	6B	H	.....1 – 83.....	S	.....61 – 84.....	H
FEF7	7A	S	.....175 – 253.....	D	.....36 – 47.....	H
	7B	S	.....18.....	D	.....233 – 240.....	H
	7C	S	.....81 – 83.....	D	.....56.....	H
FEF8	8A	S	.....144 – 358.....	D	.....32 – 41.....	H
	8B	S	.....18.....	D	.....204 – 236.....	H
	8C	H	.....51 – 87.....	S	.....18 – 57.....	D
	8D	D	.....68 – 89.....	S	.....86 – 117.....	H
FEF9	9A	S	.....212 – 393.....	D	.....12 – 40.....	H
	9B	D	.....16 – 74.....	S	.....88 – 155.....	H
	9C	H	.....36 – 56.....	S	.....57 – 60.....	D
FEF10	10A	S	.....55 – 248.....	D	.....36 – 74.....	H
	10B	D	.....69 – 82.....	S	.....86 – 96.....	H
	10C	H	.....81 – 83.....	S	.....81 – 83.....	D
FEF11	11A	S	.....209 – 246.....	D	.....36 – 41.....	H
	11B	S	.....18.....	D	.....135 – 243.....	H
FEF12	12A	H	.....1.....	S	.....56 – 61.....	D
	12B	S	.....211.....	D	.....36 – 46.....	H

S: serine. D: aspartic acid. H: histidine.

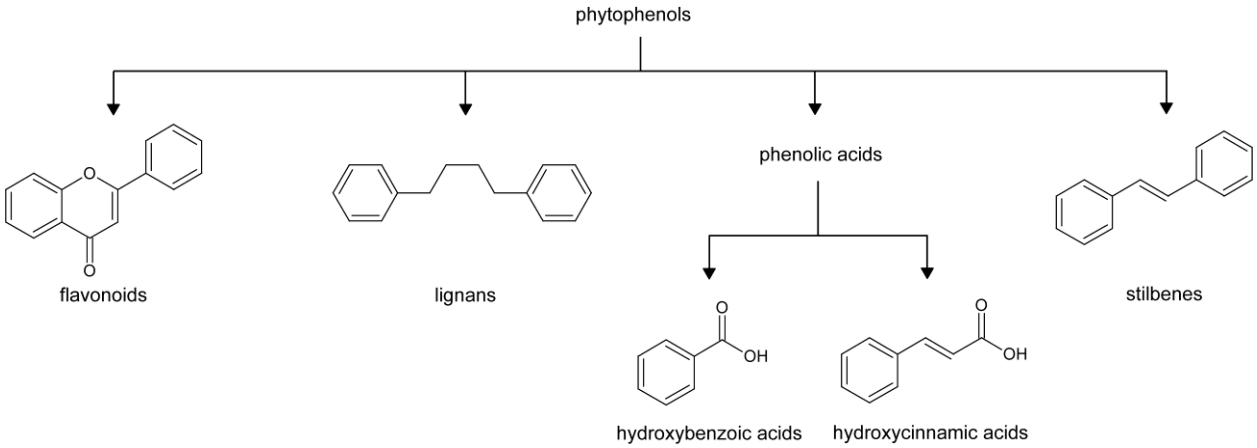

Figure 1-1. Classification of phytophenols. The figure displays the relevant backbone chemical structure of the four central phytophenols groups. The groups of flavonoids are further divided into six subclasses and the phenolic acids into two subclasses based on the position and biochemical characteristics of the subtituents groups.

Hydroxycinnamic acid derivatives

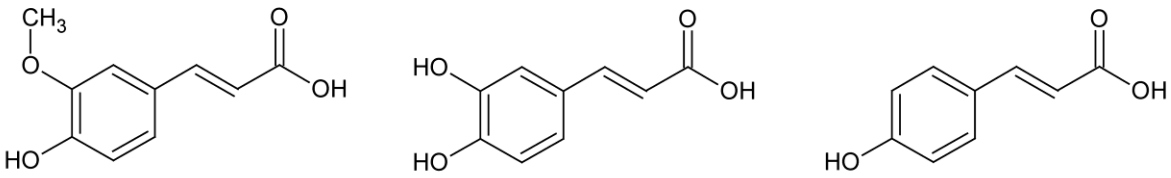

ferulic acid caffeic acid coumaric acid

Hydroxybenzoic acid derivatives

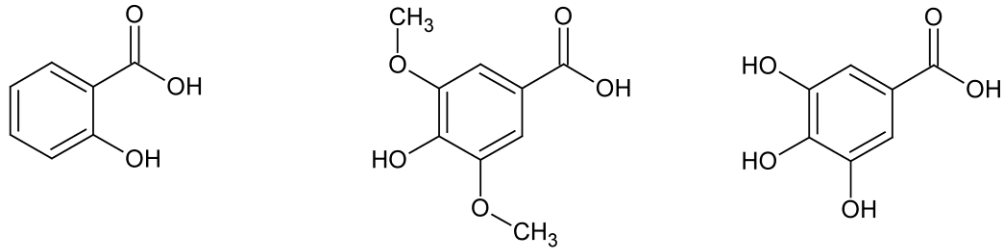

salicylic acid syringic acid gallic acid

Figure 1-2. Phenolic acid subgroups. The phenolic acid derivatives are classified into two subgroups: hydroxycinnamic and hydroxybenzoic acids. The figure displays the chemical structures of typical members of each group.

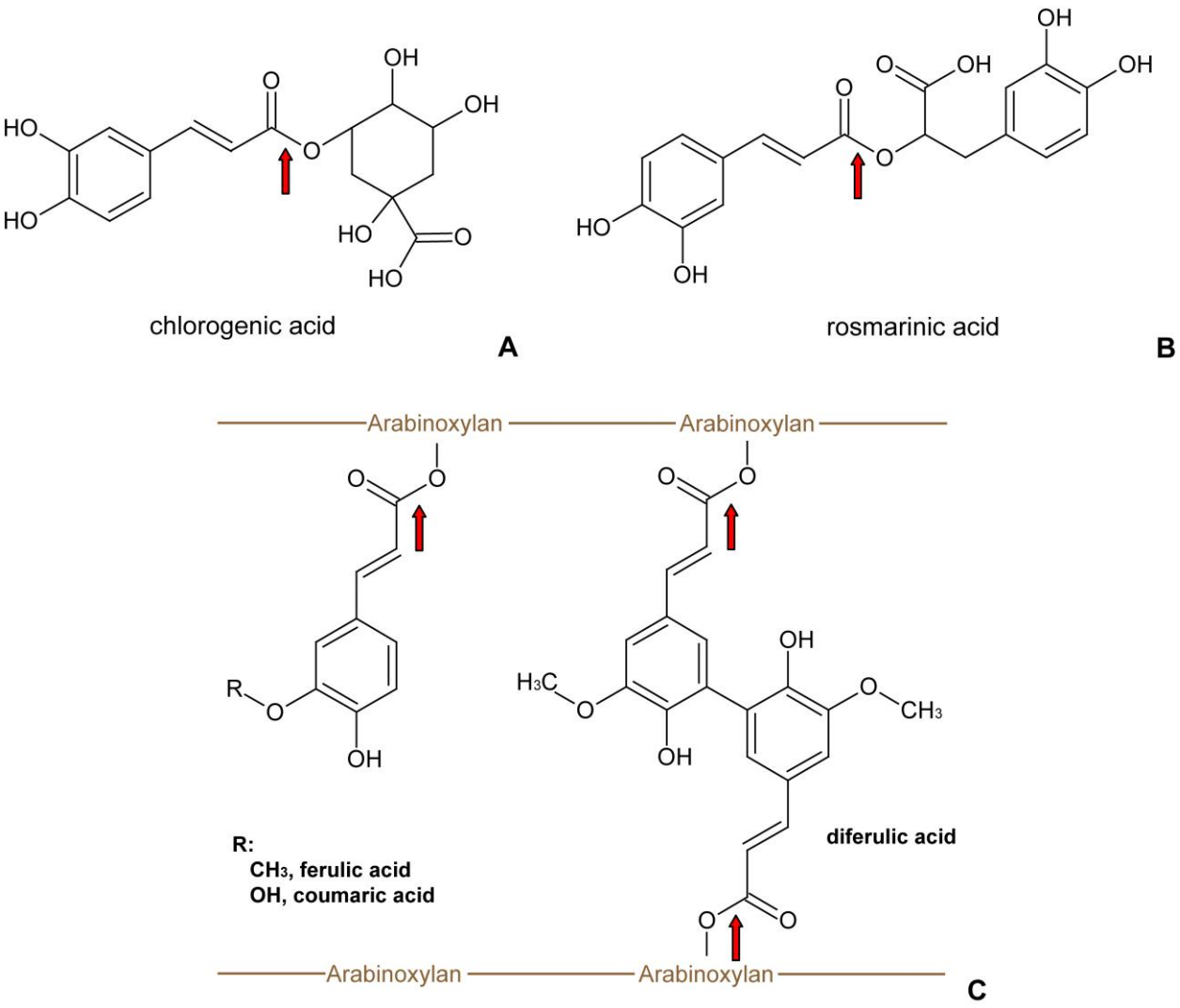

Figure 1-3. Esterification of phenolic compounds. In nature, the monophenols are usually esterified to form (A and B) soluble compounds or associated to macromolecular structures like (C) hemicellulose. The ester bonds are indicated with a red arrow. The arabinoxylan backbones are depicted in brown color.

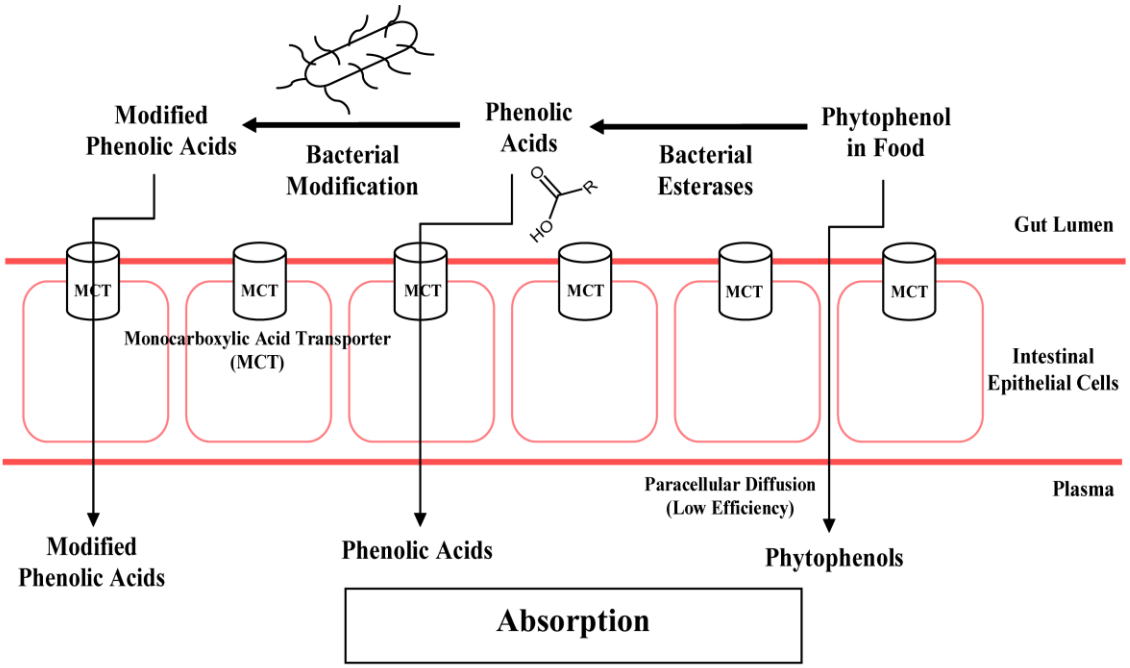

Figure 1-4. Intestinal absorption of phytophenols and phenolic acids. The majority of the dietary phytophenols and phenolic acids are absorbed at the intestinal level. A small portion of phytophenols is absorbed through paracellular diffusion with low efficiency. The remaining phytophenols are subjected to hydrolysis by bacterial esterases to release the efficiently absorbable phenolic acids. A portion of those phenolic acids can be further modified by bacterial activity. The modified phenolic acids are actively transported by the intestinal cells through the monocarboxylic acid transporter (MCT) with high efficiency. The absorbed phenols circulate in the blood stream to the different parts of the body and are further modified by the host metabolism.

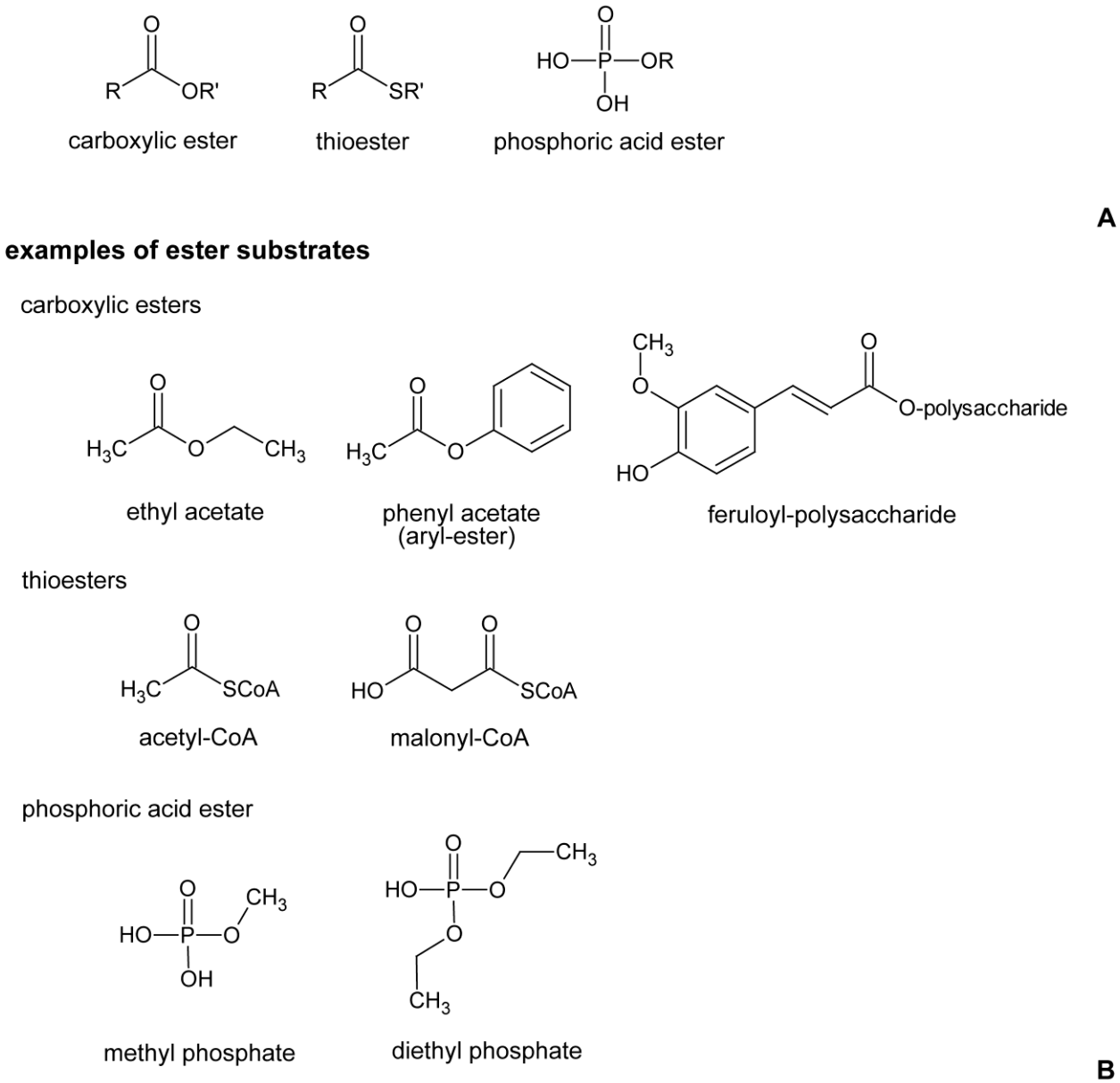

Figure 1-5. Chemical structures of ester backbones. (A) Ester bonds are present in biologically relevant substrates. (B) The chemical compounds depicted are used to illustrate carboxylic esters, thioesters, and phosphoric acid esters.

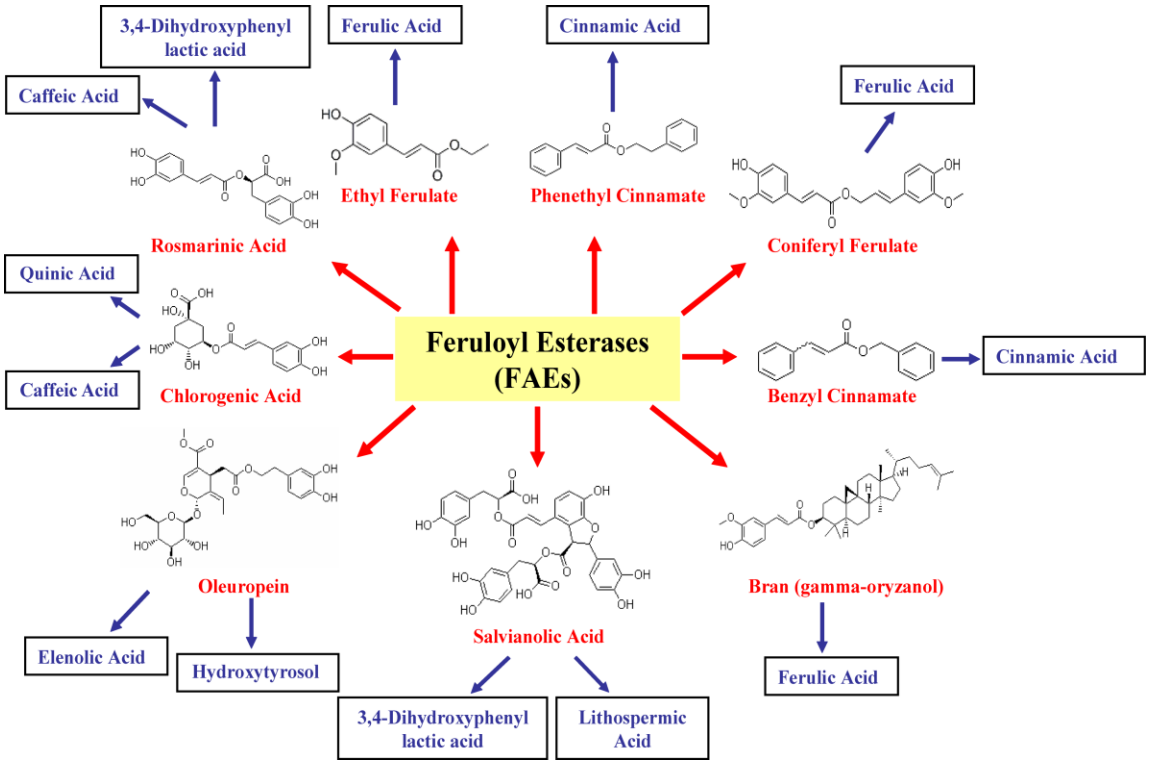

Figure 1-6. Natural phytophenols are frequently present in the human diet. The phytophenols displayed in the figure (red) are potential FAE substrates present in the human diet. The blue boxes highlight the bioactive products released after enzymatic hydrolysis.

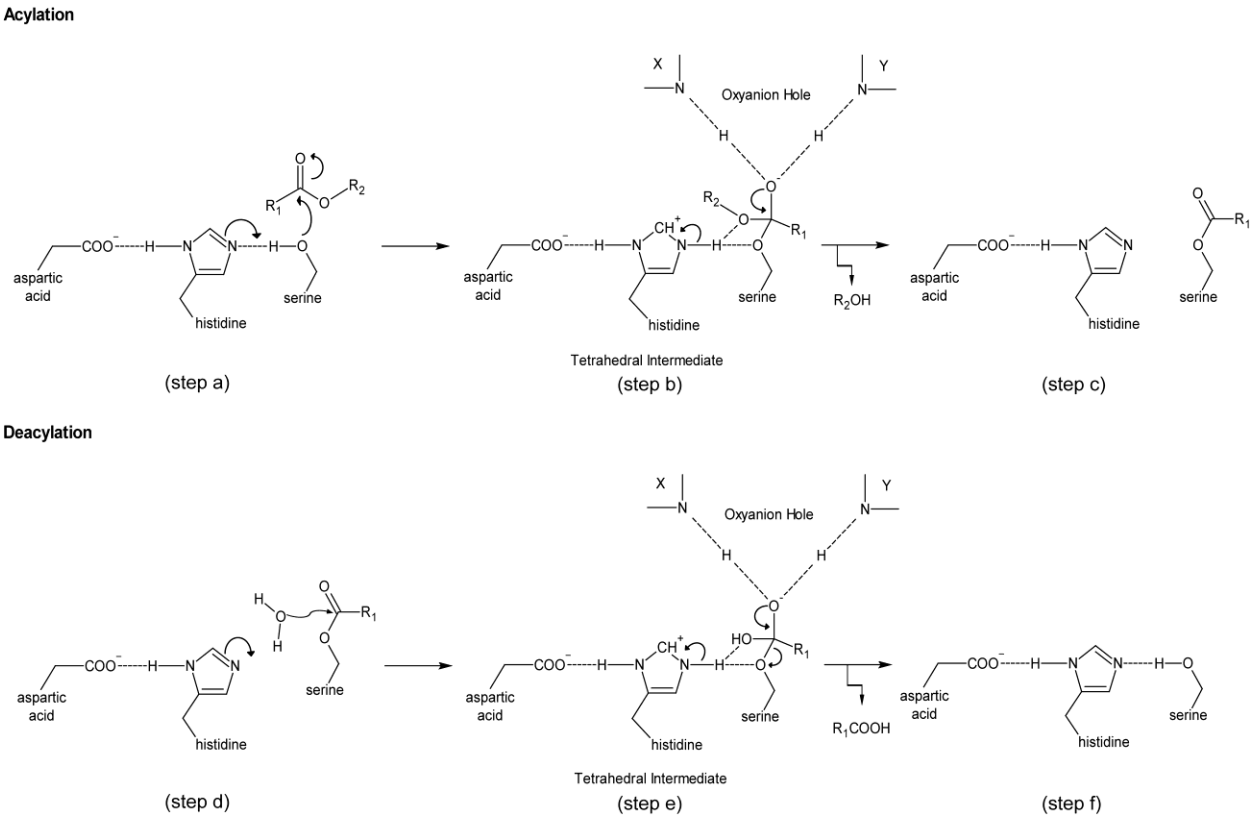

Figure 1-7. Catalytic mechanism characteristic of the carboxylesterases that use serine as the nucleophile center. The catalytic steps are illustrated using methyl ferulate as a substrate model. R1 represents the phenolic acid moiety and R2 represents methoxy group. X and Y were used to represent the unknown amino acids that will contribute with catalysis by forming the oxyanion hole. While the catalytic triad (serine, histidine, aspartic acid) is highly conserved, the amino acids of the oxyanion hole may vary.

CHAPTER 2
MATERIALS AND METHODS

Chemicals, Media, and Strains

Chemicals

All analytical grade chemicals and desalted oligonucleotides (primers) were purchased from Sigma-Aldrich (St. Louis, MO, USA). Ethyl ferulate was purchased from Apin Chemicals Ltd. (Abingbon, OX, UK). Chemicals for buffer and culture medium, reagents, and EZrun™ Protein Marker were purchased from Fisher Scientific (Atlanta, GA, USA). Restriction enzymes, T4 DNA ligase, Finnymes' Phusion™ high fidelity DNA polymerase, Quick-Load® Taq 2X Master Mix DNA polymerases, Quick-Load® 100 bp molecular weight standards, Quick-Load® 1 kb molecular weight standards, deoxyribonucleotide triphosphates (dNTPs), were purchased from New England Biolabs (lpswich, MA, USA). In-Fusion™ Dry-Down Mix was purchased from Clontech (Mountain View, CA, USA). DNeasy Blood & Tissue Kit, QIAGEN Plasmid Mini Kit, QIAquick PCR Purification Kit, and nickel-nitriloacetic acid resin (Ni-NTA Superflow) were purchased from QIAGEN (Valenia, CA, USA). Molecular biology assays were done using ultra-pure water (Synergy® UV Millipore Water Purification System).

Growth Conditions of *E. coli* Strains

Bacterial strains used for cloning and protein expression are summarized in Table 2-1, 2-3, and 2-5. *E. coli* Library Efficiency® DH5α™ strain was purchased from Invitrogen™ (San Diego, CA, USA). *E. coli* BL21-CodonPlus (DE3)-RIPL strain was purchased from Stratagene Agilent Technologies (La Jolla, CA, USA). *E. coli* DH5α strain was routinely used for plasmid purification. *E. coli* BL21 (DE3) strain was used for protein over-expression and subsequent protein purification. Wild type *E. coli* strains

were grown in Lysogeny Broth (LB) medium at 37^{o}C at 250 RPM. For purification of N-terminally labeled His_6-tagged proteins, *E. coli* strains carrying recombinant plasmid were freshly inoculated from -80^{o}C glycerol stocks into 25 mL LB medium. The medium was supplemented with ampicillin 100 $\mu g \cdot mL^{-1}$ and the cells were grown for 16 hours at 37^{o}C, 250 RPM. The cells were then sub-cultured (1% v / v) into 2 L of LB medium and grown at 37^{o}C, 250 RPM. When the optical density 600nm (OD_{600}) of the culture reached 0.6, isopropyl β-D-1-thiogalactopyranoside (IPTG) was added to the final concentration of 1 mM to initiate over-expression of recombinant proteins. The induction was carried out for 16 hours at 17^{o}C, 250 RPM. The cells were harvested by centrifugation and the cell mass was immediately used for protein purification or stored at -80^{o}C until purification.

Preparation of Competent *E. coli* Cells

The following procedures were used to prepare competent *E. coli* DH5α cells and competent *E. coli* BL21 cells. A single colony of *E. coli* was isolated from *E. coli* DH5α or *E. coli* BL21 streaked LB agar plate supplemented with 10 mM MgCl. The colony was inoculated into 5 mL TyM broth (2% tryptone, 0.5% yeast extract, 0.58% NaCl, 0.2% MgCl, w /v) and incubated for 2 hours at 37^{o}C, 250 RPM. The cells were inoculated into 300 mL TyM broth and incubated at 37^{o}C at 250 RPM until OD_{600} reached 0.5. The cell mass was collected through centrifugation at 1600 x g for 12 min at 4^{o}C. The cells were resuspended in 120 mL of Tfb1 buffer (100 mM KCl, 50 mM $MnCl_2$, 10 mM $CaCl_2$, 30 mM potassium acetate, 15% glycerol v / v , pH 5.8). The resuspended cells were incubated on ice for 90 min. The cell mass was collected again by centrifugation at 3000 1600 x g for 8 min at 4^{o}C. The cells were resuspended in 12 mL of Tfb2 buffer (10 mM

MOPS, 10 mM KCl, 75 mM $CaCl_2$, 15% glycerol v / v, pH 7) and stored at -80^{o}C in small aliquots (100 µL each) until further needed.

Isolation and Growth Condition of *Lactobacillus* strains

Lactobacilli were previously isolated by plating out aliquots of BB-DP and BB-DR rats stool samples directly in selective de Man Rogosa Sharpe (MRS) agar plates by Dr. Graciela Lorca, University of Florida. Cultures were grown at 37°C anaerobically in a gas pack system (Rogosa *et al.*, 1951). Individual colonies were picked and inoculated into 6 mL MRS broth and grown at 37°C under anaerobic conditions without shaking. The isolated strains were conserved in 96-well plates with 25% final glycerol concentration and stored at -80°C.

DNA Procedures

Lactobacillus Strain identification

Total genomic DNA was extracted using DNeasy Blood & Tissue Kit. The selected strains were identified by sequencing an internal 16S rDNA fragment from genomic DNA with Applied Biosystems model 3130 genetic analyzer (DNA Sequencing Facilities, Interdisciplinary Center for Biotechnology Research, University of Florida) using the primers listed in Table 2-2. The result sequences were blasted against NCBI Database (Benson *et al.*, 2011) to identify the donor species.

In silico Selection of Potential FAE Encoding Genes

Genes encoding proteins with potential esterase activity were selected based on *in silico* prediction using Comprehensive Microbial Resource (CMR) Database (Davidsen *et al.*, 2010). Five ORFs encoding putative/hypothetical proteins (locus tag: LJ0044, LJ0114, LJ0536, LJ0618, LJ1228) that displayed the characteristic esterase motif (Brenner, 1988; Cygler *et al.*, 1993) were selected. The genomic sequence of *L.*

johnsonii NCC 533 (GI# 41584196) was used as a reference. The primers were designed based on the genomic sequence of *L. johnsonii* NCC 533 and *L. johnsonii* N6.2 chromosomal DNA was used as template for gene cloning. Three ORFs (lotus tag: LREU1549, LREU1667, LREU1684) were selected from reference genomic sequence of *L. reuteri* DSM 20016 (GI# 148530277). The primers were designed based on the genomic sequence of *L. reuteri* DSM 20016 and *L. reuteri* TDI chromosomal DNA was used as template for gene cloning.

Cloning of Potential FAEs

Plasmid p15TV-L (Figure 2-1) contains *bla* (ampicillin resistance) gene, which serves as a selectable marker. It also contains *sacB* gene, which encodes levansucrase. Levansucrase is an enzyme that hydrolyzes sucrose to produce levan. The expression of *SacB* is toxic to *E. coli*. Thus, the growth of *E. coli* transformed with p15TV-L plasmid is inhibited when the LB medium is supplemented with 5% sucrose (w / v) unless the *SacB* gene is removed. Ligation-independent cloning (LIC) sequences are located on the flanking regions of *sacB* gene.

Primers with LIC sequence at 5' end were used to PCR amplify genes of interest. The cloning of PCR fragments into p15TV-L plasmid were done by DNA recombination in the LIC sequence using In-Fusion^{TM} Dry-Down Mix (Lorca *et al.*, 2007a). Each in-fusion pellet was resuspended in 8.5 µL of p15TV-L plasmid (75 ng $\cdot$ µL^{-1}). 0.5 µL of PCR fragment (~ 1 mg $\cdot$ µL^{-1}) was mixed with 2 µL of the resuspended pellet-plasmid to initiate DNA recombination. The mixture was incubated at room temperature for 30 min to generate a recombinant plasmid. During DNA recombination, the *SacB* gene was replaced by the PCR fragment. Thus, LB agar plates supplemented with 5% sucrose (w / v) and 100 µg $\cdot$ mL^{-1} ampicillin were used for positive selection. IPTG was used to

induce the transcription of the cloned gene. The protein possessed His_6-tagged at the N-terminus following by a TEV protease cleavage site after translation.

The genes of interest were PCR amplified from genomic DNA obtained from the isolated strains. The DNA amplification was done using *Taq* 2X master Mix DNA Polymerases. The primers used are listed in Table 2-2 and 2-6. All PCRs were performed using MyCycler^{TM} Personal Thermal Cycler (Bio-Rad Laboratories). The PCR fragments were cloned into p15TV-L as described above. The recombinant plasmids were transformed into *E. coli* DH5α. Heat shock transformation procedures were done as follows: 50 µL competent cells were mixed with 2.5 µL recombinant plasmids. The mixture was incubated on ice for 20 min, followed by 5 min in 37^{o}C water bath, and 3 min on ice. 950 µL of LB medium was added to the mixture and incubated for an additional 45 min in 37^{o}C water bath. Cells were collected by centrifugation at 7500 RPM (JLA16.250 rotor, Beckman Coulter) for 3 min. 900 µL of supernatant was discarded. The cells were resuspended in the remaining 100 µL supernatant. The cells were plated on LB agar plate supplemented with 100 µg $\cdot$ mL^{-1} ampicillin and 5% sucrose (w / v) for positive selection. Colony PCR was also used to screen for positive colonies. Plasmids were extracted using QIAGEN Plasmid Mini Kit. Sequences of PCR insert of all clones were confirmed by Applied Biosystems 3730 capillary sequencer using T7 primers (DNA Lab, Arizona State University) on the extracted plasmids. The plasmids with correct clones were further transformed into *E. coli* BL21 for protein over-production.

Cloning of Human Valacylovir Hydrolase (VACVase)

The plasmid containing the gene of interest (pET17b-VACVase) was provided by Dr. Gordon L. Amidon, University of Michigan (Lai *et al.*, 2008). The gene of interest

was cloned into p15TV-L plasmid using the primers listed in Table 2-4 and confirmed by DNA sequencing as described above.

Generating LJ0536 Protein Variants

The LJ0536 p15TV-L clone was used as a wild-type plasmid template for site directed mutagenesis assay. The 39-nucleotide long complementary primers containing the desired mutation were used to introduce individual mutations. The primers are listed in Table 2-4. The amino acids selected for modification were replaced by alanine due to its small, simple chemical structure (alanine scanning). The inert alanine methyl functional group will not introduce interaction within the protein. The mutants were constructed by PCR using Finnymes Phusion^{TM} high fidelity DNA polymerase according to manufacturer's protocol. To generate a deletion mutant of the inserted α / β domain (from V147 to A173 of LJ0536), primers LJ0536DEL147-173aa_SmaI-Fw and LJ0536DEL147-173aa_SmaI-Rv were used for PCR amplification to amplify the LJ0536 p15TV-L plasmid. The resulting PCR fragment contained a segment of *LJ0536* at the 5' end (Q174 to F249) and a segment of *LJ0536* at the 3' end (M1 to G146) connected by the sequence of p15TV-L plasmid. It was flanked with SmaI restriction sites on both ends, allowing restriction digestion and ligation to complete the recombinant plasmid. The PCR fragment was digested with SmaI restriction enzyme for 2 hours at 37^{o}C. Ligation was carried out using T4 DNA ligase at 16^{o}C for 16 hours to ligate the SmaI restriction site. The PCR amplified plasmids were then treated with 10 units of DpnI restriction enzyme 2 times at 37^{o}C for 1 hour each time to digest the methylated wild-type plasmid template. The recombinant plasmids were transformed into *E. coli* DH5α. The mutant sequences were confirmed by DNA sequencing (DNA Lab, Arizona State University).

DNA Gel Electrophoresis

DNA was separated by gel electrophoresis using 1% (w / v) agarose gel in 1X TAE electrophoresis buffer (40mM tris(hydroxymethyl)aminomethane (Tris) acetate pH 8.5, 2 mM ethylenediaminetetraacetic acid (EDTA)). Gels images were captured using ImageQuant 400 imaging system (GE Healthcare) after staining with 0.5 $\mu g \cdot mL^{-1}$ ethidium bromide.

Protein Procedures

Protein Purification

The expression of His_6-tagged proteins was carried out in *E. coli* BL21 using IPTG (1 mM) to induce gene transcription on p15TV-L. The cells were collected by centrifugation at 8000 RPM (JLA8.1000 rotor, Beckman Coulter) for 25 min. The collected cell mass was resuspended in 25 mL binding buffer (5 mM imidazole, 500 mM NaCl, 20 mM 4-(2-hydroxyethyl)-1-piperazineethanesulfonic acid (HEPES) pH 7.5) and then disrupted by French press (20000 psi). The cell free extract was collected by centrifugation at 4^oC, 17500 RPM (JA25.50 rotor, Beckman Coulter) for 25 min. The soluble His_6-tagged proteins were purified by affinity chromatography as follows: all solutions were passed through the Ni-NTA column by gravity flow. The Ni-NTA column was first washed with 30 mL of ultra-pure water to wash out any unbound nickel ions. It was then pre-equilibrated with 30 mL binding buffer. The cell free extract was applied to Ni-NTA column. During this step, the His_6-tagged proteins were bound to nickel ions that were immobilized by NTA. The resin was washed with 30 mL of binding buffer to wash out any unbound proteins. 200 mL of wash buffer (20 mM imidazole, 500 mM NaCl, 20 mM HEPES pH 7.5), which contains a higher concentration of imidazole, was used to remove unspecific proteins that were bound to the resin. Imidazole is a

competitive molecule that displaces the nickel ions bound to His_6-tagged protein. The His_6-tagged proteins were eluted using 20 mL elution buffer (250 mM imidazole, 500 mM NaCl, 20 mM HEPES pH 7.5). The purified proteins were dialyzed at 4°C for 16 hours. The dialysis buffer was composed of 50 mM HEPES buffer pH 7.5, 500 mM sodium chloride (NaCl), and 1 mM dithiothreitol (DTT). After dialysis, the samples were flash frozen and preserved at -80°C in 200 µL aliquots until needed. The His_6-tag was removed by treatment with tobacco etch virus (TEV) protease (60 ug TEV protease per 1 mg of target protein) at 4^oC for 16 hours. The sample was passed through a nickel affinity chromatography column to eliminate the released His_6-tag. Collected proteins were dialyzed at 4^oC against dialysis buffer for 16 hours. The purified proteins without His_6-tag were flash-frozen and preserved in small aliquots at -80^oC until needed.

Sodium Dodecyl Sulfate-Polyacrylamide Gel Electrophoresis (SDS-PAGE)

Purified proteins were analyzed in SDS-PAGE (120 V, 65 - 70 min.) to verify induction and to determine the purity of proteins after the affinity chromatography. Proteins were mixed with SDS-PAGE loading dye (100 mM Tris-HCl pH 6.8, 2% (w / v) SDS, 10% (v / v) glycerol, 10% (v / v) β-mercaptoethanol, 0.6 mg $\cdot$ mL^{-1} bromophenol blue) and boiled at 95^oC for 5 min prior loading to the gel. Electrophoresis was done in buffer composed of 25 mM Tris buffer, 192 mM glycine, and 0.1% (w / v) SDS. Gels were stained with Coomassie Blue (PhastGel Blue R-350) and images were captured using HP Scanjet G3010 Scanner (Hewlett-Packard).

Protein Quantification

Protein concentration was quantified using Bradford reagent (Bradford, 1976). The calibration of Bradford reagent was done using bovine serum albumin as a

standard. Absorbance at 595 nm (A_{595}) was determined using UV-1700 PharmaSpec UV-VIS Spectrophotometer (Shimadzu).

Enzyme Assays

Feruloyl esterase screening assay

The ability of *Lactobacillus* strains to produce FAEs was analyzed on MRS agar plates supplemented with 0.1% (w / v) ethyl ferulate without glucose (Donaghy *et al*., 1998). The presence of ethyl ferulate created a turbid / milky appearance of MRS agar due to the semi-soluble ethyl ferulate at 0.1% (w / v) final concentration. Ferulate assay (MRS-EF) plates were inoculated with cell obtained from individual overnight MRS cultures. The plates were incubated at 37°C in a gas pack system for a maximum of 3 days. The formation of halo (clear area) around the colonies indicated the presence of ferulate esterase activity. The strains with the highest activity (largest halos) were selected for further analysis.

Determination of optimal assay conditions

Model carboxylesterase substrates (4-nitrophenyl butyrate) was used as enzyme substrate. The optimal pH for catalysis of each purified enzyme was determined at 37^{o}C using a set of overlapping buffers: 2-(n-morpholino)ethanesulfonic acid (MES) pH 5.5 – 6.4, N,N-bis(2-hydroxyethyl)-2-aminoethanesulfonic acid (BES) pH 6.4 – 7.8, HEPES pH 6.8 – 8.2, Tris-HCl pH 7.5 – 9.0, 2-(n-cyclohexylamino)ethane Sulfonic Acid (CHES) pH 8.6 – 10. The buffers were used at 20 mM final concentration.

The optimal temperature of each purified enzyme was estimated by incubating the reaction mixture at different temperatures (13 – 40^{o}C) at the optimal pH of each enzyme. The reaction mixture consisted of 20 mM buffer, 1 mM 4-nitrophenyl butyrate, and 0.3 – 1.7 µg of enzyme per mL of reaction mixture. 4-nitrophenols were released

from 4-nitrophenyl butyrate during hydrolysis. Enzyme activity was continuously monitored for 15 min at 412 nm using UV-1700 PharmaSpec UV-VIS Spectrophotometer (Shimadzu) or Synergy™ HT Multi-Detection Microplate Reader (Biotek). The increase in absorbance due to the increase concentration of free 4-nitrophenols indicated enzyme activity. All assays and controls were performed in triplicate.

Extinction coefficient of 4-nitrophenol (16300 $M^{-1} \cdot cm^{-1}$) was used to quantify the release of 4-nitrophenol using the following equation:

$$\Delta C = \Delta Abs / \varepsilon l \qquad \text{Equation (2-1)}$$

ΔC is the change of concentration of chemical measured ($mM \cdot min^{-1}$). ΔAbs is the change of absorbance ($Abs \cdot min^{-1}$). ε is the extinction coefficient of chemical measured ($M \cdot cm^{-1}$). l is the path-length of light traveled through the sample (automatically adjusted to 1 cm by reader).

Enzyme specific activities were calculated using the following equations:

$$SA = \Delta C / [enzyme] \qquad \text{Equation (2-2)}$$

SA is the enzyme specific activity represented the amount of chemical released or hydrolyzed per mg of protein per min ($\mu mol \cdot mg^{-1} \cdot min^{-1}$). ΔC is the change of concentration of chemical measured ($mM \cdot min^{-1}$). [enzyme] is the concentration of enzyme in the reaction mixture ($mg \cdot mL^{-1}$).

Determination of enzymes substrate preference

The enzymatic substrate profiles were determined at 25^{o}C using an ester library composed of variety of ester substrates (Liu *et al.*, 2001). The enzyme activity was monitored with 4-nitrophenol (Janes *et al.*, 1998) using the following protocol. The purified enzymes were thawed from -80^{o}C and re-dialyzed against 5 mM BES buffer pH

7.2. The reactions were carried out in 96 well plates; each enzymatic reaction contained 1 mM ester substrate, 0.44 mM 4-nitrophenol (proton acceptor), 4.39 mM BES pH 7.2, 7.1% (v / v) acetonitrile, and 30 - 35 µg per mL of enzyme in a total volume of 105 µL reaction mixture. The 96 well plates were incubated at 25^{o}C using Synergy™ HT Multi-Detection Microplate Reader (Biotek). The reactions were continuously monitored for 30 min at 404 nm. The concentration of 4-nitrophenol was estimated using the extinction coefficient (ε = 16,100 $M^{-1} \cdot cm^{-1}$) and Equation 2-1. Enzyme specific activity was calculated using Equation 2-2. All assays and controls were performed in triplicate. Results are shown as mean ± standard deviation.

Determination of biochemical parameters by saturation kinetics

As enzyme reactions are saturable, the biochemical parameters such as K_m (Michaelis constant: amount of substrate required to reach half of V_{max} which associates with substrate affinity. Low value of K_m indicates high substrate affinity), V_{max} (maximum rate of reaction or maximum enzyme specific activity), K_{cat} (catalytic rate constant, s^{-1}), and K_{cat} / K_m (catalytic efficiency, $M^{-1} \cdot s^{-1}$) could be determined by measuring the initial rate of the reaction over a range of substrate concentration. K_{cat} is calculated with the following equation:

$$K_{cat} = V_{max} / [enz] \qquad \text{Equation (2-3)}$$

[enz] is the amount of enzyme in µmol $\cdot$ mg^{-1} estimated from the molecular weight of enzyme (LJ0536: 27570 g $\cdot$ mol^{-1}; LJ1228: 27454 g $\cdot$ mol^{-1}).

The model substrates (α-naphthyl acetate, β-naphthyl acetate, α-naphthyl propionate, β-naphthyl propionate, α- naphthyl butyrate, β-naphthyl butyrate, 4-nitrophenyl acetate, 4-nitrophenyl butyrate, 4-nitrophenyl caprylate) were used to determine the biochemical parameters of the purified enzymes (Gonzalez *et al.*, 2006).

The enzymatic saturation assays were conducted at the optimal pH and temperature determined for each purified enzyme. The enzyme activities of the wild type enzyme LJ0536 and all the LJ0536 mutants were carried out in 20 mM HEPES buffer pH 7.8 at 25 °C. The assays with LJ1228 were performed in 20 mM MES buffer pH 6.7 at 30°C. All reactions were continuously monitored for 15 min at 412 nm in 96-well plate using Synergy™ HT Multi-Detection Microplate Reader (Biotek). The extinction coefficients of α / β-naphthyl esters (3000 $M^{-1} \cdot cm^{-1}$) and 4-nitrophenol (16300 $M^{-1} \cdot cm^{-1}$) were used to calculate the amount of substrate hydrolyzed with Equation 2-1. Enzyme specific activities were calculated with Equation 2-2. The kinetic parameter K_m and V_{max} were estimated by non-linear fitting using Origin 8 software (OriginLab). All kinetic parameters were determined from the average of triplicated assays.

Enzyme activity assays towards aromatic esters (ethyl ferulate and chlorogenic acid) were conducted by continuously monitoring the UV-absorbance of the reaction mixture at 324 nm for 10 min. The reactions were carried out in a 96 well UV plate using Synergy™ HT Multi-Detection Microplate Reader (Biotek). The typical reaction mixture contained 20 mM buffer, 0.01 to 0.20 mM substrate, and 0.05 to 0.1 $\mu g \cdot mL^{-1}$ of purified enzyme. The extinction coefficient of ethyl ferulate (ε = 15390 $M^{-1} \cdot cm^{-1}$) and chlorogenic acid (ε = 26322 $M^{-1} \cdot cm^{-1}$) were determined experimentally and were used to estimate the amount of substrate hydrolyzed. The kinetic parameters were determined as described above from the average of triplicated assays.

Effect of bile salt component and metal ions on enzyme activity

The effect of bile salt components such as sodium glycocholate, taurocholic, and deoxycholic acid were assayed in a range of concentration (0.1 to 10 mM) using the model substrate 4-nitrophenyl butyrate. The effect of metal ions ($FeCl_2$, $FeCl_3$, $CdCl_2$,

$CaCl_2$, $CoCl_2$, $MnCl_2$, $ZnCl_2$, $CuCl_2$, $MgCl_2$) were assayed in 1 mM. The assays were conducted at the optimal pH and temperature determined for each purified enzyme. A typical enzyme reaction mixture contained 20 mM buffer, 1 mM 4-nitrophenyl butyrate, and 0.3 – 1.7 μg / mL enzyme. The reactions were continuously monitored for 10 min at 412 nm using Synergy™ HT Multi-Detection Microplate Reader (Biotek) and the enzyme activities were calculated using Equation 2-1 and Equation 2-2. All assays and controls were performed in triplicate.

LJ0536 mutants and VACVase ester screening assay

The enzymatic activities toward aliphatic (4-nitrophenyl butyrate) and aromatic (ethyl ferulate, chlorogenic acid, and rosmarinic acid) substrates were measured spectrophotometrically using a Synergy™ HT Multi-Detection Microplate Reader (Biotek). The hydrolysis of aliphatic esters was monitored at 412 nm. The hydrolysis of aromatic esters was monitored at 324 nm. A typical reaction mixture contained 20 mM HEPES pH 7.80, 0.1 mM ester substrate, and 0.3 $\mu g \cdot mL^{-1}$ purified enzymes (ethyl ferulate and chlorogenic acid) or 3 $\mu g \cdot mL^{-1}$ purified enzymes (4-nitrophenyl butyrate and rosmarinic acid). Up to 30 $\mu g \cdot mL^{-1}$ of VACVase was used to detect enzyme activity. The enzyme reactions of LJ0536 wild type and LJ0536 mutants were carried out at 25^{o}C. The enzyme reactions of VACVase were carried out at 37^{o}C. The extinction coefficients of 4-nitrophenyl butyrate (16300 $M^{-1} \cdot cm^{-1}$), ethyl ferulate (15390 $M^{-1} \cdot cm^{-1}$), chlorogenic acid (26322 $M^{-1} \cdot cm^{-1}$), and rosmarinic acid (15670 $M^{-1} \cdot cm^{-1}$) were used to estimate the amount of substrate hydrolyzed using Equation 2-1 and Equation 2-2. All assays were performed in triplicate.

Detection of phenolic acids using high performance liquid chromatography (HPLC)

HPLC was used to identify and measure the compounds released by enzymatic action from the complex substrates. A typical reaction mixture contained 20 mM HEPES pH 7.80, 1 mM ester substrate, and 20 $\mu g \cdot mL^{-1}$ enzyme. All reaction mixtures were incubated for 16 hours and filtered using 0.45 µm filter prior to HPLC analysis. HPLC analyses were performed using the HPLC L-2000 series system (Hitachi) with Symmetry® C18 5 µm 3.9 mm x 150 mm reversed-phase column protected with a Symmetry® C18 5 µm guard column (Waters). Detection of products released by enzyme activities using bran, ethyl ferulate, chlorogenic acid, and rosmarinic acid as substrates were carried out at 324 nm using linear gradient elution with water / acetic acid / 1-butanol (350:1:7, v / v / v) and methanol with a flow rate of 1 $mL \cdot min^{-1}$. (Mastihuba *et al.*, 2002).

To detect the hydrolysis of valacyclovir, the reaction mixture contained 50 mM HEPES pH 7.80, 4 mM valacyclovir, and 10 $\mu g \cdot mL^{-1}$ enzyme. Detection of enzyme activity was carried out at 254 nm using linear gradient elution with acetonitrile at a flow rate of 1 $mL \cdot min^{-1}$. (Lai *et al*., 2008).

Determination of native molecular weight using size exclusion chromatography

The native molecular weight of the proteins studied was determined by gel filtration size exclusion chromatography (SEC). The assays were performed in a LCC-501 Plus FPLC System (Pharmacia Biotech) with column Superose 12 10 / 300 GL (GE Healthcare). A linear regression fitting standard was constructed using Immunoglobulin G (150 kDa), bovine serum albumin (66 kDa), ovalbumin (45 kDa), trypsinogen (24 kDa), α-lactalbumin (14.2 kDa), cytochrome C (12.3 kDa), and vitamin B12 (1.4 kDa) as

molecular weight standards. Mobile phase was composed of 10 mM HEPES buffer and 150 mM NaCl. Data was analyzed using FPLCdirector^{TM} (Pharmacia Biotech).

Analysis of protein secondary structure by circular dichroism

Protein secondary structure was estimated using AVIV Quick Start 215 Circular Dichroism Spectrometer with 0.1 cm quartz cuvette (Hellma, Jamaica, NY). The protein samples were thawed from -80^{o}C and re-dialyzed against 2 mM HEPES buffer with 50 mM NaCl during 16 hours. The samples were adjusted to 0.2 mg $\cdot$ mL^{-1} in 0.5 mM HEPES buffer with 10 mM NaCl after dialysis. The spectra was acquired at 1 nm intervals and averaged with 10 scans. Multiple scans with buffer alone were used to correct the background. The final spectra was expressed in molar ellipticity (ME) using the following equation:

$$ME = \theta / 10nCl \qquad \text{Equation (2-4)}$$

θ is the signal acquired, n is the number of residues, C is the molar concentration of protein, and l is the path-length of the cuvette.

X-Ray Crystallization of LJ0536 and S106A

X-ray crystallization was carried out in collaboration with Banting and Best Department of Medical Research, Centre for Structural Proteomics in Toronto (University of Toronto). The crystal structures were provided by Banting and Best Department of Medical Research. Structural Analyses were done in our laboratory. All His_6-tagged proteins were crystallized using the sitting drop method with Intelliplate 96-well plates and a Mosquito Crystal liquid handling robot (TTP LabTech), mixing 0.5 µL of protein at 15 mg $\cdot$ mL^{-1}, and 0.5 µL of reservoir solution, over 100 µL reservoir solution. The protein solutions were pre-treated with the proteases subtilisin and V8 for the wild type and catalytic serine deficient (S106A) mutant of LJ0536, respectively. The

proteases stored at 1 mg · mL^{-1} stock solution were added to a final 1:10 v / v ratio protease:protein). Successful crystallization required the presence of the different proteases, a technique often used to increase the success of crystallization due to removal of disordered / flexible regions that would disrupt crystal formation (Dong *et al.*, 2007).

Reservoir solutions were identified through an in-house custom crystallization screen that was optimized based on success of common commercial sparse-matrix crystallization screens (Kimber *et al.*, 2003). The concentrations used in each case were: apo LJ0536 enzyme: 0.1 M MES pH 6 and 20% (v / v) PEG10K; catalytic serine deficient (S106A) mutant: 0.1 M sodium cacodylate pH 6.5, 0.2 M calcium acetate, 9% (v / v) PEG 8K; S106A co-crystallized with ethyl ferulate Form I: 0.1 M Tris pH 8.5, 0.2 M ammonium sulphate, 25% (v / v) PEG 3350; S106A co-crystallized with ethyl ferulate Form II: 0.1 M Tris pH 8.5, 0.2 M ammonium sulphate, 24% (v / v) PEG 3350; S106A co-crystallized with chlorogenic acid: 0.1 M Tris pH 8.5, 0.2 M lithium sulphate, 30% (v / v) PEG 4K; S106A co-crystallized with chlorogenic acid: 0.1 M Tris pH 8.5, 0.2 M lithium sulphate, 30% (v / v) PEG 4K; S106A co-crystallized with ferulic acid: 0.1 M Tris pH 8.5, 0.2 M lithium sulfate, 30% (v / v) PEG 4K.

Ligands were co-crystallized at a final ligand concentration of 5 mM (25 mM for ethyl ferulate Form II) in the sitting drop, by diluting a stock solution of 100 mM ligand 1:20 v / v with the protein/protease mix; 0.5 µL of this new solution was mixed with 0.5 µL of reservoir solution for crystallization.

All crystals were cryo-protected with reservoir solution supplemented with paratone-N oil (Hope, 1988) prior to flash freezing in an Oxford Cryosystems

cryostream. Diffraction data at 100 K at the Cu-Kα wavelength were collected at the Structural Genomics Consortium using a Rigaku FR-E Superbright rotating anode with a Rigaku R-AXIS HTC detector. Diffraction data was reduced with HKL2000 (Otwinowski & Minor, 1997).

The LJ0536 apo structure was solved by Molecular Replacement (MR) using Phaser (McCoy *et al.*, 2007), with a poly-alanine form of the structure of feruloyl esterase (Est1E, PDB: 2WTM) from *B. proteoclasticus* (Goldstone *et al*., 2010) as a search model. The successful MR solution was identified by map inspection using Coot (Emsley & Cowtan, 2004) and by a decrease in R_{free} after refinement using Refmac (Murshudov *et al.*, 1997). The structure was fully built by manual building and rounds of refinement with Refmac, Phenix.refine (Adams *et al.*, 2010) and Buster (Blanc *et al.*, 2004) at the final stages. Anisotropic B-factors were refined for protein and ligand atoms for all structures. Non-crystallographic (NCS) restraints were not utilized for any structure. All structures were refined using TLS parameterization (TLS groups were the N-terminal residue to residue 179, and 180 to the C-terminal residue), as assigned by the TLSMD server (Painter & Merritt, 2006). Additional TLS restraints resulted in lower R and R_{free} values. Water atoms were added by automatic methods using the refinement programs used in each structure (Phenix.refine, Refmac / CCP4 / ARP / wARP, or BUSTER, respectively). Ions were added after the automatic water building by inspection of magnitude of residual F_o-F_c density and hydrogen bonding patterns. The final atomic models include residues 1-245 of LJ0536, with six atoms from the expression tag at the N-terminus of one chain of the asymmetric unit.

The LJ0536 S106A structure was solved by MR using the apo structure. All ligands were identified by the presence of residual F_o-F_c density in the active site of the enzyme after molecular replacement using the apo S106A enzyme. Refinement of ligand structures was executed with geometric restraints generated by the PRODRG server (Schüttelkopf & van Aalten, 2004) and with a combination of Refmac and / or Phenix.refine. Final validation of the structure of the ligands was performed by calculating simulated annealing omit F_o-F_c maps using Phenix.refine and Cartesian simulated annealing with default parameters, after removing atoms from the ligand and any protein atoms within 5 Å of the ligand atoms. In the LJ0536 S106A + ethyl ferulate Form I complex (two chains in the asymmetric unit), one ligand was modeled with an occupancy of 1.0, the other with a manually-assigned occupancy of 0.55 (due to lower quality electron density, and higher B-factors than nearby protein atoms, at higher occupancy levels). For ethyl ferulate Form II complex (one chain in the asymmetric unit), the ligand was modeled with an occupancy of 1.0. All ligands in their respective complexes were modeled with occupancies of 1.0. The structure of Form I and Form II S106A mutant co-crystallized with ethyl ferulate are identical. Analyses of the mutant S106A co-crystallized with ethyl ferulate were carried out with Form II due to better occupancy of the ligand in the active site.

All structures were refined until convergence of R_{work} and R_{free} values, and reasonable geometries were verified using the Procheck (Laskowski *et al.*, 1993) and Molprobity (Chen *et al.*, 2010) servers.

PDB Accession Code of Proteins

The structures of apo wild type LJ0536 (PDB: 3PF8), apo S106A (PDB: 3PF9), S106A bound with chlorogenic acid (PDB: 3S2Z), S106A bound with ethyl ferulate Form

I (PDB: 3PFB), S106A bound with ethyl ferulate Form II (PDB: 3QMI), and S106A bound with ferulic acid (PDB: 3PFC) have been submitted to the PDB (Berman *et al.*, 2000). All other PDB files used in this study were achieved from PDB (Berman *et al*., 2000).

Structural Analysis

All structural images were generated using PyMOL (DeLano, 2002). Structure similarity searches were performed using the Dali database (Holm & Rosenström, 2010). Protein-protein interaction interfaces were identified and analyzed with the PDBe PISA server (Krissinel & Henrick, 2007) with default settings; a residue is considered in an interface if its change in accessible surface area between chain A and chain A complex with chain B is non-zero.

Sequence Analysis and Construction of Phylogenetic Trees

All DNA and amino acid sequences were retrieved from NCBI Database (Benson *et al*., 2011). LJ0536 protein homologs were identified by BLASTP search (Altschul *et al.*, 1997). Multiple sequence alignments were performed using CLUSTAL X2 (Larkin *et al.*, 2007). Phylogenetic analyses were conducted using neighbor-joining method and visualized with TreeView (Page, 1996). Accession numbers, locus tag, and gene identification numbers for the following figures are listed below.

Accession numbers for Figure 3-2 (phylogenetic tree of lactobacilli 16S rDNA sequences and the isolated strain N6.2 from BB-DR rats stool sample) are as follows: *L. sakei* 23K (LSA): NC_007576, locus tag LSAr01; N6.2: isolated FAE producing strain; *L. johnsonii* NCC 533 (LJO): AE017198, locus tag LJR007; *L. delbrueckii subsp. bulgaricus* ATCC BAA-365 (LDE): CP000412, locus tag LBUL_r0045; *L. acidophilus* NCFM (LBA): NC_006814, locus tag LBA2001; *L. helveticus* DPC 4571 (LHE):

CP000517, locus tag lhv_3101; *L. reuteri* JCM1112 (LRE): NC_010609, loctus tag LAR_16SrRNA01; *L. fermentum* IFO 3956 (LFE): NC_010610, locus tag LAF_16SrRNA01; *L. salivarius* UCC118 (LSL): NC_007929, locus tag LSL_RNA001. *L. brevis* ATCC 367 (LBR): CP000416, locus tag LVIS_r0082; *L. plantarum* WCFS1 (LPL): NC_004567, locus tag lp_rRNA01.

Gene identification numbers (GI#) for Figure 3-9 (multiple sequence alignment of LJ0536 and LJ1228 with their homologs and paralogs) are as follows: LJ0536: *L. johnsonii* N6.2, cinnamoyl esterase, GI# 289594369; LJ1228: *L. johnsonii* N6.2, cinnamoyl esterase, GI# 289594371; LREU1684: *L. reuteri* DSM 20016, alpha / beta fold family hydrolase-like protein, GI# 148544890; LAF1318: *L. fermentum* IFO 3956, hypothetical protein, GI# 184155794; LP2953: *L. plantarum* WCSF1, putative esterase, GI# 28379396; LGAS1762: *L. gasseri* ATCC 33323, alpha / beta fold family hydrolase, GI# 116630316; LHV1882: *L. helveticus* DPC 4571, alpha / beta fold family hydrolase, GI# 161508065; PBR1030: *Prevotella bryantii* B14, hydrolase of alpha-beta family, GI# 299776930; HMPREF9071: *Capnocytophaga sp*. oral taxon 338 str. F0234, hydrolase of alpha-beta family protein, GI# 325692879; BIF00780: *Bifidobacterium animalis* subsp. lactis BB-12, cinnamoyl ester hydrolase, GI# 289178448; BACSA1693: *Bacteroides salanitronis* DSM 18170, protein of unknown function DUF676 hydrolase domain protein, GI# 324318365; MED21706696: *Leeuwenhoekiella blandensis* MED217, hydrolase of alpha-beta family protein, GI# 85830613; HMPREF1977: *Capnocytophaga ochracea* F0287, hydrolase of alpha-beta family protein, GI# 314946466; GEOTH1777: *Geobacillus thermoglucosidasius* C56-YS93, alpha / beta hydrolase fold protein, GI# 335362064; SMBG3706: *Clostridium acetobutylicum* DSM

1731, alpha / beta fold family hydrolase, GI# 336291846; CUW2274: *Turicibacter sanguinis* PC909, conserved hypothetical protein, GI# 292644698; TMATH1585: *Thermoanaerobacter mathranii* subsp. mathranii str. A3, BAAT / Acyl-CoA thioester hydrolase, GI# 296842777; EUBIFOR00351: *Eubacterium biforme* DSM 3989, hypothetical protein EUBIFOR_00351, GI# 218217536.

Gene identification numbers (GI#) for Figure 3-10 (phylogenetic tree of LJ0536 with its homologs and other cinnamoyl esterases), Table 5-6 (Structural prediction of LJ0536, LJ1228, and homologs / paralogs using SWISS-MODEL, automatic modeling) and Table 5-7 (Structural prediction of LBA-1 and BFI-2 using SWISS-MODEL, manual modeling) are as follows: *L. johnsonii* N6.2 cinnamoyl esterase LJ0536 (LJO-1), GI# 289594369. *L. johnsonii* N6.2 cinnamoyl esterase LJ1228 (LJO-2), GI# 289594371. *L. gasseri* ATCC 33323 alpha/beta fold family hydrolase LGAS1762 (LGA), GI# 116630316. *L. acidophilus* NCFM alpha/beta superfamily hydrolase LBA1350 (LBA-1), GI# 58337623. *L. acidophilus* NCFM, alpha/beta superfamily hydrolase LBA1842 (LBA-2), GI# 58338090. *L. helveticus* DPC 4571 alpha / beta fold family hydrolase LHV1882 (LHV), GI#161508065. *L. plantarum* WCSF1 putative esterase LP2953 (LPL), GI# 28379396. *L. fermentum* IFO 3956 hypothetical protein LAF1318 (LAF), GI# 184155794. *L. reuteri* DSM 20016 alpha/beta fold family hydrolase-like protein LREU1684 (LRE), GI# 148544890. *Butyrivibrio fibrisolvens* E14 cinnamoyl ester hydrolase CinI (BFI-1), GI# 1622732. *B. fibrisolvens* E14 cinnamoyl ester hydrolase CinII (BFI-2), GI# 1765979. *Treponema denticola* ATCC 35405 cinnamoyl ester hydrolase TDE0358 (TDE), GI# 41815924. *Eubacterium ventriosum* ATCC 27560 hypothetical protein EUBVEN_01801 (EVE), GI# 154484090.

Gene identification numbers (GI#) for Table 5-2 (Structural prediction of fungal FAEs using SWISS-MODEL, automatic modeling) and Table 5-3 (Structural prediction of fungal FAEs using SWISS-MODEL, manual modeling) are as follow: *Neurospora crassa* feruloyl esterase (NCR), GI# 9955721. *Penicillium funiculosum* feruloyl esterase (PFU), GI# 25090320. *Piromyces equi* feruloyl esterase (PEQ), GI# 23821548.

Gene identification numbers for Table 5-4 (Structural prediction of putative FAEs in subfamily 1B using SWISS-MODEL, automatic modeling) and Table 5-5 (Structural prediction of putative FAEs in subfamily 1B using SWISS-MODEL, manual modeling) are as follows: *Leptospira biflexa* serovar Patoc strain putative feruloyl esterase (LBI), GI# 183222795. *Paenibacillus* sp. W-61 putative feruloyl esterase (PAE), GI# 133251525. *Clostridium cellulovorans* 743B putative esterase (CCE), GI# 242261429. *Geobacillus* sp. Y412MC10 putative esterase (GEO), GI# 192811693. *Spirosoma linguale* DSM 74 hypothetical protein SlinDRAFT_02770 (SLI), GI# 229867621. *Algoriphagus* sp. PR1 Possible xylan degradation enzyme (ALG), GI# 126648512.

Gene identification numbers (GI#) for Table 5-8 (Structural prediction of bacterial FAEs using SWISS-MODEL, automatic modeling) and Table 5-9 (Structural prediction of bacterial FAEs using SWISS-MODEL manual modeling) are as follow: *Treponema denticola* F0402 cinnamoyl ester hydrolase (TDE-2), GI# 325475449. *Streptococcus sanguinis* VMC66 cinnamoyl ester hydrolase (SSA), GI# 322123198. *Ruminococcus albus* 8 feruloyl esterase family protein (RAL), GI# 324108892. *Cellulosilyticum ruminicola* feruloyl esterase III (CRU), GI# 326781741. *Prevotella oris* F0302 feruloyl esterase (POR), GI# 281401992.

Table 2-1. Strains and plasmids used in Chapter 3

Strains or Plasmids	Genotype / Description	Source or Reference
E. coli		
DH5α	F- φ80*lacZ*ΔM15 Δ((*lacZYA-argF*)U169 *recA1 endA1 hsdR17*(rk-, mk+) *phoA supE44* λ thi-1 *gyrA96 relA1*	Invitrogen
BL21	F– *ompT hsdS*(rB– mB–) *dcm*+ Tetr *gal* λ(DE3) *endA* Hte [*argU proL* Cam^r] [*argU ileY leuW* Strep/Spec^r]	Stratagene Agilent Technologies
Lactobacillus spp.		
N6.1	*Lactobacillus* sp. isolated from BB-DR rat stool sample.	This study
N6.2	*Lactobacillus* sp. isolated from BB-DR rat stool sample.	This study
N6.4	*Lactobacillus* sp. isolated from BB-DR rat stool sample.	This study
INT173	*Lactobacillus* sp. isolated from BB-DR rat stool sample.	This study
TD1	*Lactobacillus* sp. isolated from BB-DR rat stool sample.	This study
PN2	*Lactobacillus* sp. isolated from BB-DR rat stool sample.	This study
Plasmid		
p15TV-L	Amp^r, T7 promoter driven expression, LIC sequence for DNA recombination cloning, N-terminal 6X His fusion tag followed by a TEV cleavage site	(Guthrie *et al.*, 2007)

Amp^r: ampicillin resistance. TEV: tobacco etch virus.

Table 2-2. Primers used in Chapter 3

Primer Names	Primer Sequences	Description
LJ_0044 Forward	5'-**TTGTATTTCCAGGGC**ATGAAATTACTTCTTACCGGCG-3'	Generate coding region of LJ0044 using template genomic DNA of isolated *Lactobacillus* strain
LJ_0044 Reverse	5'-**CAAGCTTCGTCATCA**TCAATTAGAAATTTGATTTAATTTTTGAACAATT-3'	
LJ_0114 Forward	5'-**TTGTATTTCCAGGGC**ATGAAAATAGATAATTTAACGTTAACAAATTTT-3'	Generate coding region of LJ0114 using template genomic DNA of isolated *Lactobacillus* strain
LJ_0114 Reverse	5'-**CAAGCTTCGTCATCA**CTAAACGTAAATTCTTCTATCTTTCAA-3'	
LJ_0536 Forward	5'-**TTGTATTTCCAGGGC**ATGGCAACAATTACACTTGAGC-3'	Generate coding region of LJ0536 using template genomic DNA of isolated *Lactobacillus* strain
LJ_0536 Reverse	5'-**CAAGCTTCGTCATCA**TTAAAACGCATTATTATTCTGTAAAAAATC-3'	
LJ_0618 Forward	5'-**TTGTATTTCCAGGGC**ATGAAAAAAATTATTCTTTTTGGTGATTC-3'	Generate coding region of LJ0618 using template genomic DNA of isolated *Lactobacillus* strain
LJ_0618 Reverse	5'-**CAAGCTTCGTCATCA**TTATGATATAGCAGCTGTTTCTTTC-3'	
LJ_1228 Forward	5'-**TTGTATTTCCAGGGC**ATGGAGACTACAATTAAACGTGAT-3'	Generate coding region of LJ1228 using template genomic DNA of isolated *Lactobacillus* strain
LJ_1228 Reverse	5'-**CAAGCTTCGTCATCA**TTATTTTATTAAAAACTCACCAACTAATTTTAA-3'	
LREU_1549 Forward	5'-**TTGTATTTCCAGGGC**ATGGAAATTAAAAGTGTTAACTTAGATC-3'	Generate coding region of LREU1549 using template genomic DNA of isolated *Lactobacillus* strain
LREU_1549 Reverse	5'-**CAAGCTTCGTCATCA**CTAAATTAAATTCAGTTCAGTTAACCA-3'	

LIC sequences for DNA recombination are in bold.

Table 2-2. Continued

Primer Names	Primer Sequences	Description
LREU_1667 Forward	5'-**TTGTATTTCCAGGGC**ATGGTACCGGGGCATAAG-3'	Generate coding region of LREU1667 using template genomic DNA of isolated *Lactobacillus* strain
LREU_1667 Reverse	5'-**CAAGCTTCGTCATCA**CTATTTAATATAGTGATCTAAAAATCTTG-3'	
LREU_1684 Forward	5'-**TTGTATTTCCAGGGC**ATGGAAATAACAATCAAACGAGATG-3'	Generate coding region of LREU1684 using template genomic DNA of isolated *Lactobacillus* strain
LREU_1684 Reverse	5'-**CAAGCTTCGTCATCA**CTAATTTTTTAAAAAGTTAGCTACCAG-3'	
T7 Forward	5'-TTAATACGACTCACTATAGGG-3'	Confirm gene insertion in p15TV-L plasmid and sequencing
T7 Reverse	5'-GCTAGTTATTGCTCAGCGG-3'	
Lacto-F	5'-TGGAAACAGRTGCTAATACCG-3'	Universal primers of lactobacilli for strain identification which amplify 233 bp 16s rDNA fragment for sequencing
Lacto-R	5'-GTCCATTGTGGAAGATTCCC-3'	
D88-F	5'-GAGAGTTTGATYMTGGCTCAG-3'	Universal primers of lactobacilli for strain identification which amplify 1.5kb 16s rDNA fragment for sequencing
D94-R	5'-GAAGGAGGTGWTCCARCCGCA-3'	

LIC sequences for DNA recombination are in bold.

Table 2-3. Plasmids used in Chapter 4

Strains or Plasmids	Genotype / Description	Source or Reference
Plasmid		
LJ0536 p15TV-L	Amp^r, T7 promoter driven expression, N-terminal 6X His fusion tag followed by a TEV cleavage site and LJ0536 coding region cloned by DNA recombination with LIC sequence	This study
pET17b-VACVase	Amp^r, T7 promoter driven expression, N-terminal T7 tag, VACVase coding region	(Lai *et al*., 2008)

Table 2-4. Primers used in Chapter 4

Primer Names	Primer Sequences	Description
LJ0536_H32A Forward	5'-GACATGGCAATCATTTTT***GCT***GGTTTTACCGCTAACCGT-3'	Generate coding region of LJ0536 with histidine residue at position 32 mutated to alanine residue using LJ0536 p15TV-L plasmid as template
LJ0536_H32A Reverse	5'-ACGGTTAGCGGTAAAACC***AGC***AAAAATGATTGCCATGTC-3'	
LJ0536_D61A Forward	5'-ATTGCTAGTGTTCGCTTT***GCT***TTTAATGGCCATGGTGAT-3'	Generate coding region of LJ0536 with aspartic acid residue at position 61 mutated to alanine residue using LJ0536 p15TV-L plasmid as template
LJ0536_D61A Reverse	5'-ATCACCATGGCCATTAAA***AGC***AAAGCGAACACTAGCAAT-3'	
LJ0536_S68A Forward	5'-TTTAATGGCCATGGTGAT***GCA***GATGGTAAATTTGAAAAT-3'	Generate coding region of LJ0536 with serine residue at position 68 mutated to alanine residue using LJ0536 p15TV-L plasmid as template
LJ0536_S68A Reverse	5'-ATTTTCAAATTTACCATC***TGC***ATCACCATGGCCATTAAA-3'	
LJ0536_D83A Forward	5'-GTTTTAAATGAAATTGAA***GCT***GCAAATGCCATTTTAAAT-3'	Generate coding region of LJ0536 with aspartic acid residue at position 83 mutated to alanine residue using LJ0536 p15TV-L plasmid as template
LJ0536_D83A Reverse	5'-ATTTAAAATGGCATTTGC***AGC***TTCAATTTCATTTAAAAC-3'	
LJ0536_S106A Forward	5'-ATTTATCTAGTCGGCCAT***GCT***CAAGGTGGTGTCGTTGCT-3'	Generate coding region of LJ0536 with serine residue at position 106 mutated to alanine residue using LJ0536 p15TV-L plasmid as template
LJ0536_S106A Reverse	5'-AGCAACGACACCACCTTG***AGC***ATGGCCGACTAGATAAAT-3'	

Mutation sites are in bold with italic.

Table 2-4. Continued

Primer Names	Primer Sequences	Description
LJ0536_D138A Forward	5'-GCTGCCACTTTAAAAGGT***GCT***GCTCTTGAAGGTAATACA-3'	Generate coding region of LJ0536 with aspartic acid residue at position 138 mutated to alanine residue using LJ0536 p15TV-L plasmid as template
LJ0536_D138A Reverse	5'-TGTATTACCTTCAAGAGC***AGC***ACCTTTTAAAGTGGCAGC-3'	
LJ0536_Q145A Forward	5'-GCTCTTGAAGGTAATACA***GCA***GGAGTTACCTATAATCCA-3'	Generate coding region of LJ0536 with glutamine residue at position 145 mutated to alanine residue using LJ0536 p15TV-L plasmid as template
LJ0536_Q145A Reverse	5'-TGGATTATAGGTAACTCC***TGC***TGTATTACCTTCAAGAGC-3'	
LJ0536_D197A Forward	5'-TTAATCCACGGTACAGAT***GCT***ACCGTTGTTTCCCCTAAT-3'	Generate coding region of LJ0536 with aspartic acid residue at position 197 mutated to alanine residue using LJ0536 p15TV-L plasmid as template
LJ0536_D197A Reverse	5'-ATTAGGGGAAACAACGGT***AGC***ATCTGTACCGTGGATTAA-3'	
LJ0536_H218A Forward	5'-TATCAAAACAGCACTTTA***GCC***TTAATCGAAGGTGCAGAC-3'	Generate coding region of LJ0536 with histidine residue at position 218 mutated to alanine residue using LJ0536 p15TV-L plasmid as template
LJ0536_H218A Reverse	5'-GTCTGCACCTTCGATTAA***GGC***TAAAGTGCTGTTTTGATA-3'	
LJ0536_H225A Forward	5'-TTAATCGAAGGTGCAGAC***GCT***TGTTTTAGTGATAGCTAT-3'	Generate coding region of LJ0536 with histidine residue at position 225 mutated to alanine residue using LJ0536 p15TV-L plasmid as template
LJ0536_H225A Reverse	5'-ATAGCTATCACTAAAACA***AGC***GTCTGCACCTTCGATTAA-3'	

Mutation sites are in bold with italic.

Table 2-4. Continued

Primer Names	Primer Sequences	Description
LJ0536Δ147-173aa_SmaI Forward	5'-TCC*CCCGGG*AACAATTGCCTATTTATGAA-3'	Generate coding region of LJ0536 with deletion of amino acid residue from position 147 to position 173 using LJ0536 p15TV-L plasmid as template
LJ0536Δ147-173aa_SmaI Reverse	5'-TCC*CCCGGG*TCCTTGTGATTACCTTCAA-3'	
VACVase Forward	5'-**TTGTATTTCCAGGGC**ATGTCGGTAACCTCTGCCAAAG-3'	Generate coding region of VACVase using pET17b-VACVase plasmid as template
VACVase Reverse	5'-**CAAGCTTCGTCATCA**TTATTGTAGGAAGTCTTCTGCTAACTTG-3'	

Restriction sites are in italic.

LIC sequences for DNA recombination are in bold.

Table 2-5. Strains used in Chapter 5

Strains or Plasmids	Genotype / Description	Source or Reference
Lactobacillus spp.		
L. gasseri	Wild type *L. gasseri* ATCC 33323	(Lorca *et al.*, 2007b)
L. acidophilus	Wild type *L. acidophilus* ATCC 4356	(Lorca *et al*., 2007b)

Table 2-6. Primers used in Chapter 5

Primer Names	Primer Sequences	Description
LGAS_1762 Forward	5'-**TTGTATTTCCAGGGC**ATGAAGTTAAAGAAAAAGAAAGTAGG-3'	Generate coding region of LGAS1762 using template genomic DNA of isolated *L. gasseri*
LGAS_1762 Reverse	5'-**CAAGCTTCGTCATCA**TTAAAAAGTATTATTATCTTGTAAAAATTCTG-3'	
LBA_1350 Forward	5'-**TTGTATTTCCAGGGC**ATGTTGAAAAAAAGATTTTTATATATTTTTTTGG-3'	Generate coding region of LBA1350 using template genomic DNA of isolated *L. acidophilus*
LBA_1350 Reverse	5'-**CAAGCTTCGTCATCA**TCAATTATTTAAAAAATCATCGATTAATCCT-3'	

LIC sequences for DNA recombination are in bold.

T7 promoter	5230-5246
N-terminal tag	5317-5379
N-terminal cloning site	5365-5379
C-terminal cloning site	7395-7409
T7 terminator	7488-7534
bla coding sequence	209-1066
pBR322 origin	1827
lacI coding sequence	3764-4843
sacB coding sequence	5901-7319
LIC Fw	5365-5379
LIC Rv	7395-7409

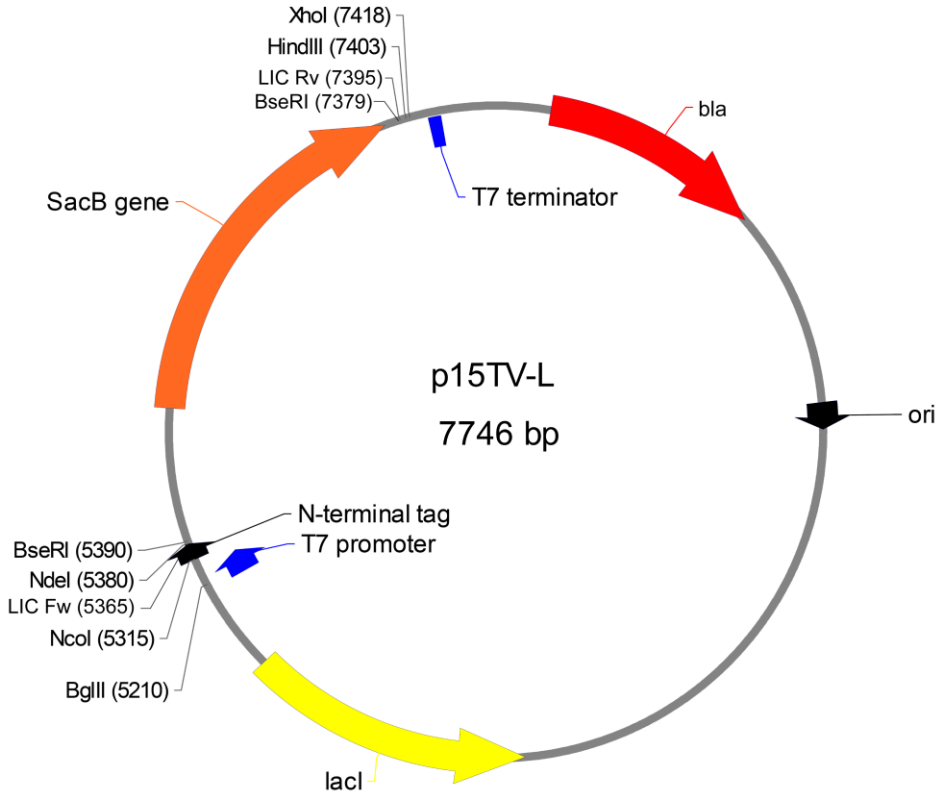

Figure 2-1. Expression vector, p15TV-L map. Image was captured from http://www.sgc.utoronto.ca/SGC-WebPages/Vector_PDF/p15TV-L.pdf and modified.

CHAPTER 3
IDENTIFICATION OF FAES FROM GUT MICROBIOTA

Background

The commensal microbiota residing in the different niches of the higher organism bodys are critical for maintaining good health. However, the mechanisms by which microorganisms interact with the host are still unclear and difficult to study. Important technological advances such as rapid sequencing methods, bioinformatics, and identification using 16S rDNA made possible to describe the variability and composition of the small “ecosystems”. One of the most interesting applications of commensal microbiota is the identification of species potentially responsible for specific host diseases. One clear example is the noticeable changes in the composition of the gut microbial ecosystem of diabetes patients compared to healthy individuals (Vaarala *et al.*, 2008). A recent study (Roesch *et al.*, 2009) showed that Bio Breeding Diabetes Prone (BB-DP) rats have differences in gut microbiota composition when compared to the isogenic Bio Breeding Diabetes Resistant (BB-DR) animals. The results obtained indicated that BB-DR rats have a predominant presence of probiotic bacteria such as *L. johnsonii*, *L. reuteri*, and *Bifidobacterium* species when compared with the microbial ecosystem in BB-DP rats.

The microbial ecosystem described before is not unique. In the past decade, a study carried out in Japan found that oral administration of probiotic bacterium *L. casei* prevents the onset of diabetes in NOD mice by altering the immune response and inhibiting the disappearance of insulin-secreting β cells in Langerhans islets (Matsuzaki *et al.*, 1997b). Other studies showed that oral administration of several *Lactobacillus* spp. can help reduce blood glucose levels by stimulating insulin secretion (Yamano *et*

al., 2006) via changes in the autonomic neurotransmission (Tanida *et al.*, 2005). However, the direct mechanisms behind how probiotic bacteria benefit the host are still unclear.

A feeding study which involves feeding BB-DP rat with *L. johnsonii* has shown that oral administration of the probiotic bacterium *L. johnsonii* mitigates the incidence of type 1 diabetes by decreasing the intestinal oxidative stress response (Valladares *et al.*, 2010). The decreased oxidative stress at the intestinal level could be a consequence of multiple factors. The interaction of probiotics with the animal foods is probably one of the first aspects to be analyzed in order to generate a rationale understanding of the problem.

The rat chow is formulated with many ingredients containing 6% to 8% (w / w) of fiber in the form of sugar beet pulp. The sugar beet pulp is an important source of ferulic acid, a phytophenol with anti-oxidative and anti-inflammatory effects (Couteau & Mathaly, 1998). It has been demonstrated that low dosage of cinnamic acids (especially ferulic acid) has been related with the stimulation of insulin secretion (Balasubashini *et al.*, 2003; Adisakwattana *et al*., 2008), prevention of oxidative stress, lipid peroxidation (Balasubashini *et al.*, 2004; Srinivasan *et al*., 2007), and inhibition of diabetic nephropathy progression (Fujita *et al.*, 2008). The phytophenols and its derivatives are tightly attached to plant cell wall materials by ester bonds which limits intestinal assimilation and functioning of phytophenols. Specific enzymes with good FAE activity are required to hydrolyze and release phenolic acids from the macromolecular structures.

I hypothesized that the probiotic bacteria *Lactobacillus johnsonii* could produce the necessary enzymes to release the antioxidative phenolics. The lactic acid bacteria (lactobacilli) are well known probiotic bacteria used as food supplements and are present in human intestine. It has been found that several lactobacilli, such as *L. fermentum*, *L. reuteri*, *L. leichmanni*, and *L. farciminis*, possess FAE activity but the genes encoding these enzymes were not identified (Donaghy *et al*., 1998).

In this chapter, I described the strain isolation and identification of several colonies of *Lactobacillus* with the ability to hydrolyze ethyl ferulate (EF) in MRS-agar plates. The best FAE producer, identified with the name of *Lactobacillus johnsonii* strain N6.2, was isolated from BB-DR rats' stool samples (Lai *et al.*, 2009). Using a genomic approach, I was able to identify and purify several enzymes with esterase activity. The best enzymes with FAE activity were selected. This chapter summarizes the biochemical characteristic of two FAEs purified to homogeneity from the probiotic strain *L. johnsonii* N6.2.

Result and Discussion

FAEs Producing Strain Isolation and Identification

Colonies of *Lactobacillus* were previously isolated by Dr. Graciela Lorca, University of Florida, directly from the stool samples obtained from the same BB-DR and BB-DP rats analyzed by Roesch (Roesch *et al*., 2009). The isolated colonies were individually transferred to MRS-EF agar plates, with no glucose. The glucose was omitted to prevent a potential catalytic repression of the hydrolytic enzymes. The screening plates were used to evaluate the ability of the isolated strains to produce FAE activity. The strains that displayed evident FAE in MRS-EF agar generated a clear halo around the colonies (Figure 3-1A). The colonies that displayed the best FAE activity

produced clear halo zones of 0.8 - 0.9 cm in diameter. More than 300 colonies were analyzed using this method. Interestingly, 80 ± 5% (mean ± standard deviation) of the *Lactobacillus* colonies isolated from BB-DR rats demonstrated excellent FAE activity. Only 41 ± 7% of the *Lactobacillus* colonies isolated from BB-DP rats were able to hydrolyze the embedded ethyl ferulate. Six colonies isolated from the BB-DR samples showed the largest clear zones “halos” on MRS-EF screening plates. The colonies N6.1, N6.2, N6.4, TDI, INT173, and PN2 were selected and preserved in glycerol at -80°C to be further identified.

The 16S rDNA sequence amplified from the selected isolated colonies belongs to three different *Lactobacillus* spp. The strain, with a colony identification number PN2, showed 96% sequence identity with *L. helveticus*. The strain TDI and INT173 showed 99% sequence identity with *L. reuteri*. Strains N6.1, N6.2, and N6.4 showed 99% to 100% sequence identity with *L. johnsonii* (Figure 3-2). Among all of the isolated *Lactobacillus* strains, *L. johnsonii* N6.2 and *L. reuteri* TDI displayed the highest FAE activities (largest clear halo zones) and were selected as DNA donors to clone potential FAE encoding genes.

In Silico Selection of Targets for Cloning

The precise identification of *L. johnsonii* and *L. reuteri* in the stool samples allowed the use of comparative genomics to select FAE targets *in silico*. Five open reading frames (ORFs) encoding proteins that displayed the characteristic motif previously described for esterases were selected (Brenner, 1988; Cygler *et al*., 1993). The target genes from *L. johnsonii* were selected from a group of 346 ORFs encoding hypothetical (306 ORFs) or putative (40 ORFs) proteins as they are annotated in the genome used as a reference, strain *L. johnsonii* NCC 533 (http://cmr.jcvi.org/tigr-

scripts/CMR/CmrHomePage.cgi). Based on the genome sequence of *L. johnsonii* NCC 533, primers were designed, and *L. johnsonii* N6.2 chromosomal DNA was used as a template for gene cloning. To identify potential FAEs in *L. reuteri*, the genomic sequence of the strain *L. reuteri* DSM 20016 was used to design the primers. Three *L. reuteri* genes were selected for cloning.

Purification and Quick Evaluation of Purified Enzymes

All eight potential FAE encoding genes (*LJ0044, LJ0114, LJ0536, LJ0618, LJ1228, LREU1549, LREU1667, LREU1684*) were cloned successfully into the expression vector p15TV-L and expressed in *E coli* BL21 as recombinant proteins. Seven out of eight potential FAEs (LJ0114, LJ0536, LJ0618, LJ1228, LREU1549, LREU1667, LREU1684) were purified using nickel affinity chromatography. The purity of the His_6-tagged proteins was analyzed by SDS-PAGE and stained with Coomassie Blue. The results are shown in Figure 3-3.

A rapid method to evaluate the FAE activity was used immediately after purification. An aliquot of the purified proteins (3-5 µl equivalent to 0.1 µg total protein) were dropped on the surface of the MRS-EF screening plate. Three out of seven proteins (LJ0536, LJ1228, LREU1684) displayed FAE activity, as it was demonstrated by the formation of halos in the MRS-EF screening plates (Figure 3-1B). It was evidenced that LREU1684 displayed less enzyme activity than the enzymes identified from *L. johnsonii*. The halos in Figure 3-1B look similar; however, 0.4 µg of LREU1684 protein were required to generate a clear zone of similar size to that produced by 0.1 µg protein of LJ0536 or LJ1228. Thus, only LJ0536 and LJ1228 were selected to be further analyzed.

Determination of Optimal pH and Temperature for Activity

The optimal conditions of both enzymes were determined using the model substrates 4-nitrophenyl acetate and 4-nitrophenyl butyrate. These substrates, the 4-nitrophenyl esters, are routinely using to detect esterase activity because the technique is simple and reproducible. The release of 4-nitrophenol after hydrolysis can be easily detected at 412 nm using a visible spectrum spectrophotometer. Since enzymes follow the induced fit model (Koshland, 1958) and esterases are able to hydrolyze a wide range of substrates, it is not necessary to use the “best fit” substrate to determine the optimal conditions for activity. The maximal activity of LJ0536 was achieved at pH 7.8 and 20 °C (Figure 3-4) while the optimal pH and temperature of LJ1228 were pH 6.8 and 30°C (Figure 3-5). The optimal temperature determined *in vitro* is low for proteins that were purified from bacteria living in rat intestines. However, they demonstrated up to 70% residual activity in a wide range of temperature (15 to 38°C), indicating the proteins could be still active in the intestine.

Analysis of Enzymatic Substrate Profile

The substrate profile of the selected enzymes (LJ0536 and LJ1228) was determined in parallel using a panel of 27 different substrates. The panel was an array of aliphatic and aromatic esters representing a variety of chemical scaffolds. These assays clearly demonstrated that both selected enzymes showed the highest activity towards aromatic esters (ethyl ferulate, chlorogenic acid, and rosmarinic acid). The screening also revealed the catalytic flexibility characteristic of the esterases. Several aliphatic esters were also substrates for both enzymes in the study. In Figure 3-6, it is evident that LJ0536 showed high activity towards ethyl ferulate but lower activity towards chlorogenic and rosmarinic acids. The results obtained with the enzyme

LJ1228 demonstrated similar hydrolytic ability towards the aromatic esters (Figure 3-6). This assay is used only to demonstrate the enzyme substrate preferences since it allows the use of several substrates in parallel. This technique utilizes specific conditions to detect the release of hydrogen ion (proton) during hydrolysis. The buffer (BES buffer) and the pH indicator (4-nitrophenol) to be used in this kind of assays must have similar affinity (BES buffer pK_a = 7.09; 4-nitrophenol pK_a = 7.15) for the protons released. In this way, the ratio of protonated buffer and the protonated indicator remains constant. The pH, produced by the proton release during the enzymatic reaction, shifts and it is detected as a change in the yellow color of the indicator present in the mixture. Thus, this technique is not flexible enough in order to re-create the best conditions (pH, type of buffers, ions etc) that the enzymes require in order to work at its maximal initial velocity. The specific enzyme activity determined using this method does not reflect the true specific enzyme activity. In addition, the stability of several enzymes could be affected because of the exhaustive dialysis in BES buffer. The dialysis was done using 120 - 150 times in excess to the volume of enzyme suspension. Consequently, the technique was valid only to demonstrate the substrate preferences even when the conditions (BES buffer pH 7.2, 25^{o}C) were not the best for the enzymes herein studied.

Biochemical Properties of LJ0536 and LJ1228

The selected enzymes, LJ0536 and LJ1228, purified as a single band with an apparent molecular weight of 30 kDa (Figure 3-3). The apparent monomeric molecular weight determined was consistent with the theoretical molecular weight predicted. LJ0536 has a molecular weight of 27.6 kDa, while the LJ1228 enzyme has a molecular weight of 27.4 KD. The estimated molecular mass includes the TEV cleavage site and the His_6-tag encoded in the plasmid (amino acid sequence:

MGSSHHHHHHSSGRENLYFQG, 2.4 kDa). The His_6-tag was removed by TEV treatment. The enzymes do not showed catalytic differences when tagged and un-tagged proteins were evaluated in parallel. Consequently, the assays described in this work were carried out with tagged protein.

When the activity of LJ0536 was evaluated in the presence of divalent cations or iron chloride (Fe^{3+}), only Cu^{2+} (1 mM) inhibited the activity by 90%. LJ1228 enzyme activity was arrested with 1 mM of Zn^{2+}, Fe^{3+}, or Cu^{2+}. The activity of LJ1228 was five times more sensitive to Fe^{3+} than the FAE activity described from *L.acidophilus* (Wang *et al*., 2004b). The addition of EDTA to the reaction mixtures did not affect the activity of these enzymes. Both enzymes were fully inhibited by phenylmethanesulfonyl fluoride (PMSF) and resistant to N-ethylmaleimide (NEM) and iodoacetate. These results confirm the presence of serine as the nucleophilic residue in the active center, which is suggested by the data from the bioinformatic analysis.

The enzymatic parameters obtained by steady state saturation kinetics using a variety of ester substrates are summarized in Table 3-1. In the saturation assays all enzymes followed a canonical Michaelis-Menten hyperbolic kinetic. The biochemical parameters were estimated as described in the Material and Methods section (Chapter 2). As it was determined by the substrate screening method, the enzymes in this study displayed activity on a wide range of ester substrates. Both enzymes showed the highest substrate affinity towards aromatic esters when compared to aliphatic esters. Ethyl ferulate and chlorogenic acids were the best substrate for both enzymes (LJ0536: K_m = 0.020 ± 0.01 mM; LJ1228: K_m = 0.063 ± 0.03 mM). The affinity obtained with ethyl ferulate was comparable with the affinity obtained with chlorogenic acid (LJ0536: K_m

0.053 ± 0.01 mM; LJ1228: K_m= 0.010 ± 0.00 mM). The chemical scaffold of these two substrates is clearly different. The leaving group, alkoxy group of the chlorogenic acid, is a cyclic polyol (quinic acid), which is bigger than the ethyl group released from the ethyl ferulate. This is an important observation and could be used as the first piece of evidence to suggest that the enzymes recognize only the phenolic moiety of the phytophenol. The molecular aspects of substrate binding will be discussed at the light of the protein structure (Chaper 4). LJ0536 also demonstrates to have high substrate affinity towards 4-nitrophenyl butyrate (0.040 ± 0.00 mM). However, the catalytic efficiency was lower than those observed for phenolic esters (4-nitrophenyl butyrate: 4.30 E+04 $M^{-1} \cdot s^{-1}$). The hydrolysis of chlorogenic acid and rosmarinic acid were also confirmed using HPLC by detecting the free caffeic acid released in the reaction mixture by enzymatic action.

Chlorogenic and rosmarinic acids are important components of the human diet. Chlorogenic acid is present in coffee and rosmarinic acid is an aromatic compound produced by many herbs, such as rosemary, sage, and oregano (Wang *et al*., 2004a). The efficient intestinal absorption of these compounds can only occur after microbial enzymatic degradation of the ester bond. The FAE hydrolysis will expose the carboxyl group specifically recognized by the monocarboxylic acid transporter (Plumb *et al.*, 1999). The release of ferulic acid from bran, the hard outer layer of grains usually produced as a by-product of refining, was also confirmed using HPLC. Bran is another important component of the human diet present in bread and fibers from cereal origin.

FAE activity was detected in several bacterial species such as *B. lactis* and *L. gasseri* including *E. coli* (Couteau *et al*., 2001). However, before this work, there are no

records of enzymes purified from bacteria residing in the intestinal tract with efficient chlorogenic acid esterase activity.

The substrate affinity (K_m) of both *L. johnsonii* enzymes towards chlorogenic acid are comparable to the K_m described in *A. niger* FAE (0.01 mM) (Asther *et al.*, 2005). The enzymes of fungal origin require different conditions to be catalytically efficient. For example, the FAE purified from *A. niger*, one of the most studied, requires pH 6.0 and 55^{o}C of temperature. As it was discussed in recent reviews, most FAEs have been isolated from phytopathogenic fungi (Fazary & Ju, 2007; Topakas *et al.*, 2007). Thus, an important contribution of this work is related exclusively with the biochemistry of two new bacterial enzymes that display FAE activity. Since lactobacilli are GRAS (Generally Recognized As Safe) organisms, these two enzymes could have important industrial applications and could be used in the modification of the texture and flavor of fermented food.

Effect of Bile Salt Components

The catalytic ability of LJ0536 and LJ1228 in the presence of conjugated (glycocholic acid and taurocholic acid) and unconjugated bile salts (deoxycholic acid) were evaluated *in vitro*. These components were selected since they can potentially inhibit the activity of hydrolytic enzymes (Schmidt *et al.*, 1982). Conjugated bile acids are more efficient at emulsifying fats because they are more ionized than unconjugated bile acids. The enzyme activity assays in the presence of bile salts using 4-nitrophenyl butyrate as substrate indicate that glycocholic acid is able to improve the activity of LJ0536 (Figure 3-7A). The enzymatic activity of LJ0536 increased almost 40 $\pm$ 10.2% with respect to the control reaction when 0.1 mM of sodium glycocholate was present in the mixture (salt of glycocholic acid). The enzyme activity increased 2.5 fold when the

concentration of sodium glycocholate was increased to 10 mM in the reaction mixture (Figure 3-7B). Interestingly, the enzymatic activity of LJ1228 was not affected at all by any of the salts assayed. The result suggests that both enzymes could work efficiently at bile salt concentrations comparable to those found in the gastrointestinal tract.

In Silico Analysis of FAE Genomic Context

The genomic context of the genes encoding the purified FAEs was investigated using the genome of *L. johnsonii* NCC 533 as reference. It was found that the genes encoding LJ0536 and LJ1228 are located in two poorly characterized regions of the chromosome. Both genes *LJ0536* and *LJ1228* are flanked by hypothetical ORFs. *LJ0536* is transcribed in the opposite direction with respect to the surrounding hypothetical ORFs. *LJ1228* is transcribed in the same direction with respect to the surrounding hypothetical ORFs. The bioinformatics analysis was conclusive for predicting potential associations of those two genes in the same transcriptional unit.

Analysis of FAEs Primary Sequences

Proteins encoded in different groups of bacteria (*Lactobacillus*, *Prevotella*, *Capnocytophaga*, *Bifidobacterium*, *Bacteroides*, *Leeuwenhoekiella*, *Geobacillus*, *Clostridium*, *Turicibacter*, *Thermoanaerobacter*, *Eubacterium*) demonstrate high homology with LJ0536 and LJ1228. All the sequences retrieved from the database belong to proteins without further characterization and are annotated as putative esterases. In the multiple sequence alignment, several amino acids showed full conservation. It was possible to identify two main highly conserved clusters. In both regions the characteristic esterase motif is present; the serine residue in the GxSxG motif is usually the catalytic serine (Figure 3-9). The presence of a second motif is an exception to the general rule that carboxylesterases follow. They could be the

consequence of protein fusions, internal duplications, or by chance. However, the sequence analysis performed was not solid evidence proving duplication or potential fusions with other proteins. It is also possible that some FAEs carry two active sites of hydrolysis. Further studies using site-directed mutagenesis and x-ray crystallography are required to confirm the existence of two esterase motifs with a catalytically functional serine (Chapter 4). The catalytic triad (serine, histidine, and aspartic acid) should be completed with full conserved in all sequences analyzed.

LJ0536 and LJ1228 share 42% amino acid sequence identity. The region of the first motif, which is closer to the N-terminus, is not highly conserved when it is compared to the region of the second motif. The second motif (GHSQGGVV) is thought to be the catalytic motif due to the full cluster of 17 amino acids. It is highly conserved in all homologs and paralogs. The conservation of amino acids suggests that the sequence context is imperative for the catalytic properties of the enzyme.

A tree diagram of proteins was constructed with the closest sequences obtained (Figure 3-10). The proteins grouped in cluster III are LJ0536 (LJO-1) homologous proteins. They share between 71% (LHV) to 87% (LGA) amino acid sequence identity with LJ0536 and present only in homofermentative LAB (*L. gasseri*, *L. helveticus*, and *L. acidophilus*). LJ1228 (LJO-2) in cluster II has a lower amino acid sequence identity from 51% (LPL) to 74% (LRE) with its homologs encoded only in the chromosome of heterofermentative strains. Cluster I is constructed by proteins that share only 18% (BFI-1: CinI) to 33% (BFI-2: CinII) amino acid sequence identity of LJ0536 or 21% (BFI-1: CinI) to 24% (BFI-2: CinII) amino acid sequence identity of LJ1228. The CinI and CinII proteins were included because CinI and CinII from *B. fibrisolvens* are annotated

as cinnamoyl ester hydrolases and are the closest related bacterial protein previously purified (Dalrymple *et al.*, 1996). Only one copy of homolog is identified in each of the *Lactobacillus* spp. except for *L. acidophilus* which has two homologs (LBA-1 in cluster I grouped with CinI and LBA-2 in cluster III grouped with LJ0536).

Summary

The genomic approach using the genome of sequenced strains was successfully used to analyze the wild type strain isolated and identified in our laboratory. The *in silico* prediction of esterases based on the presence of the canonical esterase motif was successfully applied. According to the scientific records, the two enzymes herein purified are the first to be cloned and biochemically characterized from probiotics. Despite that the bacteria was isolated from rat fecal samples, the microorganism studied is a commensal member present in the human gut. The FAE activity was previously described in several microorganisms representative of the different bacterial groups (Couteau *et al*., 2001). However, in the publications consulted, the genes encoding the enzymes were not identified. There is only one article (Wang *et al*., 2004b) that describes the isolation of a FAE gene from *L. acidophilus*. These authors used classical methods to purify the enzyme from crude extract. The N-terminal amino acid sequences of that FAE was provided in the article: ARVEKPRKVILVGDGAVGST. The *L. acidophilus* genome was fully sequenced a year later (Altermann *et al.*, 2005). The sequence described by Wang *et al*. matches only with the L-lactate dehydrogenase. No enzymes, in the 3 different, fully sequenced and annotated strains of *L. acidophilus,* matched the sequence provided. During the course of this work, a similar protein was purified from *Butyrivibrio proteoclasticus*. The protein identified as EstE1 was not

extensively characterized. The work on EstE1 focused on the structure of the protein; thus, it is included in the discussion of the chapter 4 of the present work.

The biological importance of LAB as probiotics is extensively documented and discussed (Walter, 2008). The amelioriating effects of LAB against diabetes symptoms were recently described. However, there is still no satisfactory explanation for this observation (Matsuzaki *et al.*, 1997a; Matsuzaki *et al*., 1997b; Matsuzaki *et al.*, 1997c; Yamano *et al*., 2006). The present work does not answer that question but joins important elements to enrich the discussion in pursuing the understanding of the bacterium-diabetic host relationship. Based on the microflora analysis of BB-DP and BB-DR rats, LAB is one of the groups of bacteria that are naturally enriched in the gut of a nondiabetic host (Roesch *et al*., 2009). It has been shown that an important amount of the cinnamoyl esterase activity is provided by the enzymes produced by the gut microflora (Plumb *et al*., 1999; Williamson *et al.*, 2000) and that ferulic acid can stimulate insulin secretion (Adisakwattana *et al*., 2008; Balasubashini *et al*., 2004; Fujita *et al*., 2008; Balasubashini *et al*., 2003). These three important elements together suggest that the ability of LAB to produce FAEs could play a role in releasing ferulic acid from the diet in the digestive tract, prevent oxidative stress, and to overcome diabetes symptoms of genetically predisposed diabetic hosts. A direct piece of evidence regarding oxidative stress diminution by probiotics was recently published (Valladares *et al*., 2010). The BB-DP rats fed with the *L. johnsonii* N6.2 strain demonstrated to have less oxidative damage and lower rate of diabetes development. These findings, together with the high feruloyl esterase activity described in this work, are in direct agreement with the initial hypothesis that the probiotic bacteria *Lactobacillus johnsonii* could

produce the necessary enzymes to release the antioxidative phenolics. Further *in vivo* evidence using knockout FAE mutants will be necessary to discuss this observation in detail.

Table 3-1. Saturation kinetic parameters of LJ0536 and LJ1228

	K_m (mM)		V_{max} (μmol · min^{-1} · mg^{-1})		K_{cat} (s^{-1})	K_{cat} / K_m (M^{-1} · s^{-1})
LJ0536		standard deviation		standard deviation		
α-naphthyl acetate	0.30	±0.03	21.20	±1.23	9.75	3.27 E+04
α-naphthyl propionate	0.16	±0.01	14.00	±0.05	6.43	3.97 E+04
α-naphthyl butyrate	0.15	±0.01	12.70	±0.24	5.82	3.87 E+04
β-naphthyl acetate	0.90	±0.22	1.83	±0.25	0.84	9.37 E+02
β-naphthyl propionate	0.22	±0.02	0.53	±0.05	0.25	1.09 E+03
β-naphthyl butyrate	0.22	±0.01	0.25	±0.01	0.11	5.10 E+02
4 nitrophenyl acetate	0.47	±0.14	8.40	±1.03	3.86	8.23 E+03
4 nitrophenyl butyrate	0.04	±0.00	3.77	±0.18	1.73	4.30 E+04
4 nitrophenyl caprylate	0.20	±0.00	0.27	±0.01	0.12	6.20 E+02
ethyl ferulate	0.02	±0.01	17.20	±3.24	7.89	3.93 E+05
chlorogenic acid	0.05	±0.01	61.20	±2.75	28.10	5.32 E+05
LJ1228						
α-naphthyl acetate	0.74	±0.08	2.97	±0.17	1.36	1.85 E+03
α-naphthyl propionate	0.40	±0.07	2.25	±0.15	1.03	2.61 E+03
α-naphthyl butyrate	0.19	±0.03	0.85	±0.05	0.39	2.10 E+03
β-naphthyl propionate	0.32	±0.06	0.25	±0.02	0.11	3.65 E+02
β-naphthyl butyrate	0.12	±0.01	0.10	±0.00	0.04	3.87 E+02
4 nitrophenyl acetate	0.95	±0.22	0.64	±0.09	0.29	3.11 E+02
4 nitrophenyl butyrate	0.22	±0.02	0.56	±0.01	0.26	1.14 E+03
4 nitrophenyl caprylate	0.26	±0.01	0.15	±0.01	0.06	2.58 E+02
ethyl ferulate	0.06	±0.03	1.11	±0.28	0.50	7.80 E+04
chlorogenic acid	0.01	±0.00	8.68	±0.49	3.97	3.69 E+05

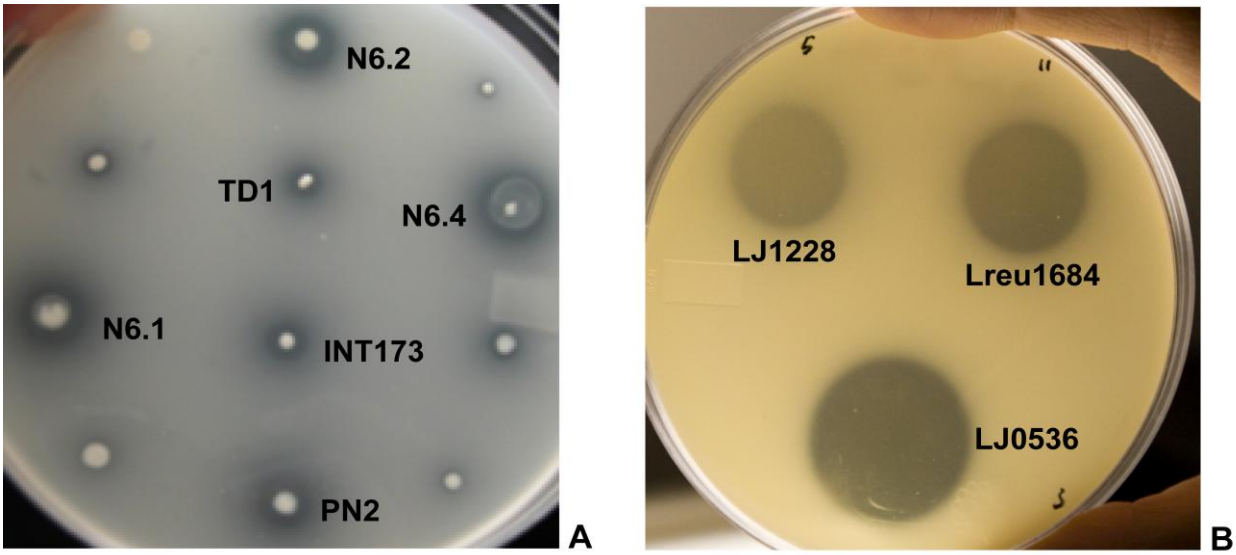

Figure 3-1. Identification of FAE-producing strains. The assays were carried out using MRS agar without glucose supplemented with 0.1% ethyl ferulate. The colonies producing FAEs hydrolyzed the embedded ethyl ferulate and generated a halo-like zone on the plate. (A) Isolated *Lactobacillus* strains. N6.1, N6.2, N6.4: *L. johnsonii*-like colonies; TD1, INT173: *L. reuteri*-like colonies; PN2: *L. helveticus*-like colony. (B) The same plates were used to check the enzymes immediately after purification. The enzymes LJ1228, LREU1684 and LJ0536 are used to illustrate the results obtained with this technique.

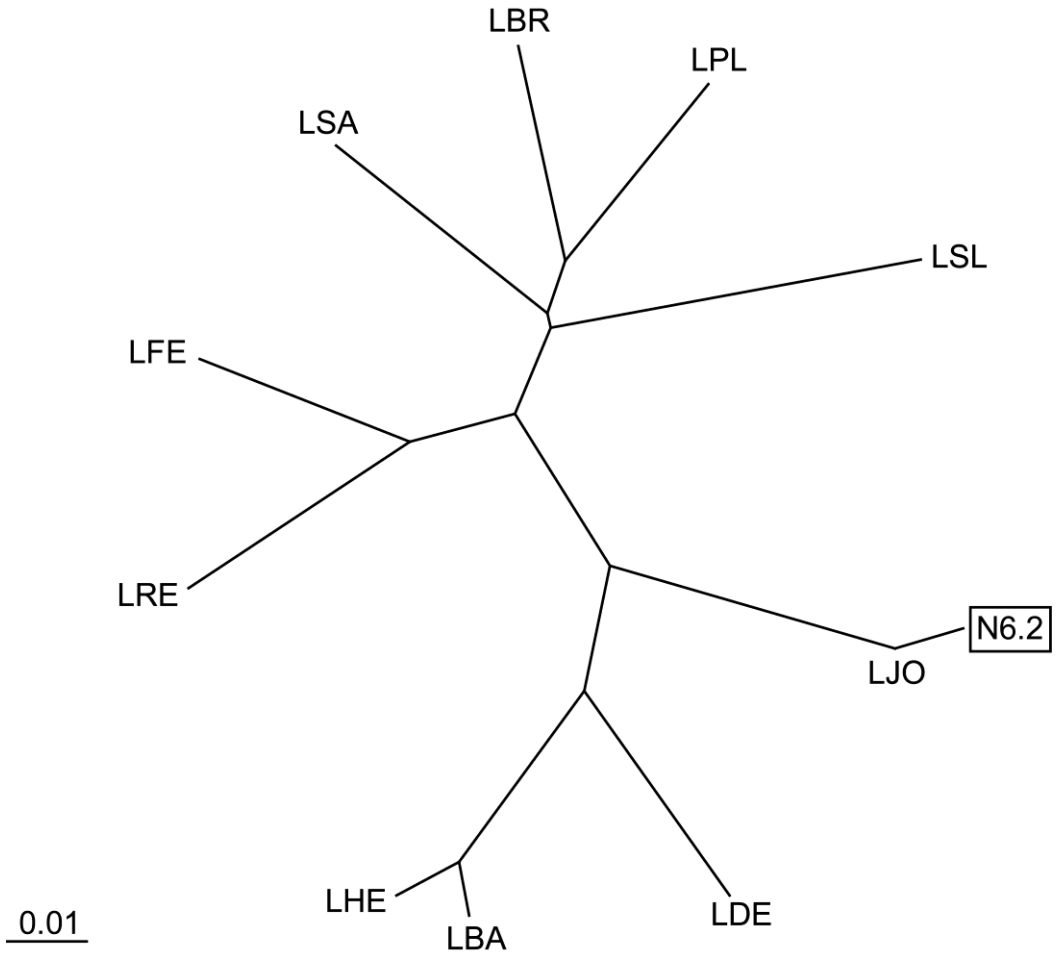

Figure 3-2. Identification of the colonies isolated from BB-DR rats. Phylogenetic relationships of lactobacilli 16S rDNA sequences and the isolated strain N6.2 from BB-DR rats stool sample. The analysis shows that the isolated N6.2 is one strain of *L. johnsonii*. The alignment of the sequences was done using ClustalX2 (neighbor-joining method) and the phylogenetic relationships were visualized with TreeView. LSA, *L. sakei* 23K (locus tag = LSAr01); N6.2: isolated strain; LJO, *L. johnsonii* NCC 533 (locus tag = LJR007); LDE, *L. delbrueckii subsp. bulgaricus* ATCC BAA-365 (locus tag = LBUL_r0045); LBA, *L. acidophilus* NCFM (locus tag = LBA2001); LHE, *L. helveticus* DPC 4571 (locus tag = lhv_3101); LRE, *L. reuteri* JCM1112 (locus tag = LAR_16SrRNA01); LFE: *L. fermentum* IFO 3956 (locus tag = LAF_16SrRNA01); LSL, *L. salivarius* UCC118 (locus tag = LSL_RNA001).LBR, *L. brevis* ATCC 367 (locus tag = LVIS_r0082); LPL, *L. plantarum* WCFS1 (locus tag = lp_rRNA01).

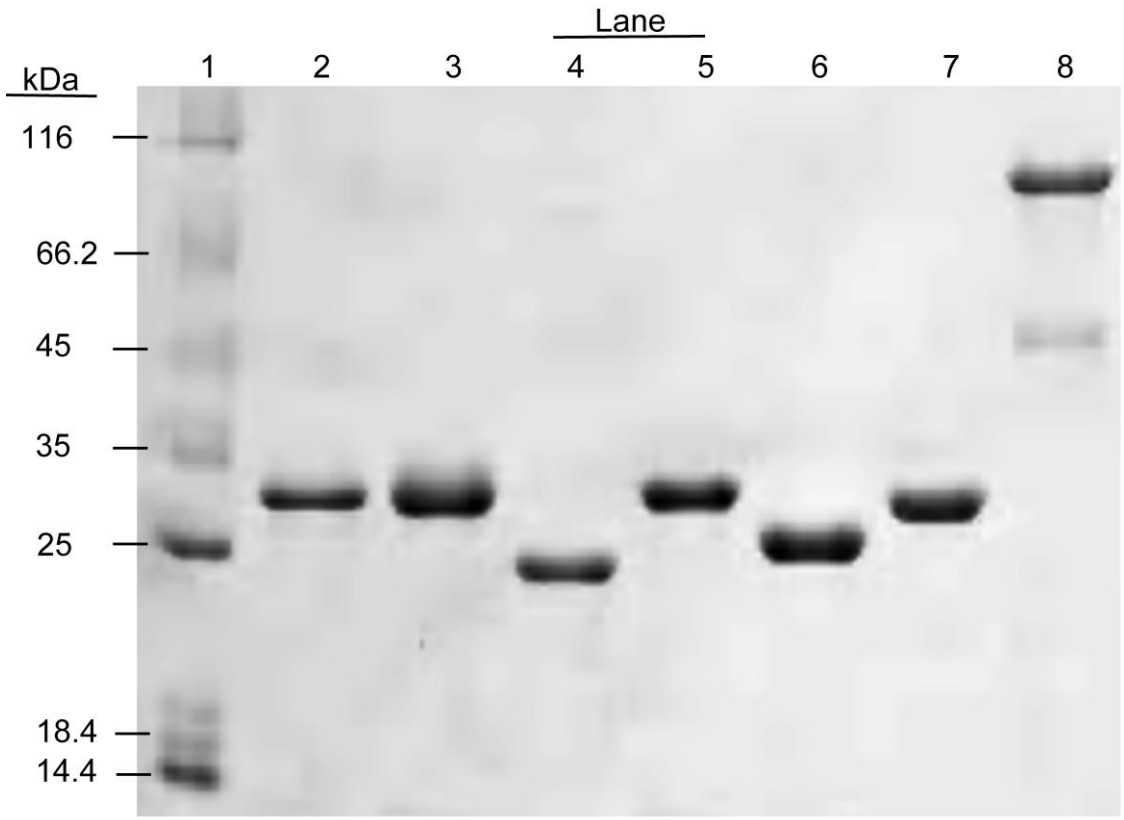

Figure 3-3. Purified enzymes on SDS-PAGE stained with Coomassie Blue. Enzymes were purified using nickel affinity chromatography. Lane 1: EZrun molecular weight marker (Fisher Scientific). Lane 2: LJ0114 (30.3 kDa). Lane 3: LJ0536 (27.6 kDa). Lane 4: LJ0618 (21.2 kDa). Lane 5: LJ1228 (27.5 kDa). Lane 6: LREU1549 (26.6 kDa). Lane 7: LREU1684 (27.5 kDa). Lane 8: LREU1647 (90.4 kDa).

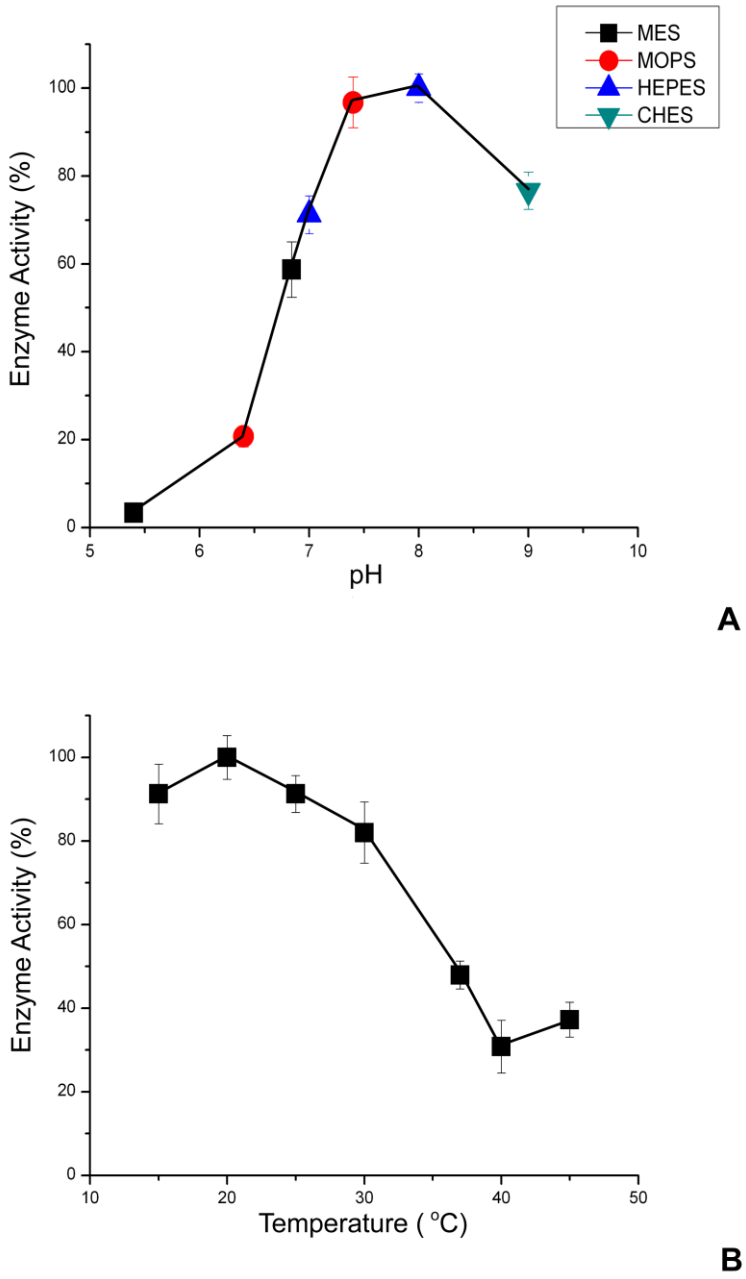

Figure 3-4. Optimal pH and temperature of LJ0536. (A) The optimal pH was determined by measuring the enzyme activity at 37°C using 1 mM 4-nitrophenyl butyrate as model substrate. The assay was done using overlapping buffers from pH 5.4 to pH 9. The optimal pH was estimated as pH 7.8. (B) The optimal temperature for enzyme activity was determined in a range of temperature from 15°C to 45°C using 1 mM 4-nitrophenyl butyrate as a model substrate. The optimal temperature determined was 20°C.

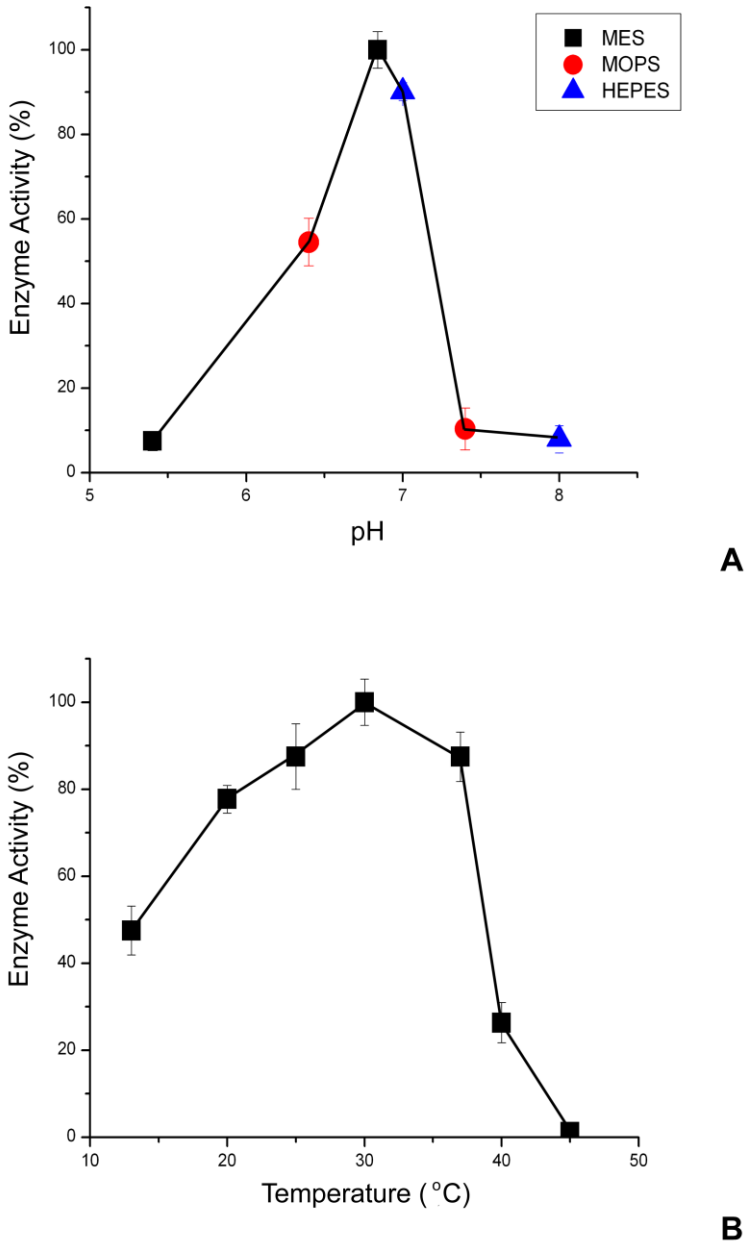

Figure 3-5. Optimal pH and temperature of LJ1228. (A) The optimal pH was determined by measuring the enzyme activity at 37°C using 1 mM 4-nitrophenyl butyrate as model substrate. The assay was done using overlapping buffers from pH 5.4 – pH 8.0. The optimal pH was estimated as pH 6.8. (B) The optimal temperature was determined by measuring the enzyme activity in a range of 13°C to 45°C using 1 mM 4-nitrophenyl butyrate as a substrate. The optimal temperature determined was 30°C.

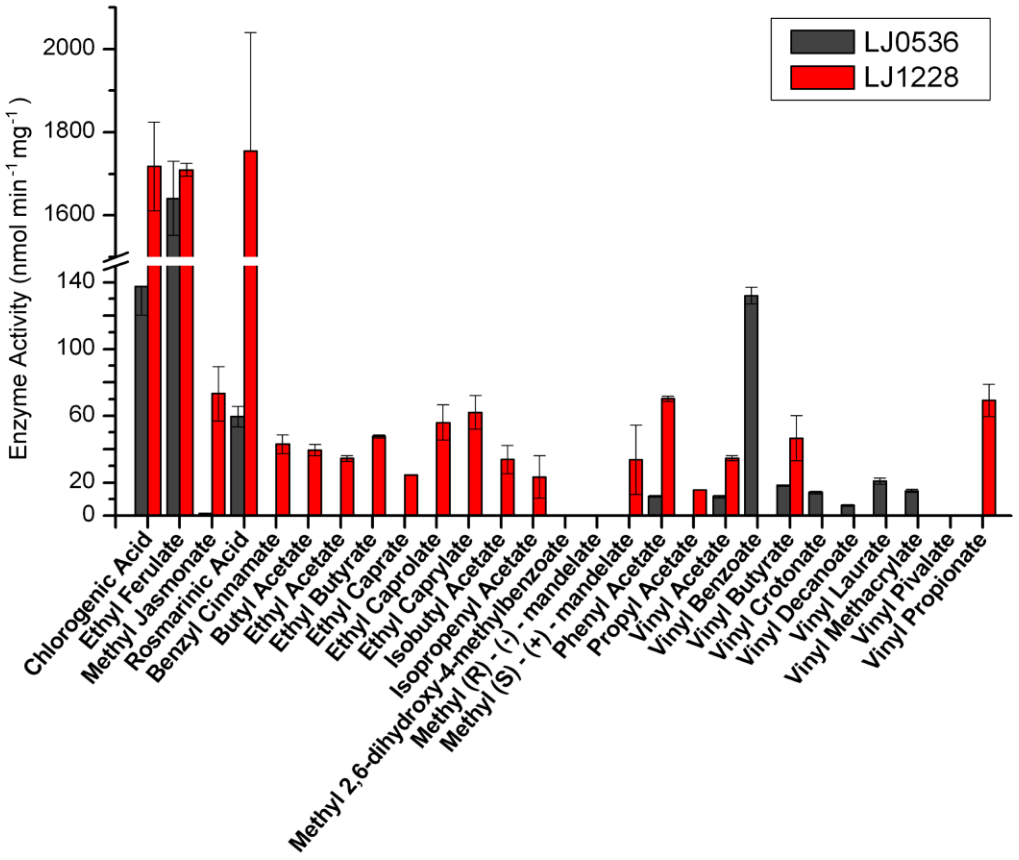

Figure 3-6. Enzymatic substrate profile of the enzymes LJ0536 and LJ1228. The assays were carried out following the protocol described by Janes and co-workers using 4-nitrophenol as a proton trapper (Janes *et al*., 1998). The hydrogen ion generated during ester hydrolysis reduced the free 4-nitrophenol in solution, leading to a decrease in absorbance at 404 nm. The enzyme activity was estimated from the amount of hydrogen ion released. The reaction mixture was formulated with 4.39 mM BES buffer pH 7.2, 0.44 mM of 4-nitrophenol, 1 mM of substrate, and 30 to 35 $\mu g \cdot mL^{-1}$ of the purified enzymes.

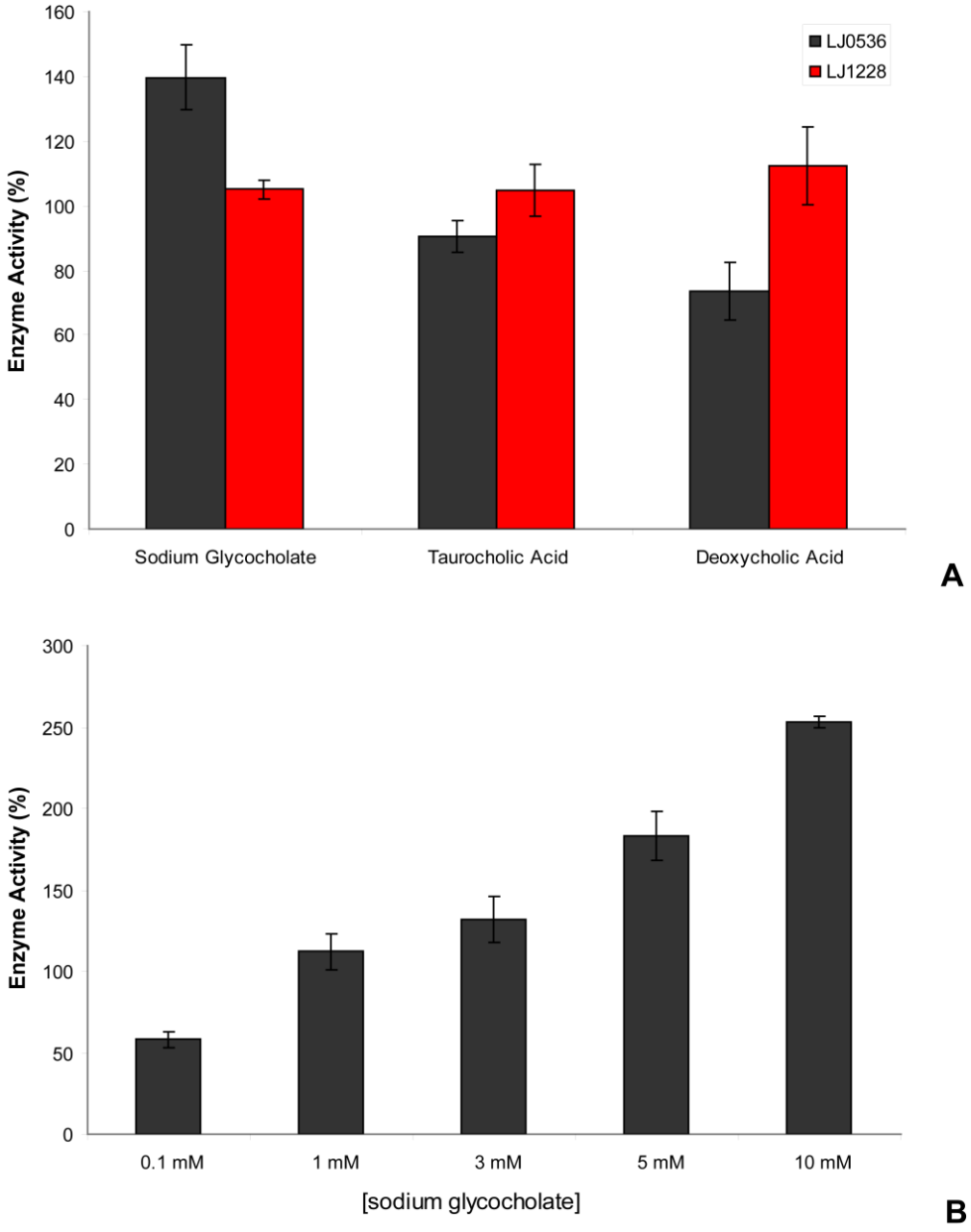

Figure 3-7. Effect of bile salts on LJ0536 and LJ1228 enzyme activity. (A) The activity was evaluated with 0.1 mM of the three bile salt components using 4-nitrophenyl butyrate as the model substrate. Only sodium glycocholate significantly improved on LJ0536 activity. LJ1228 was not affected by any of the tested bile salts. (B) The activity of LJ0536 improved as the concentration of sodium glycocholate increased in the reaction mixture.

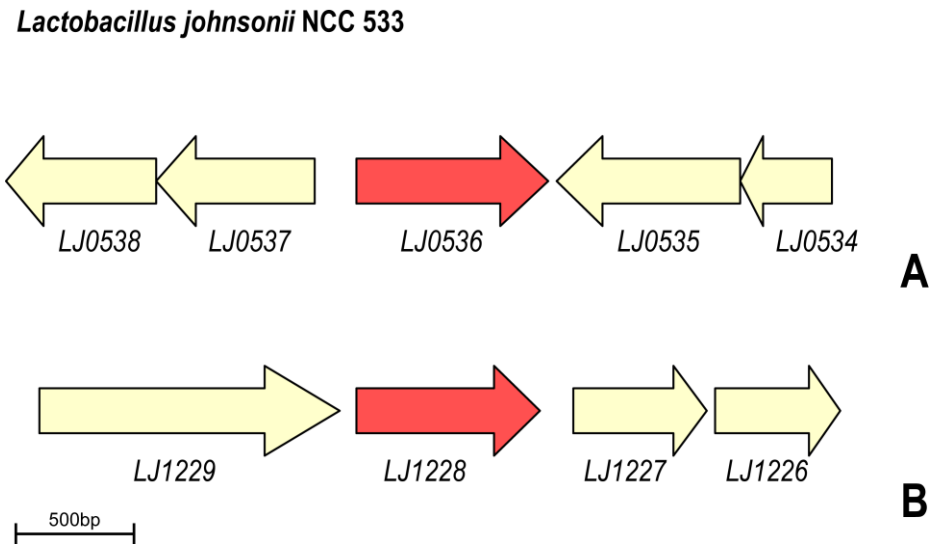

Figure 3-8. Genomic context of (A) LJ0536 and (B) LJ1228 (colored red) in the reference strain *L. johnsonii* NCC 533. All the open reading frames in the neighborhood and the genes of interest are annotated as hypothetical proteins (colored Ivory).

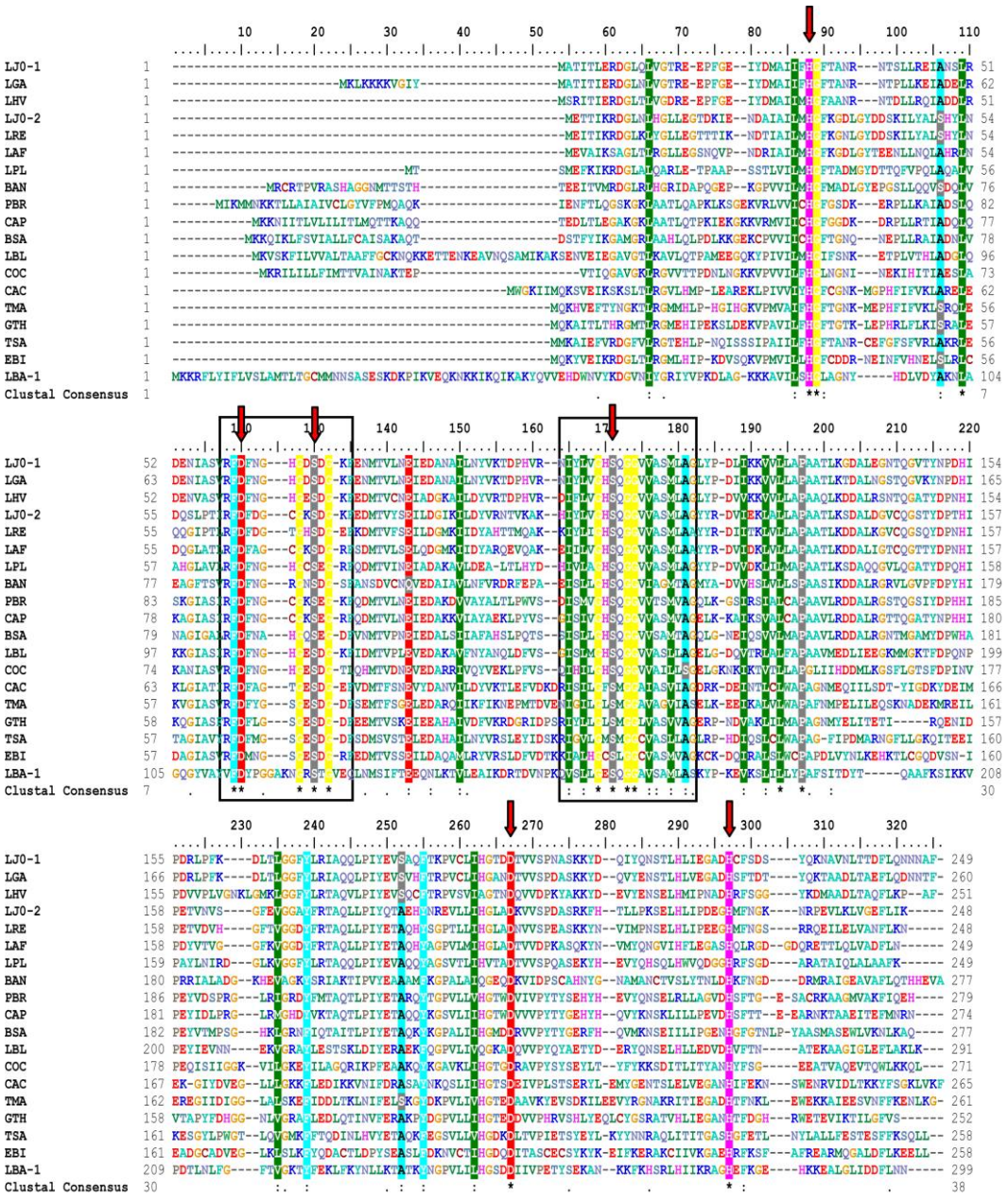

Figure 3-9. Multiple sequence alignment of LJ0536 and proteins with high sequence identity. The protein sequences retrieved from the database are annotated as putative or hypothetical esterase / hydrolase. Gene identification numbers are listed in Chapter 2. The two classical serine esterase catalytic motifs (GxSxG) are clearly identified (boxed in rectangles). The cluster containing the first motif, which belongs to the positions Gly66-Ser68-Gly70 in LJ0536, is less conserved compared to the location of the second motif Gly_{104}-Ser_{106}-Gly_{108}. The serine present in the second motif is thought to be the nucleophile residue during catalysis since the cluster is highly conserved. The potential catalytic triad residues (fully conserved serine, histidine, and aspartic acid) are indicated by red arrows. Amino acids are colored in different colors.

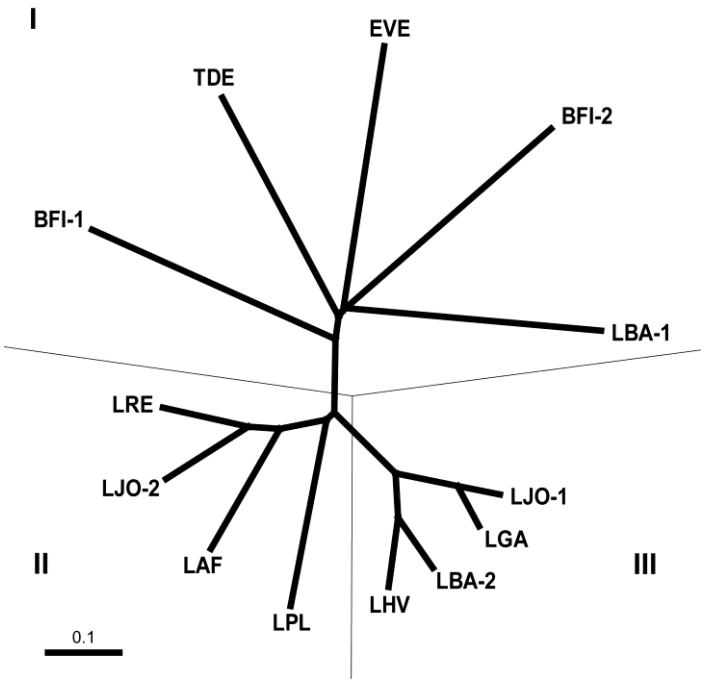

Figure 3-10. Tree representation of LJ0536 and LJ1228 relationships with the proteins that displayed the highest sequence identity. Three clusters are clearly identified. Based on the sequence analysis, the proteins studied are clustered in two different groups. LJO-1: *L. johnsonii* N6.2, cinnamoyl esterase LJ0536. LJO-2: *L. johnsonii* N6.2, cinnamoyl esterase LJ1228. LGA: *L. gasseri* ATCC 33323, alpha/beta fold family hydrolase LGAS1762. LBA-1: *L. acidophilus* NCFM, alpha/beta superfamily hydrolase LBA1350. LBA-2: *L. acidophilus* NCFM, alpha/beta superfamily hydrolase LBA1842. LHV: *L. helveticus* DPC 4571, alpha/beta fold family hydrolase LHV1882. LPL: *L. plantarum* WCSF1, putative esterase LP2953. LAF: *L. fermentum* IFO 3956, hypothetical protein LAF1318. LRE: *L. reuteri* DSM 20016, alpha/beta fold family hydrolase-like protein LREU1684. BFI-1: *B. fibrisolvens* E14, cinnamoyl ester hydrolase CinI. BFI-2: *B. fibrisolvens* E14, cinnamoyl ester hydrolase CinII. TDE: *Treponema denticola* ATCC 35405, cinnamoyl ester hydrolase TDE0358. EVE: *Eubacterium ventriosum* ATCC 27560, hypothetical protein EUBVEN_01801.

CHAPTER 4
X-RAY CRYSTALLIZATION AND SUBSTRATE BINDING MECHANISM OF LJ0536

Background

The enzymes that hydrolyze the ferulic and *p*-coumaric ester cross-linking bonds present in hemicellulose are used industrially to improve the degradation of biomass with vegetable origins. It is well known that the natural systems often serve as inspirations for finding the necessary elements needed to improve “man made” methods. The natural flora associated with decaying wood are composed primarily of several species of fungi. Thus, several mass-produced commercial enzymes used in plants biomass saccharification were obtained from different species of fungi. Due to ease of obtaining such enzymes, it is not surprising that practically all FAEs that had been biochemically and structurally studied are of fungal origin (Benoit *et al.*, 2007; Faulds *et al.*, 2005; Hermoso *et al*., 2004).

The scientific literature describing the biochemistry and 3-dimensional structures of bacterial FAEs is limited. It was mentioned previously (Chapter 3) that no proteins isolated from bacteria of the human normal flora with FAE activity were biochemically characterized before this work. Once LJ0536 and LJ1228 were identified as *L. johnsonii* FAEs, the *in silico* predicted 3-dimensional structure partially matched with only one protein of the PDB database (PDB: 2OCG). The best match was the human protein valacyclovir hydrolase (VACVase), produced in the liver and involved in the activation of the antiviral valacyclovir (Lai *et al*., 2008). During the course of this study, the first structure of a bacterial FAE (Goldstone *et al*., 2010) was deposited in the PDB database (PDB: 2WTM). This protein (Est1E) was purified from *Butyrivibrio proteoclasticus* (Firmicutes, Clostridiales), a bacterium that thrives in the rumen of several herbivores.

The overall predicted structure of LJ0536 had a good correlation with the structure of Est1E.

Esterases are classical members of one of the most versatile proteins structural groups, the α / β superfamily, sub-family α / β fold hydrolases (Ollis *et al*., 1992). The α / β fold provides a stable scaffold for the active site of a variety of enzymes, including lipases, proteases, and haloalkane dehydrogenases. The canonical α / β fold hydrolases mostly consist of several β-strands (normally 8), surrounded by α-helices (Figure 4-1). The central β-sheet usually displays a left-handed superhelical twist. Thus, in the overall structure, the first and last strands cross each other at an angle of 90°. The catalytic center always consists of a triad composed of a nucleophile (serine, cysteine, or aspartic acid), a fully conserved histidine, and an acidic residue (usually aspartic acid). The nucleophile, usually serine in carboxylesterases, is always located in a sharp turn exposed to the solvent, which is generally called the “nucleophilic elbow”. This architecture ensures easy contact between the substrate and water molecules in the solvent (Ollis *et al*., 1992; Nardini & Dijkstra, 1999; Holmquist, 2000).

The hydrolytic mechanism of serine esterases was described in detail in Chapter 1. The sequence of steps previously described is generally accepted for all enzymes with a similar mechanism of hydrolysis. The acylenzyme intermediate was “captured” in a crystallized protein (Mangel *et al.*, 1990; Ding *et al*., 1994). The only elusive link in this reaction is the tetrahedral intermediate (Dodson & Wlodawer, 1998). Thus, the formation of the two tetrahedral intermediates steps is assumed to occur and probably they will be never captured due to the instability of the complex (Hedstrom, 2002). Since

most of the secrets of catalysis have already been uncovered, the focus of this study is on characterizing the mechanisms of substrate binding.

The identification of protein scaffolds that recognize the substrates to be hydrolyzed is one of the most interesting aspects of modern enzymology. Catalytic pockets can be predicted using 3-dimensional models. However, the information in the protein structure database is still too fragmented to identify the intimate relationship between the amino acids of the binding cavity and the substrate. Due to limited knowledge of FAE structures, *in silico* approaches are used to predict potential substrate orientations within the catalytic pockets of the enzymes. However, the techniques used, generally called molecular docking, face serious problems when the proteins to be studied can function with several substrates. The phenomenon, described as “enzyme promiscuity”, is actually more frequent than the model of “one enzyme, one substrate” traditionally associated with enzymatic catalysis. The catalytic flexibility of carboxylesterases, enzymes that can use ester compounds with a variety of chemical scaffolds (Pindel *et al.*, 1997; Bornscheuer, 2002; Lai *et al*., 2009) makes this group of enzymes excellent models of study. The catalytic flexibility is well represented by the FAEs purified from *L. johnsonii* N6.2. Both LJ0536 and LJ1228 proteins were demonstrated to be active on a large variety of ester substrates, from phenolic to aliphatic esters, including substrates of high molecular weight like steryl esters (Lai *et al*., 2009).

This chapter is dedicated to the structural studies carried out with the FAEs purified from *L. johnsonii* N6.2. The overall structure of the apo-enzyme is described, together with the analysis of the catalytic amino acids. As mentioned before, the main

focus of the study is directed towards describing the structures involved in the conformation of the catalytic pocket. The structures of the crystallized protein and protein co-crystallized with the substrates of interest are discussed along with the site-directed mutagenesis studies. The unique features of LJ0536 were compared with the characteristics of the closest structural homologous as identified by 3-dimensional alignments.

Result and Discussion

Architecture of LJ0536

The structure of the apo-LJ0536 was determined by Banting and Best Department of Medical Research, Centre for Structural Proteomics in Toronto (University of Toronto). Structural Analyses were done in our laboratory. The apo-LJ0536 structure has a resolution of 2.35 Å using Molecular Replacement (MR) with feruloyl esterase Est1E from *Butyrivibrio proteoclasticus* (PDB: 2WTM) (Goldstone *et al*., 2010). Crystallization and diffraction statistics are summarized in Table 4-1. LJ0536 was crystallized as homodimer (Figure 4-2A and B), which is consistant with size exclusion analysis (Figure 4-3) showing that the native molecule weight of LJ0536 is 46.0 ± 3.2 kDa (monomeric apparent molecular weight: 27.6 kDa). LJ0536 displays a classical α / β hydrolase fold (Ollis *et al*., 1992). The overall structure of LJ0536 is composed of twelve β-strands and nine α–helices (Figure 4-4A). It has a central β-sheet core which contains one antiparallel (β_2) and seven parallel (β_1, β_3, β_4, β_5, β_6, β_{11}, β_{12}) β-strands. The central β-sheet core shows a left-handed superhelical twist with an approximate angle of 120^o between β_1 and β_{12} (Figure 4-4B). It is flanked by five α–helices of which two α–helices (α_1, α_9) are externally located and three α–helices (α_3, α_4, α_8) are internally located towards the dimer interface (Figure 4-2A). The dimer interface is

formed by α_4, α_6, and β_1. It comprises 34 and 37 residues of chain A and chain B respectively, burying a total of 2373 $Å^2$ between the two chains. Five hydrogen bonds are formed within the interface (one from chain A R8 to chain B D9, one from chain A G117 to chain B Q175, two from chain A R171 to chain B D121, and one from chain A R171 to chain B L118). A sequence of 54 amino acids (P131 to Q184) forms an inserted α / β domain between β_6 and β_{11} (Figure 4-5). This domain is composed of two short β-hairpins (β_7 - β_8 and β_9 - β_{10}), and three α–helices (α_5, α_6, α_7). The two β-hairpins project towards the entrance of the substrate binding cavity. The two protruding hairpins from the inserted α / β domain decorate the entrance of this cleft and form the “roof” of the catalytic compartment. The substrate binding cavity resembles an open canal-like feature with the shape of a boomerang (Figure 4-6). The binding cavity is formed by two clefts (Figure 4-6A). One is approximately 13 Å long and ends in a hydrophobic pocket buried between the α_5 and α_6 of the inserted α / β domain. It is large enough to accommodate the aromatic acyl group of the substrate. The other cleft is about 12 Å long and can accommodate the alkoxyl group plus additional atoms from larger substrates.

The S106 is the Catalytic Residue

An intriguing feature of LJ0536 is the presence of two GXSXG motifs, which are conserved among LJ0536 orthologs. Previously, two conserved classical GXSXG motifs (G66-X-S68-X-G70 and G104-X-S106-X-G108) were identified in the primary sequences of LJ0536. These two clusters were fully conserved in all of the homologs retrieved from the database with a Blast search. Typically, the carboxylesterases display only one GXSXG motif. In order to confirm LJ0536 is using serine as catalytic residue, the enzyme activity was evaluated in the presence of specific serine or cysteine

inhibitors. The enzymatic activity of LJ0536 was arrested by the serine protease inhibitor phenylmethanesulphonylfluoride (PMSF), but it resisted the action of the cysteine alkylating compounds N-ethylmaleimide (NEM) and iodoacetate (Figure 4-7). These results confirmed the presence of a serine as the nucleophilic residue in the active center, which was suggested by the bioinformatic analysis.

The crystal structure of LJ0536 showed that the catalytic triad is composed of S106, H225, and D197 (Figure 4-6). The role of H225 is to deprotonate S106. Then S106 can perform a nucleophilic attack on the carbon atom of the carbonyl group of the substrate, while D197 stabilizes the protonated H225. The distance between S106 and H225 is 3.03 Å, and the distance between H225 and D197 is 3.01 Å. The catalytic serine residue (S106) is located at the center of the boomerang shape crevice which is on the nucleophilic elbow formed between β_5 and α_4 (Figure 4-6B and D). S68 is located 18 Å away from S106 (Figure 4-8A). Two amino acids that are conserved within homolog proteins, H32 and D61, are found in the sequence (Figure 3-9). Although S68 together with H32 and D61 seem able to form a catalytic triad, S68 is not located on the nucleophilic elbow. Catalytic serine located on ucleophilic elbow is one of the conserved features of the α / β fold subfamily. The nucleophilic elbow structure is one of the requirements to consider the serine as a catalytically active residue. There is not a binding cavity exposed to the solvent around S68. The apparent contact of the residue (S68) with the solvent is not enough to support a role in hydrolysis (Figure 4-8B). The highly conserved histidine of the triad, in this case H32, has a good orientation in space, but it is not in a close proximity to S68 (9.48 Å apart from each other). Consequently, it is unlikely that H32 can perform the deprotonation of S68. There is no other potential

candidate in the region to fulfill the critical deprotonation step during catalysis. Thus, S68, H32, and D61 do not reunite the typical characteristics to be considered as a triad of catalytic active residues.

In order to confirm experimentally that S68, H32, and D61 are not involved in the forming of catalytic triad, enzymes with specific site-directed mutations were made. The mutations were directed to the conserved serine, histidine, or aspartic acid residues as identified with the multiple alignment of the lineal sequences of several proteins with high identity (Figure 3-9). All mutants were purified successfully (Figure 4-9). It was confirmed that the active catalytic triad is S106, H225, and D197 since the mutants S106A and D197A do not displayed enzymatic activity (Table 4-2, Figure 4-10). Interesting, the enzyme activity of S68A, H32A, and D61A was also hindered. A second look to the structures indicates that the S68 form extensive hydrogen bonds with the amino acids of the neighborhood (Figure 4-8C). I hypothesized that the conserved S68 was an important residue in order to maintain the proper folding of the enzyme. Circular dichroism analysis of the S68A mutant confirmed a significant shift in the secondary structure of the protein (Figure 4-11). The secondary structure analysis indicates that the activity of S68A is affected by an overall change in the protein structure rather than a change in the catalytic residues.

Analysis of the Crystal Structures of S106A-Substrate Complexes Reveals Critical Residues for Substrate Binding and Catalysis

The structure of the catalytic deficient mutant (S106A) and the S106A co-crystallized with ferulic acid, ethyl ferulate, or chlorogenic acid (Figure 4-12) were determined by Banting and Best Department of Medical Research, Centre for Structural Proteomics in Toronto (University of Toronto). Structural Analyses were done in our

laboratory. The S106A ethyl ferulate complex crystallized in two forms (Form I and Form II with a dimer and a single chain in the asymmetric units, respectively). The two ethyl ferulate crystal forms are nearly identical in structure (root mean square deviation (RMSD) values of 244 Cα atoms of both chains of Form I onto Form II are 0.25 and 0.3 Å respectively), and the dimer from Form II is essentially identical with the Form I dimer. Analysis was focused on Form II due to better occupancy of the ligand in the active site. Overall, no appreciable differences in the backbone structure between the apo wild type (WT) enzyme and the S106A mutant (RMSD of 0.33 Å over all 244 Cα atoms) was observed. The ligand binding did not induce major structural changes in the active site, except for a rotamer change in Q145 and a slight rotation of the side chain of H225 (Figure 4-13), which presumed the active conformation of the catalytic triad.

The excellent diffraction of apo-S106A, S106A bound with ethyl ferulate, S106A bound with ferulic acid, and S106A bound with caffeic acid (resolutions between 1.58 Å – 1.75 Å) allowed us to compare the positions of different substrates and the conformation of the active site residues (Figure 4-14). Q145 from the inserted α / β domain adopted a different conformation, creating a bridge-like structure on top of the catalytic site (Figure 4-12). The feature of Q145, along with the side chains of F34 and V199, limits the size of the substrate that can enter the catalytic pocket to 7 Å in width. In all three complexes, the substrates in the catalytic groove were oriented with the aromatic acyl moiety of the carbonyl group bound in the deepest part of the pocket (Figure 4-12). The opposite end of the ligands, on the far side of the ester moiety such as the ethoxyl group of ethyl ferulate, rests on a more solvent-exposed area of the groove and has no interactions with the protein. The electron density for the C2 atom of

ethyl ferulate has missing electron density in the structure (Figure 4-15A), which is consistent with the C2 atom being part of the leaving group (ethyl group) after hydrolysis. As well, no clear electron density was resolved for the quinic acid moiety of chlorogenic acid (labeled as caffeic acid-bound) (Figure 4-15C and D), perhaps due to residual enzymatic activity or a lack of productive interactions with the enzyme. The substrate specificity only depends on the type of phenolic acid presents in the ester, binding of the leaving group is not necessary, resulting in poor electron density map on the leaving group. This hypothesis is supported by Faulds (Faulds *et al*., 2005) which shown that crystallization of S133A AnFaeA mutant (catalytic deficient mutant of feruloyl esterase from *Aspergillus niger*) with feruloylated trisaccharide substrate shows only the ferulic acid moiety but not the carbohydrates moiety. A similar scenario is observed in the crystal structure of catalytic serine deficient S172A FAE-XynZ mutant in complex with feruloyl arabinoxylan (Schubot *et al.*, 2001). Only the ferulic acid is visible in the structure, even though the authors took extra precaution to avoid substrate hydrolysis during crystallization. Both studies lead to the same conclusion that the lack of leaving group in the structure is due to the lack of interaction between the enzyme and the leaving group. The enzyme does have an area of the binding cleft that could accommodate the quinic acid group (Figure 4-14B), or other groups of a similar size, formed by the side chains of H32, A36, T40, L42, L43, H105 and C226. The binding cavity is occupied by water molecules in each of the structures (Figure 4-13).

The LJ0536 catalytic deficient mutant S106A forms extensive hydrogen bonding networks at both ends of the ligands. Thus, it forms a molecular ruler where the distance between the aromatic ring and the site of hydrolysis is constrained by these

hydrogen bonds and the position of the catalytic triad. Other than the catalytic residues and the oxyanion hole, the enzyme does not contribute any hydrogen bonds on the end of the ligand with the ester group (Figure 4-13 and 4-16). This suggests that substrate discrimination is accomplished by the hydrogen bonds to the aromatic ring and its substituents. More hydrogen bonds are formed with the phenolic rings of the ligands, including the presence of an ordered water molecule in all of the complexes (Figure 4-13). The 4-hydroxyl group (ethyl ferulate, ferulic acid, and caffeic acid) and 3-hydroxyl group (caffeic acid) of the aromatic ring of the substrates are hydrogen bonded to D138 and Y169, respectively, from the inserted α / β domain at the back of the enzyme cavity. The 3-methoxy (3-hydroxyl in case of caffeic acid) and 4-hydroxyl groups also interact with an ordered water molecule in all of the complexes. This water is also coordinated by the Oγ1 atom of T144 from the inserted α / β domain. The 3-methoxy group of ethyl ferulate or ferulic acid is accommodated by a small hydrophobic cavity formed by the benzyl moieties of F34 and F160, plus the L165 residue (Figure 4-16). The aliphatic chain separating the aromatic ring from the site of hydrolysis is accommodated by the hydrophobic side chains of F34, A132, V199, and V200. One oxygen atom of the carbonyl group that forms the ester interacts directly with the oxyanion hole formed by the backbone nitrogen atomes of F34 and Q107. Whereas the other oxygen interacts with H225 and an ordered water molecule present in the caffeic and ferulic acid structures (the ethoxy group of ethyl ferulate occupies the space of this water molecule). Ethyl ferulate rotates slightly and positions the ester bond perpendicular to A106 at a distance of 2.73 Å due to these interactions. The ester bond is strained from planarity by the active site (bond angle of 116º), suggesting the hydrolytic mechanism involves a

typical tetrahedral enzyme-ester intermediate of esterases. The different configuration of the ester bonds of the substrate ethyl ferulate and the product ferulic acid that is parallel to the main axis of the groove further suggests the validity of the tetrahedral enzyme-ester intermediate mechanism (Figure 4-13B and C, 4-14A).

A water molecule was observed, 3.3 Å from the non-carbonyl oxygen of the ester bond of ethyl ferulate towards the solvent-exposed face of the pocket (Figure 4-13B and 4-14A). It is possible that this corresponds to the water molecule that is targeted for deprotonation by H225 in order to hydrolyze the tetrahedral intermediate between the ligand and S106. Thus, the enzyme is regenerated and the product is released. After hydrolysis, the new hydroxyl group forms a polar interaction with the Nε2 of H225.

The caffeic acid moiety of chlorogenic acid adopts a similar position to and interaction with the catalytic pocket as ferulic acid. However, caffeic acid has two hydroxyl groups in the benzyl ring (positions 3 and 4), which interact with the side chain of D138 and Y169 through hydrogen bonding (Figure 4-13D and 4-16D). These differences between enzyme and substrate interaction explain the differences in the turnover number previously reported (chlorogenic acid K_{cat} = 28.1 s^{-1}; ethyl ferulate K_{cat} = 7.9 s^{-1}) (Lai *et al*., 2009).

The size of the binding pocket as revealed in the crystal structure helps explain the results of a previous study showing that LJ0536 has lower substrate affinity (based on K_m) with 1 / 2-naphthyl acetate compared to 1 / 2-naphthyl propionate and butyrate (1-Naphthyl-acetate: 0.298 $\pm$ 0.03 mM. 1-Naphthyl propionate: 0.162 $\pm$ 0.01 mM. 1-Naphthyl butyrate: 0.150 $\pm$ 0.01 mM. 2-Naphthyl acetate: 0.897 $\pm$ 0.22 mM. 2-Naphthyl propionate: 0.225 $\pm$ 0.02 mM. 2-Naphthyl butyrate: 0.222 $\pm$ 0.01 mM) (Lai *et al*., 2009).

It is possible that the size of acetate is not long enough to exploit the binding pocket for interactions.

Site-Directed Mutagenesis of the Inserted α / β Domain Demonstrates a Role in Substrate Preference

The analysis of the catalytic site of LJ0536 indicated that the inserted α / β domain from P131 to Q184 could be important for substrate binding. I hypothesized that the inserted α / β domain is critical for holding the phenolic ring of the phenolic esters in the correct position for catalysis, but it has a less important role when aliphatic esters are used as the enzyme substrate. The hypothesis was assessed by introducing a dramatic change to the enzyme by expressing a deletion mutant of the inserted α / β domain (ΔCAP). ΔCAP showed low activity when 4-nitrophenyl butyrate was used as the model substrate. In contrast, no activity was detected with any of the phenolic esters (ethyl ferulate, chlorogenic acid, and rosmarinic acid), even when excessive amounts of enzyme (50 $\mu g \cdot mL^{-1}$) were used in the reaction mixtures and the release of products was analyzed using HPLC. A deeper analysis of site-directed mutants confirmed the importance of the inserted α / β domain in phenolic ester catalysis (Table 2, Figure 4-10). Among these mutants, D138A and Q145A had the highest impact on the enzymatic activity. A direct comparison using four different substrates at a fixed concentration (0.1 mM) indicated that D138A and Q145A showed 73.1 $\pm$ 2.8% and 87.6 $\pm$ 0.3% of percentage activity respectively on 4-nitrophenyl butyrate (Figure 4-10A). The activity of these mutants dropped to less than 10% activity when caffeic acid esters (chlorogenic acid and rosmarinic acid) were used as substrates (Figure 4-10C and D). Interestingly, the mutant Q145A retained 21.7 $\pm$ 2.8% of percentage activity when ethyl ferulate was used as the substrate (Figure 4-10B). These results suggested that the residues D138

and Q145 play a role in interactions and/or restricting access to the binding pocket for caffeic and feruloyl esters, but not for nitrophenyl-based esters. A possible explanation could be that the orientation of the ester bond in 4-nitrophenyl butyrate is such that to maintain proper orientation in the binding site for catalysis, the substrate would need to be oriented with the 4-nitrophenol moiety bound in the other pocket of the boomerang-shaped binding canal. This hypothesis would have to be tested by mutation, such as to T40 or H105. Other random mutation (T148A, N150A, and D152A) were also created (Figure 4-9B) to test the sensitive of the inserted α / β domain. Even though the enzyme activity of T148A and N150A were severly impaired (Table 4-2, Figure 4-10), there are no functional roles of these residues can be seen in crystal structural analysis. The only explanation is that the mutation caused a change in the architecture of inserted α / β domain which affected the binding cavity. D152A achieved even a higher enzyme activity when compared to wild type LJ0536 (Table 4-2, Figure 4-10). It could be the result of D152A caused a local realignment of the inserted α / β domain and improve the binding affinity. These results together with the crystallographic data indicated that D138 and Q145 from the inserted α / β domain are important in recognizing the caffeic and ferruloyl esters.

Comparisons of LJ0536 and Proteins with Similar Folding

A structural similarity search using the Dali Database (Holm & Rosenström, 2010) identified many proteins with structural homology to LJ0536 with a range of primary sequence identities between 17% and 32%. The top matches were Est1E from *B. proteoclasticus* (PDB: 2WTM) (Goldstone *et al*., 2010), human mono-glyceride lipase (PDB: 3JW8 and 3HJU) (Bertrand *et al.*, 2010), bromoperoxidase A1 from *Streptomyces aureofaciens* (PDB 1A8Q) (Hofmann *et al.*, 1998), human valacyclovir

hydrolase VACVase (PDB: 2OCG) (Lai *et al*., 2008), and aryl esterase from *Pseudomonas fluorescens* (PDB: 3HI4) (Yin *et al.*, 2010).

Superposition of these structures showed that the enzymes are highly similar in their architecture of general folding, but there is variation in the inserted domains (Figure 4-17). Only Est1E shows a highly identical structure with LJ0536. However, the inserted domains from the other structural homologs have different secondary structures, even though the architecture of the central core of the enzymes is highly identical. These inserted domains are formed by α-helices, which differ from the inserts of LJ0536 and Est1E that are composed of both α-helices and β-sheets.

However, even with the same secondary structure, the specific features of the inserted domain promote different substrate binding mechanism. The overall structural features of *L. johnsonii* cinnamoyl esterase LJ0536 resemble those recently described in Est1E, a predominant esterase encoded in the genome of *Butyrivivrio proteoclasticu*s (Goldstone *et al*., 2010). However, the specific structural differences in the architecture of the catalytic pocket promote different substrate binding preferences. The differences in the catalytic pocket scaffolds become evident when both protein structures are superimposed. The protruding hairpins of LJ0536 at the entrance of the catalytic groove are slightly shifted (2.30 Å and 1.85 Å) with respect to Est1E. The inserted α / β domain of LJ0536 adopts a rigid structure as the same conformations are seen in the apo and ligand-bound structures. In contrast, Est1E adopts a conformational change upon substrate binding (Goldstone *et al*., 2010). The specific binding features of Est1E are based on the rotation of W160 which is located on the second protruding hairpin of the inserted α / β domain. This corresponds to the hairpin formed between β_9 and β_{10} in

LJ0536. The protruding hairpins of Est1E shift when ligand is bound to the catalytic site. W160 flips and creates a small hydrophobic cavity for binding of the substrate. The dynamic flipping mechanism of W160 is not present in LJ0536. F160 of LJ0536 corresponds to W160 of Est1E. It adopts the same conformation in apo and each of the ligand-bound complexes. Instead, LJ0536 forms a bridge-like structure created by Q145 in both apo and ligand bound structure to hold the substrate in the catalytic cavity. L44 of Est1E forms a hydrogen bond to the 4-hydroxyl group on the aromatic ring of ferulic acid. L144 of Est1E corresponds to Q145 of LJ0536. Instead, hydrogen bonds are formed between D138 and Y169 to the hydroxyl groups on the aromatic ring of ferulic acid and caffeic acid in case of LJ0536.

Structural variation in the inserted α / β domain is reflected in substrate preferences. Due to its its activity on feruloyl esters, Est1E is indeed a closely related enzyme to LJ0536 (Goldstone *et al*., 2010). Thus the inserted domain of LJ0536 and Est1E are highly identical (Figure 4-18A, B, D, and E). Using VACVase as another example, the inserted domain is comprised of four α-helices (Figure 4-18C and F). An optimal superimposition of LJ0536 and VACVase was found when the inserted domains were excluded, and only the central cores of the enzymes were compared. VACVase is a biphenyl hydrolase-like protein which is produced in large amounts in the liver. It is involved in prodrug activation and was originally identified from human breast carcinoma. This enzyme was also detected in Caco-2 cells as well as in the intestinal mucosa (Lai *et al*., 2008; Kim *et al.*, 2003). Since VACVase shows a similar architecture of the central core to LJ0536, it could potentially share similar enzyme activity and contribute to phenolic ester hydrolysis in human intestine. Unlike most of the esterases,

VACVase demonstrated a high specificity for amino acid esters (Lai *et al*., 2008). VACVase was purified (Figure 4-9C) and its enzyme activity was compared in parallel with LJ0536 to assess their substrate preferences. VACVase was only active with valacyclovir and L-amino acid benzyl esters; it was not active towards 4-nitrophenyl esters, ethyl ferulate, chlorogenic acid, or rosmarinic acid. Despite the fact that LJ0536 has a large range of catalytic specificity, no activities were detected when valacyclovir and L-amino acid benzyl esters were used as enzyme substrates. Although the overall enzyme structures are similar, the substrate preferences of these enzymes are completely different. These results further suggest the architecture of the inserted α / β domain of esterases plays a critical role in substrate specificity.

Summary

The proteins LJ0536 and LJ1228 purified and biochemically characterized from Chapter 3 were successfully crystallized. There were no significant structural differences between LJ0536 and LJ1228. It is expected that both enzymes share identical substrate binding mechanism as the critical amino acid residues discussed herein for LJ0536 are also conserved in LJ1228. Thus, only LJ0536 was used for deep analysis. All the structures generated in this work were deposited in the PDB database.

The α / β domain, inserted as an accessory of the canonical α / β fold structure, is relevant to the shape of the catalytic pocket of the enzyme studied. LJ0536 showed clear differences with the previously published enzyme EstE1. The inserted α / β domain of EstE1 is flexible, and the hydrophobic catalytic pocket is “formed” once the protein adopts the open conformation to bind the substrate. Instead, the LJ0536 inserted α / β domain is a rigid structure present both in the apo-enzyme and when it is in complex with the substrate. Several enzymes involved in the catalysis of a variety of

substrates display similar central core architecture. Interestingly, the major variations are observed in the inserted domains. The specific features of the inserted domain contribute to the substrate binding.

In term of substrates binding, the biggest difference between the enzymes herein studied and the esterases of fungal origin is related to the architecture of the catalytic pocket as well as substrate binding. The *Aspergillus niger* AnFaeA (PDB: 2BJH) pocket (Hermoso *et al*., 2004) is a narrow open cleft formed by a small loop of 13 amino acids and a short α helix. The ferulic acid is wedged between the two walls of the crevice. The hydrophobicity which stabilizes the aromatic ring of ferulic acid is contributed by the amino acids on one of the walls; the methoxy group that decorates the benzyl ring of ferulic acid is oriented toward a small cavity composed of polar amino acids. These structures clearly differ from the inserted α / β domain of LJ0536. The full comparison of LJ0536 and AnFaeA is discussed in Chapter 5.

Table 4-1. Statistics of X-ray diffraction and structure determination

PDB code	3PF8	3PF9	3S2Z	3PFB	3QM1	3PFC
Enzyme	LJ0536 (wild-type)	LJ0536 S106A	LJ0536 S106A	LJ0536 S106A	LJ0536 S106A	LJ0536 S106A
Ligands	None	None	Caffeic acid (from soak of chlorogenic acid)	Ethyl ferulate, Form I	Ethyl ferulate, Form II	Ferulic acid
Data collection						
Wavelength (Å)	*Cu-Kα* 1.54178	*Cu-Kα* 1.54178	*Cu-Kα* 1.54178	*Cu-Kα* 1.54178	*Cu-Kα* 1.54178	*Cu-Kα* 1.54178
Resolution (Å)	50.0 – 2.35	50.0 – 1.75	50.0 – 1.75	50.0 – 10.0.58	23.80 – 1.82	50.0 – 1.75
Space group	$R3_2$	$C222_1$	C2	C2	$C222_1$	$C222_1$
Cell dimensions						
a, b, c (Å)	149.9, 149.9, 130.3	72.7, 85.7, 81.9	72.3, 84.2, 87.6	72.3, 83.9, 88.9	71.9, 85.4, 81.1	72.0, 85.4, 81.0
a, b, g (°)	90, 90, 120	90, 90, 90	90, 97.6, 90	90, 98.2, 90	90, 90, 90	90, 90, 90
Number of observed reflections	143192	140545	208914	101781	139955	146324
Number of unique reflections	23389	26002	51281	46265	22853	25396
R_{sym}	0.105 (0.442)[a]	0.057 (0.460)[b]	0.047 (0.462)[c]	0.046 (0.260)[d]	0.048 (0.327)[e]	0.058 (0.484)[f]
I / σI	13.44 (4.81)	37.87 (3.75)	21.86 (2.57)	31.21 (3.09)	27.56 (3.18)	22.20 (2.88)
Completeness (%)	99.0 (100.0)	99.1 (96.1)	99.7 (97.6)	73.1 (21.6)	100 (99.9)	99.5 (94.0)
Redundancy	6.1 (5.5)	5.4 (4.1)	4.1 (3.3)	2.0 (1.3)	6.1 (4.8)	5.8 (5.1)
Refinement						
Programs	Refmac, PHENIX, BUSTER	Refmac	Refmac	PHENIX, Refmac	PHENIX	PHENIX
Resolution (Å)	31.49 – 2.34	50.0 – 1.75	50.0 – 1.76	44.20 – 1.58	23.07 – 1.82	17.65 – 1.75
Number of reflections: working, test	22192, 1194	23365, 1310	48659, 2615	47130, 2673	21234, 1119	23466, 1237
R_{work} / $R_{free,\ 5\%}$	22.3/29.9 (27.3/36.5)	14.1/19.9 (23.6/30.7)	14.3/20.8 (19.0/28.2)	21.1/30.4 (30.2/36.2)	14.7/19.1 (22.8/26.7)	14.7/17.9 (23.6/26.1)
No. atoms						
Protein	3836	1988	3935	3939	1991	1964
Ligands	N/A	N/A	26	32	16	14
Solvent	3	4	16	20	61	17
Water	146	275	432	907	173	224
Average *B*-factors						
Protein	56.7	29.9	33.9	23.6	19.4	22.9
Ligand	N/A	N/A	35.9	33.0	19.1	21.8
Solvent	39.2	41.9	58.0	26.0	55.9	49.4
Water	44.9	43.3	46.7	39.2	31.5	24.4
R.m.s. deviations						
Bond lengths (Å)	0.010	0.025	0.023	0.021	0.016	0.016
Bond angles (°)	1.23	1.843	1.812	1.933	1.710	1.611
Ramachandran analysis						
Most favoured (%)	86.4	89.1	89.3	88.4	90.8	90.7
Additionally favoured (%)	12.0	9.5	9.1	10.0	7.3	7.9
Generously favoured (%)	0.9	0.5	1.1	1.1	1.4	1.4
Disallowed (%)	0.7	0.9	0.5	0.5	0.5	0

[a]Values in brackets refer to the highest resolution shell of 2.39 – 2.35 Å
[b]Values in brackets refer to the highest resolution shell of 1.78 – 1.75 Å
[c]Values in brackets refer to the highest resolution shell of 1.78 – 1.75 Å
[d]Values in brackets refer to the highest resolution shell of 1.61 – 1.58 Å
[e]Values in brackets refer to the highest resolution shell of 1.85 – 1.82 Å
[f]Values in brackets refer to the highest resolution shell of 1.78 – 1.75 Å

Table 4-2. Saturation kinetic parameters of LJ0536 variants

Mutants	V_{max} (μmol · mg^{-1} · min^{-1})	K_m (mM)	k_{cat} (s^{-1})	K_{cat} / K_m (M^{-1} · s^{-1})
H32A	0.09 ± 0.02	0.13 ± 0.08	0.04	3.18 E+02
D61A	n.d.	n.d.	0.00	n.d.
S68A	0.47 ± 0.04	0.08 ± 0.02	0.22	2.70 E+02
D83A	n.d.	n.d.	n.d.	n.d.
S106A	n.d.	n.d.	n.d.	n.d.
D121A	0.97 ± 0.06	0.20 ± 0.03	0.45	2.23 E+03
D138A	1.23 ± 0.08	0.22 ± 0.03	0.57	2.57 E+03
Q145A	2.05 ± 0.10	0.29 ± 0.04	0.94	3.25 E+03
T148A	2.15 ± 0.15	0.14 ± 0.02	0.99	7.06 E+03
N150A	0.62 ± 0.03	0.14 ± 0.01	0.28	2.03 E+03
D152A	4.27 ± 0.30	0.08 ± 0.01	1.96	2.45 E+04
D197A	0.00 ± 0.00	0.19 ± 0.06	0.00	0.00 E+00
H218A	3.64 ± 0.05	0.07 ± 0.06	1.67	2.39 E+04
H225A	0.65 ± 0.06	0.19 ± 0.04	0.30	1.57 E+03
ΔCAP	0.28 ± 0.03	0.65 ± 0.12	0.13	1.98 E+02
WT	3.34 ± 0.15	0.16 ± 0.02	1.53	9.59 E+03

n.d.: note detected.

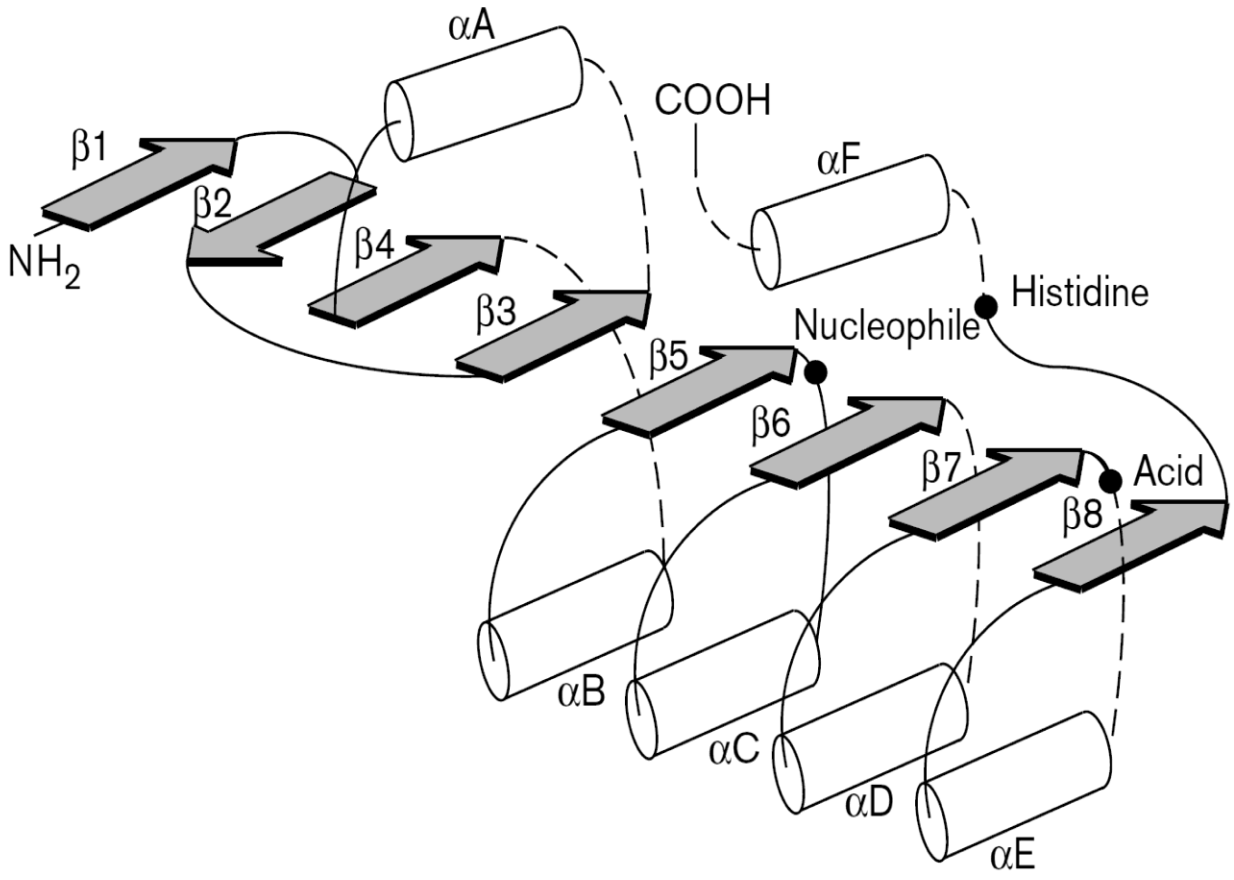

Figure 4-1. General secondary structure of α / β fold. α-helices, β-strands, and catalytic triad location are represented by white barrel, gray arrows, and black dots, respectively. Solid lines represent random coils. Dashed lines indicate possible locations of inserted domains.[1]

[1] Reprinted with permission from Nardini, M. & B. W. Dijkstra, (1999) [alpha]/[beta] Hydrolase fold enzymes: the family keeps growing. *Curr Opin Struct Biol* **9**: 732-737.

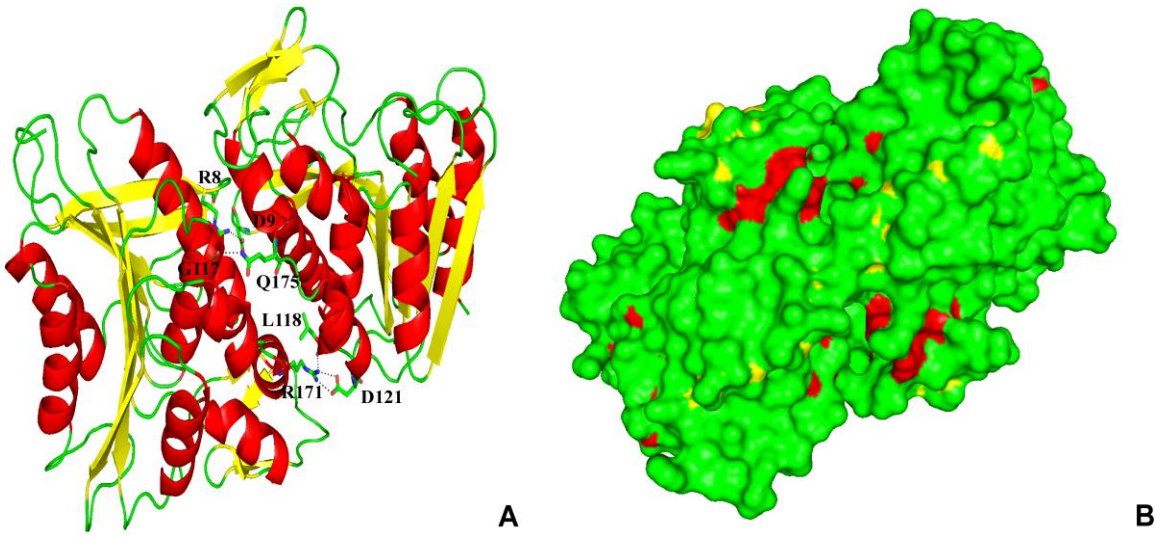

Figure 4-2. Representation of the overall LJ0536 structure. (A) Ribbon diagram showing LJ0536 dimer. The residues connecting the monomers are shown in the interface of the two molecules. (B) Surface Illustration of the native protein. α-helices are colored red. β-sheets are colored yellow. Random coils are colored green.

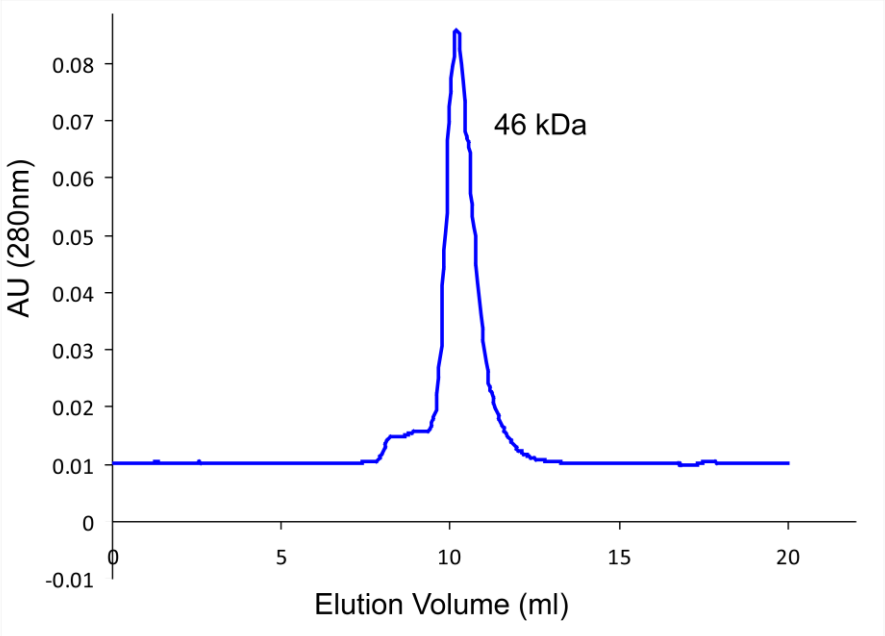

Figure 4-3. Determination of the native molecular weight of the enzyme by gel filtration assays. The figure displays the molecular weight of the wild type protein LJ0536. The assay was carried out using a Superose 12 10 / 300 GL column in a Pharmacia FPLC System according to the protocol described in Materials and Methods. The native molecular weight determined was 46 ± 3.2 KDa.

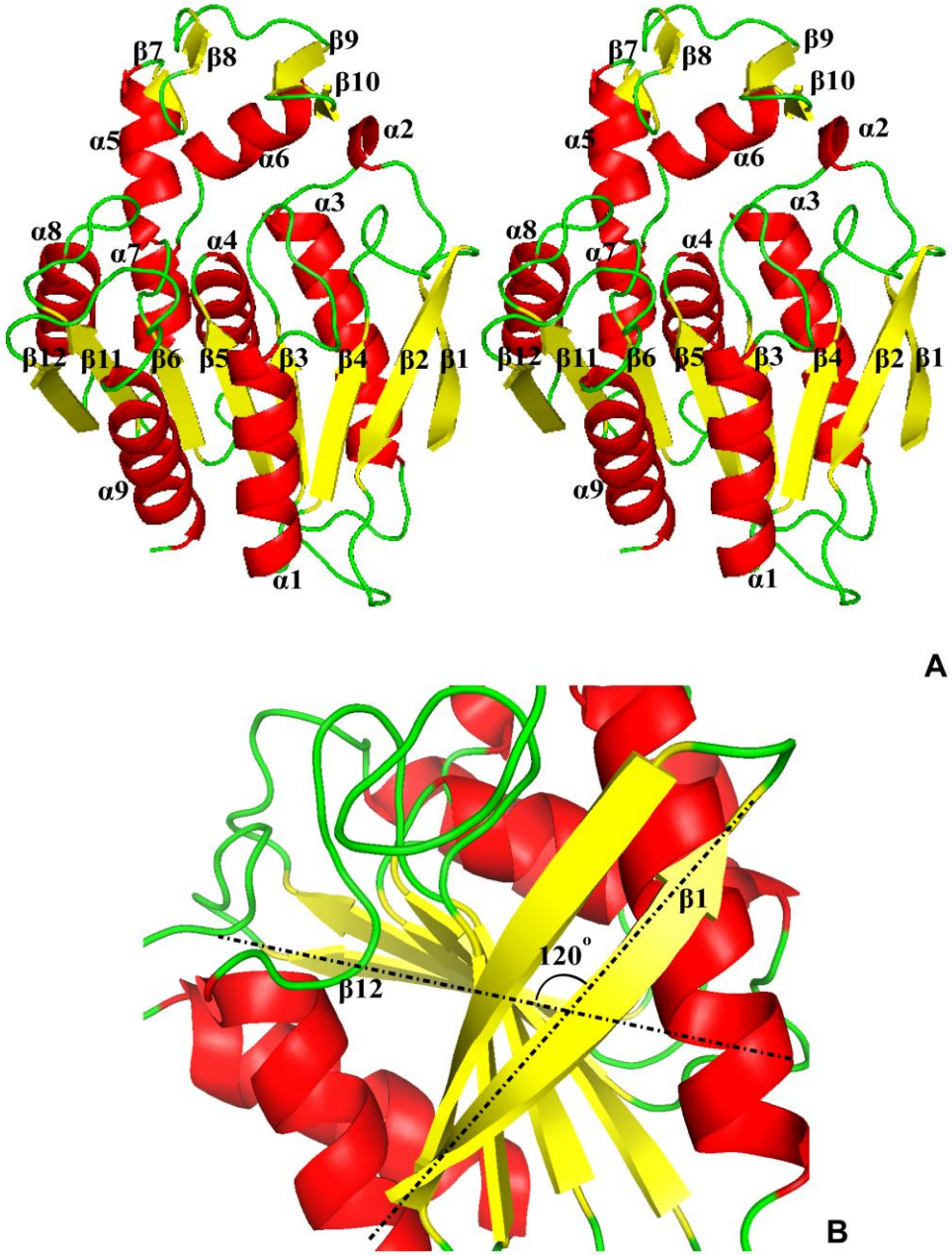

Figure 4-4. Representation of the single chain LJ0536 structure. (A) Ribbon representation of LJ0536 monomer structure (stereo view). (B) Details of the left hand superhelical twist of the central β-sheet core. α-helices are colored red. β-sheets are colored yellow. Random coils are colored green.

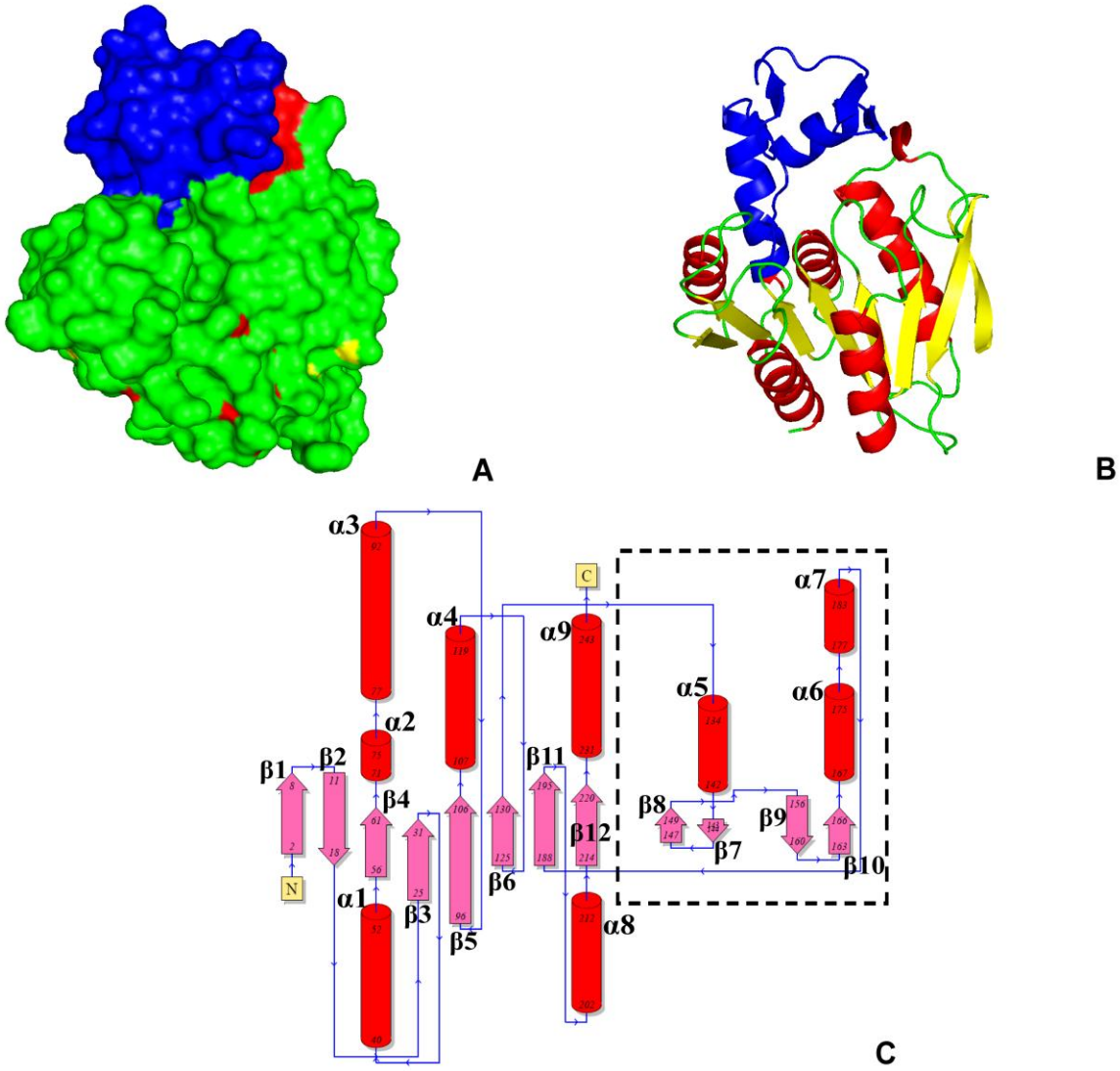

Figure 4-5. Details of α / β inserted domain in the LJ0536 structure. (A) Surface representation and (B) ribbon representation of the LJ0536 (monomer). (C) Topology diagram of the monomer structure. The diagram was generated using PDBsum software (Laskowski, 2009). The box depicted with dotted lines indicates the inserted α / β domain. The inserted α / β domain is colored blue. α-helices are colored red. β-sheets are colored yellow. Random coils are colored green.

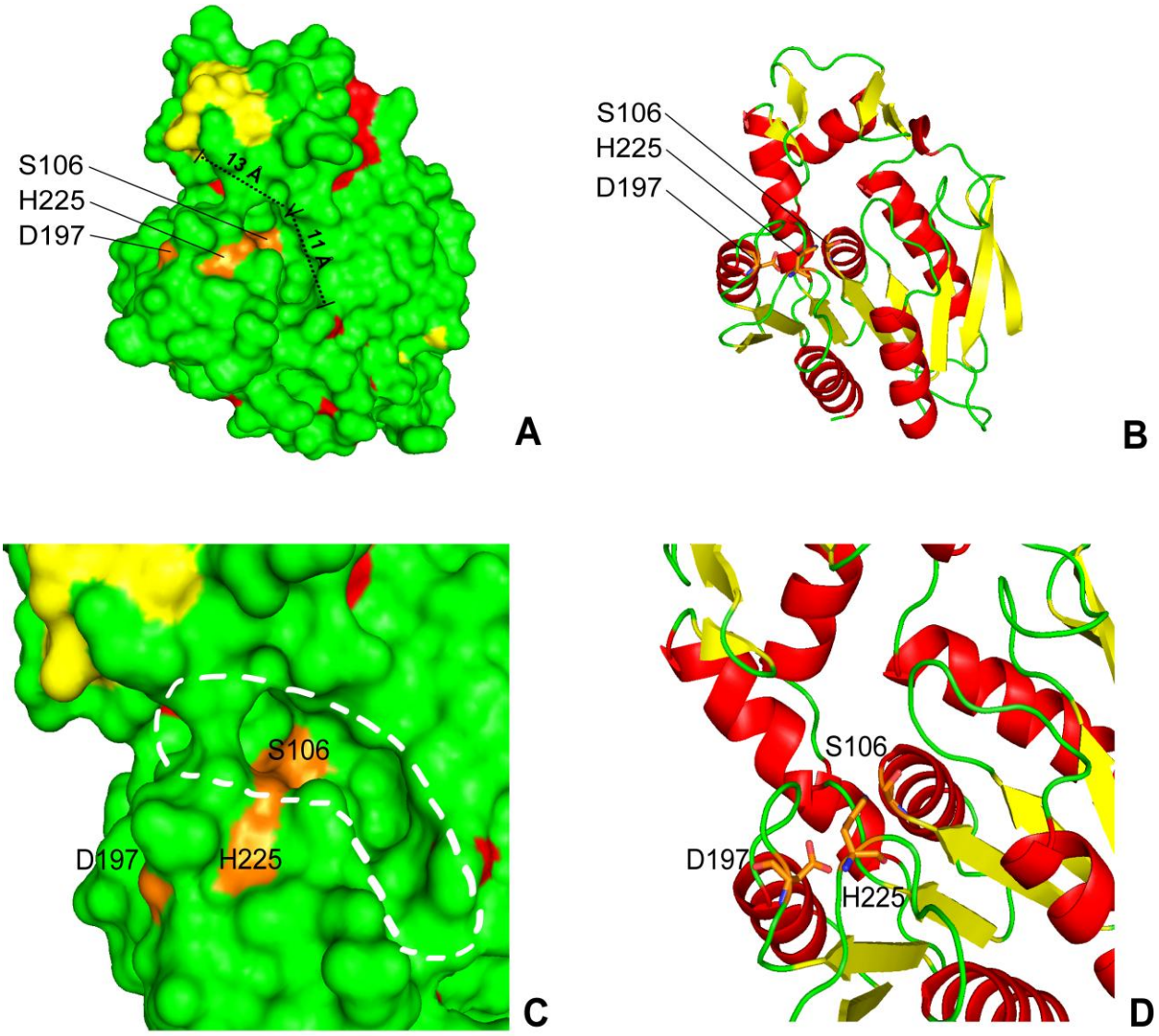

Figure 4-6. Surface and ribbon representation of LJ0536 catalytic site. (A) Surface representation of single chain LJ0536 with the binding cavity located in the middle. (B) Ribbon diagram of single chain LJ0536. The figure has the same magnification used in the panel A for direct comparison. (C) A close surface view of binding cavity of LJ0536. The boomerang-like shape of the binding cavity is indicated with dashed lines. (D) A close cartoon view of binding cavity of LJ0536. The figure has the same magnification used in the panel C for direct comparison. Catalytic triad is composed of S106, H225, and D197. Catalytic residues are colored orange. α-helices are colored red. β-sheets are colored yellow. Random coils are colored green.

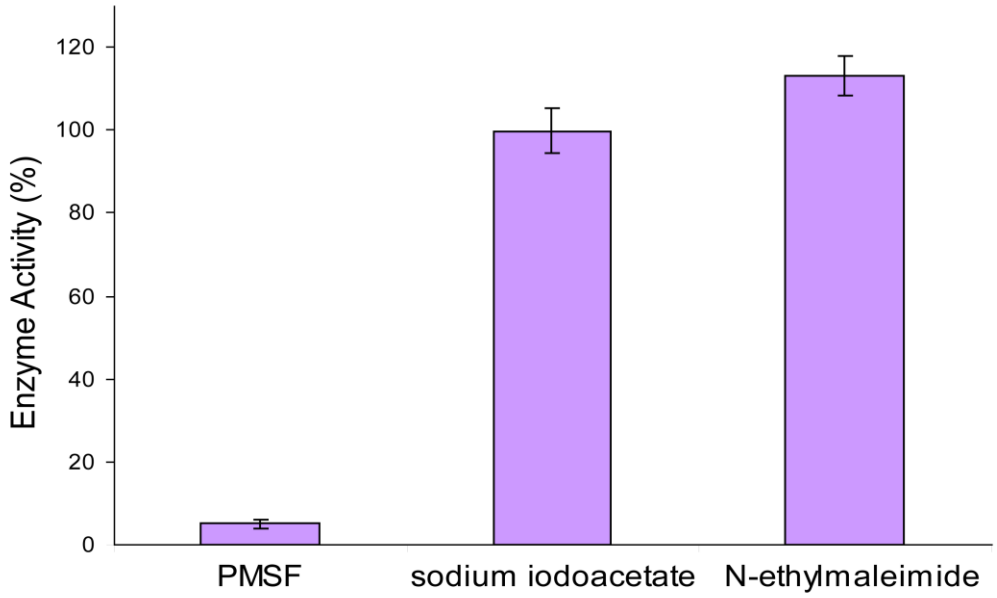

Figure 4-7. Enzyme activity in presence of specific inhibitors. The activity of LJ0536 was inhibited with 1 mM PMSF. No effects were observed with 1 mM sodium iodoacetate or N-ethylmaleimide. The results confirmed that LJ0536 is a serine esterase. The assay was carried out using 4-nitrophenyl butyrate as enzyme substrate in buffer HEPES pH 7.8, 25^{o}C.

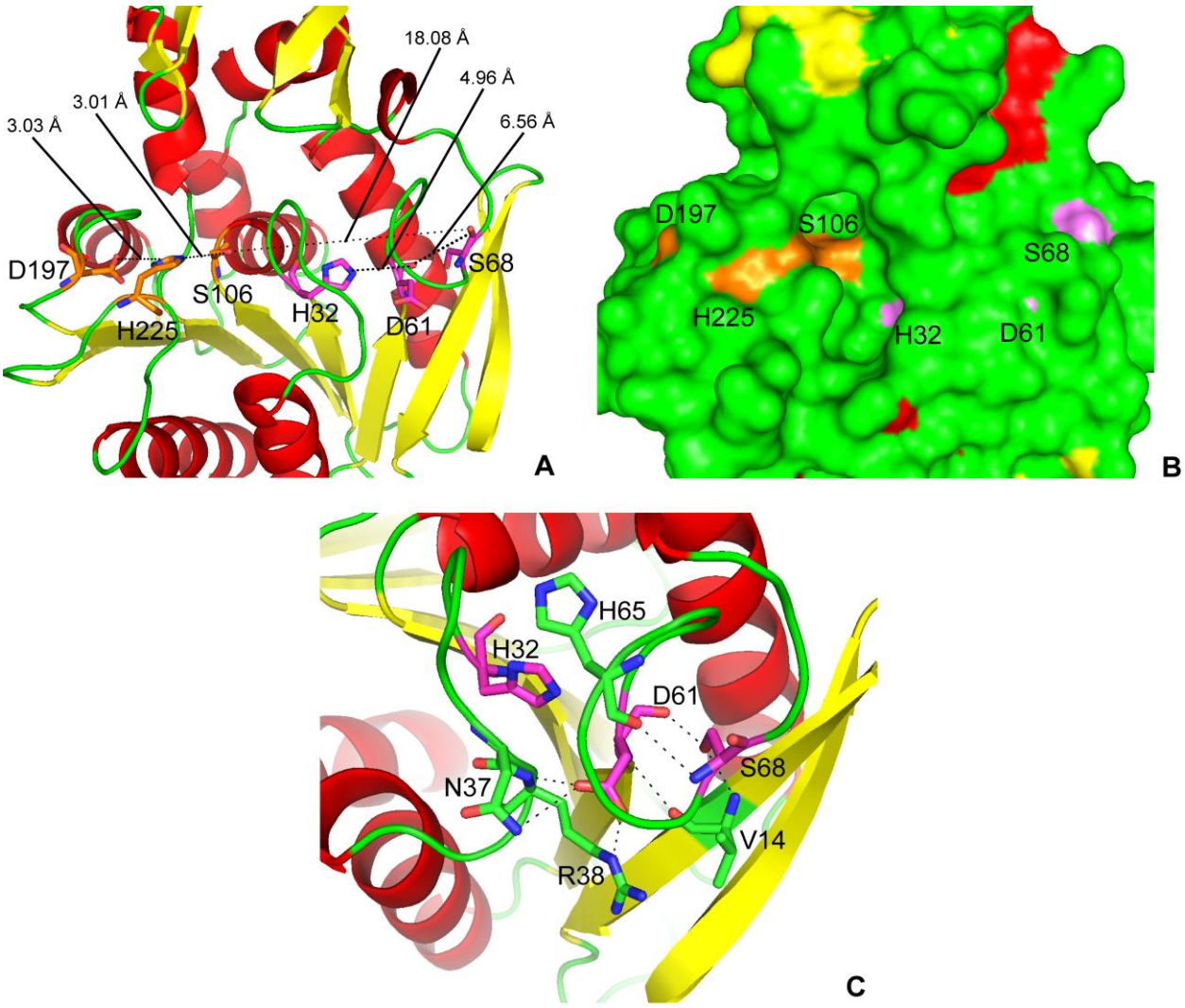

Figure 4-8. Identification of the two GXSXG motifs in the overall LJ0536 structure. (A) Ribbon representation showing the distance between the two serine residues S106 and S68. (B) The surface representation indicates the absence of catalytic pockets associated to S68. (C) S68 forms hydrogen bonds to D61, H65, and V14 located on one of the central β-strand. D61 forms hydrogen bonds with S68, R38, and N37. These extensively hydrogen bond formation could contribute to maintain proper folding of the enzyme. Catalytic triad (S106, H225, D197) is colored orange. Putative triad (S68, H32, D61) is depicted in purple color. α-helices are colored red. β-sheets are colored yellow. Random coils are colored green. Dotted lines indicate distance between residues in panel A or hydrogen bonds in panel C.

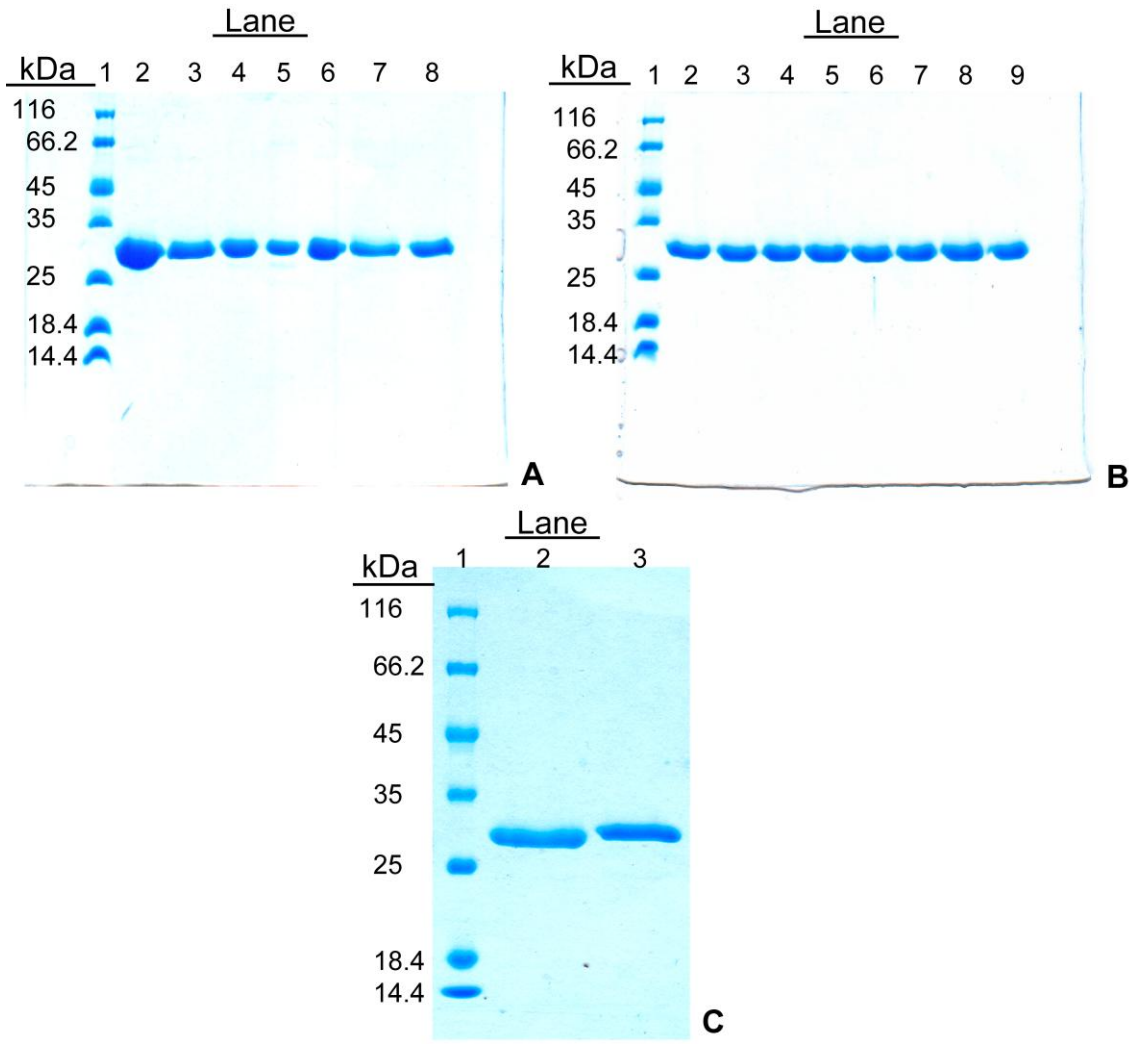

Figure 4-9. SDS-PAGE. The pictures show the purified LJ0536 wild type together with the LJ0536 mutants obtained from site-directed mutagenesis. (A) Lane 1: EZrun molecular weight marker. Lane 2: wild type LJ0536. Lane 3: H32A. Lane 4: D61A. Lane 5: S68A. Lane 6: D83A. Lane 7: S106A. Lane 8: D121A. (B) Lane 1: EZrun molecular weight marker. Lane 2: D138A. Lane 3: Q145A. Lane 4: T148A. Lane 5: N150A. Lane 6: D152A. Lane 7: D197A. Lane 8: H218A. Lane 9: H225A. C) Lane 1: EZrun molecular weight marker. Lane 2: mutant ΔCAP. The inserted α / β domain was deleted from 147 position to 173 position. Lane 3: purified human VACVase.

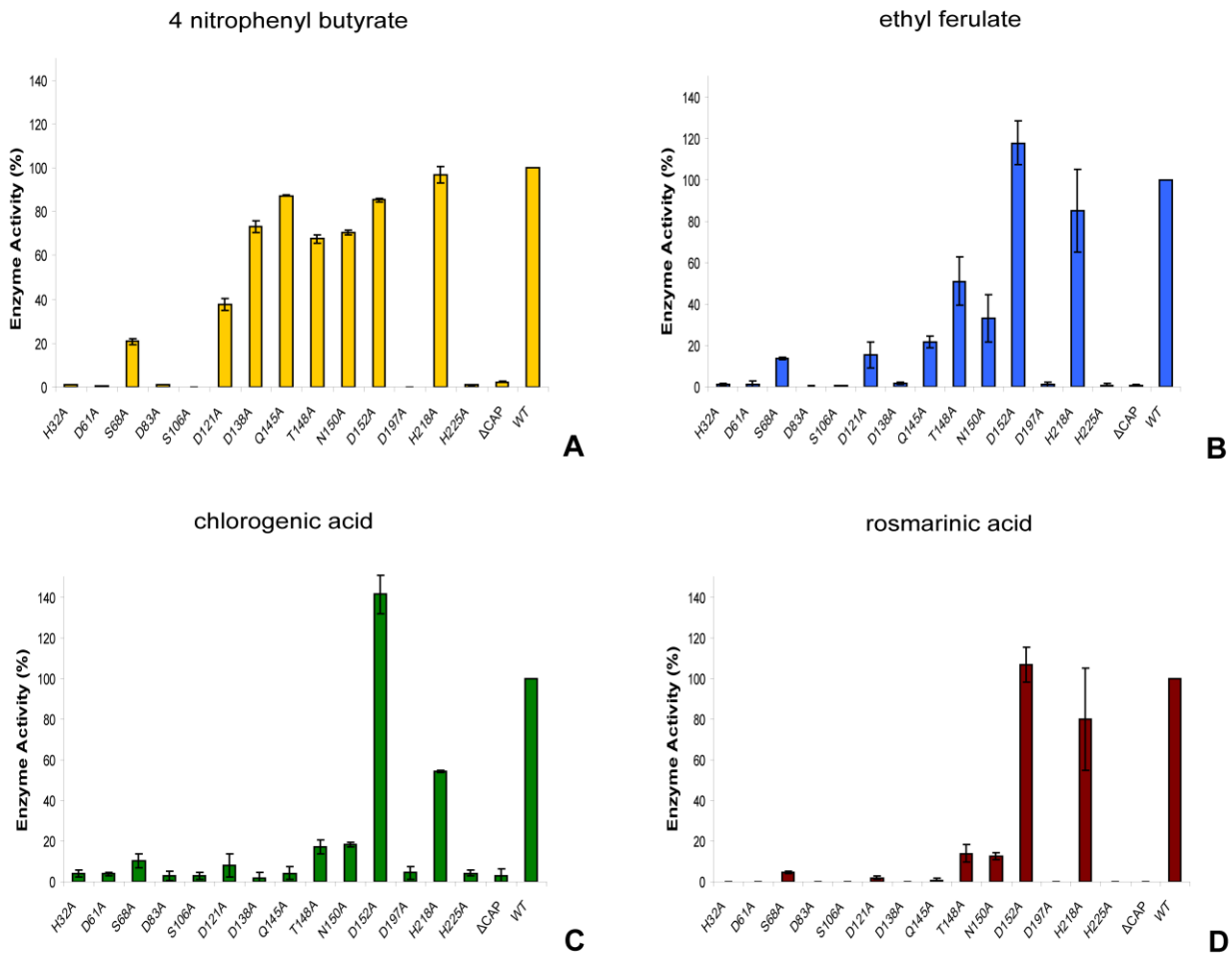

Figure 4-10. Comparative enzymatic activity of LJ0536 variants. The substrates used in each panel were: (A) 0.1 mM 4-nitrophenyl butyrate. (B) 0.1 mM ethyl ferulate. (C) 0.1 mM chlorogenic acid. (D) 0.1 mM rosmarinic acid. The enzymatic assays were carried out using aliphatic and aromatic esters as enzyme substrates. The reaction mixtures consisted of 0.1 mM substrate, 20 mM buffer HEPES pH 7.8, 25^{o}C.

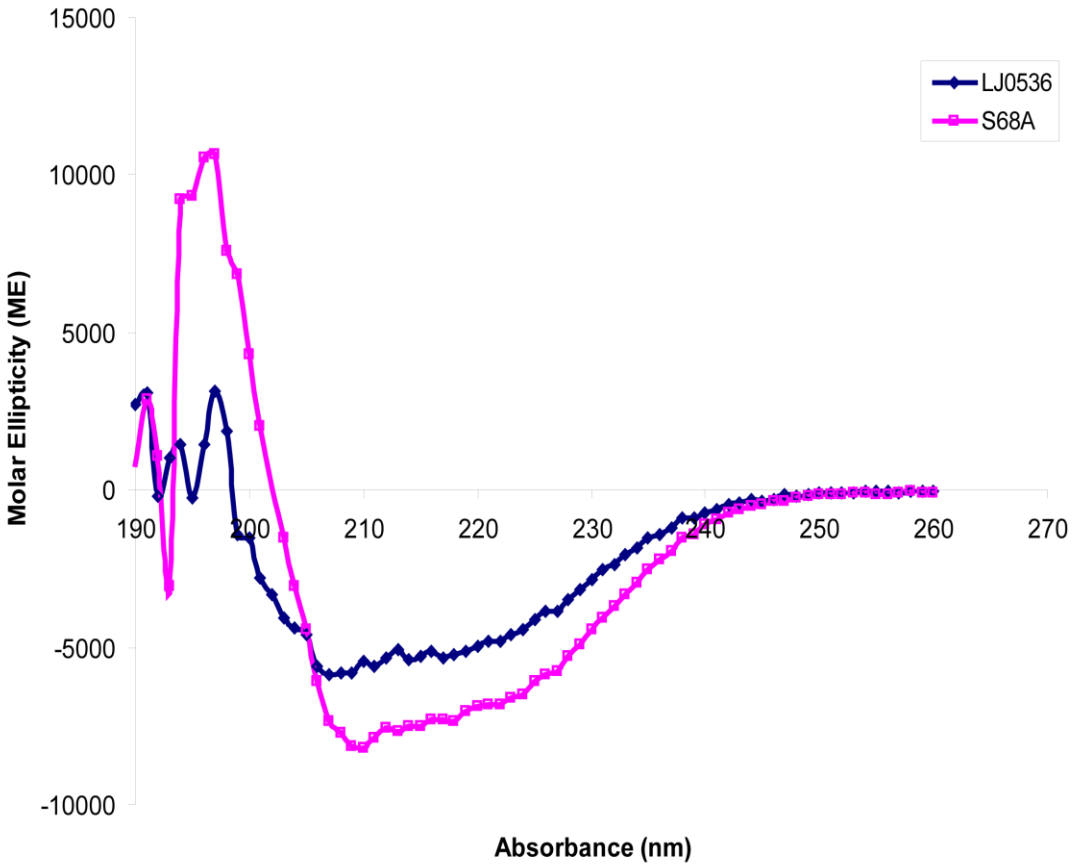

Figure 4-11. Circular dichroism spectra of LJ0536 and mutant S68A. The spectrum displayed by the enzyme changed when S68 was mutated to alanine. The assay supports the important role of S68 to maintain the structure of the central core of the protein. The mutation should have an important impact on the overall folding since the enzyme activity was severely impaired. Molar ellipticity was calculated using Equation 2-4.

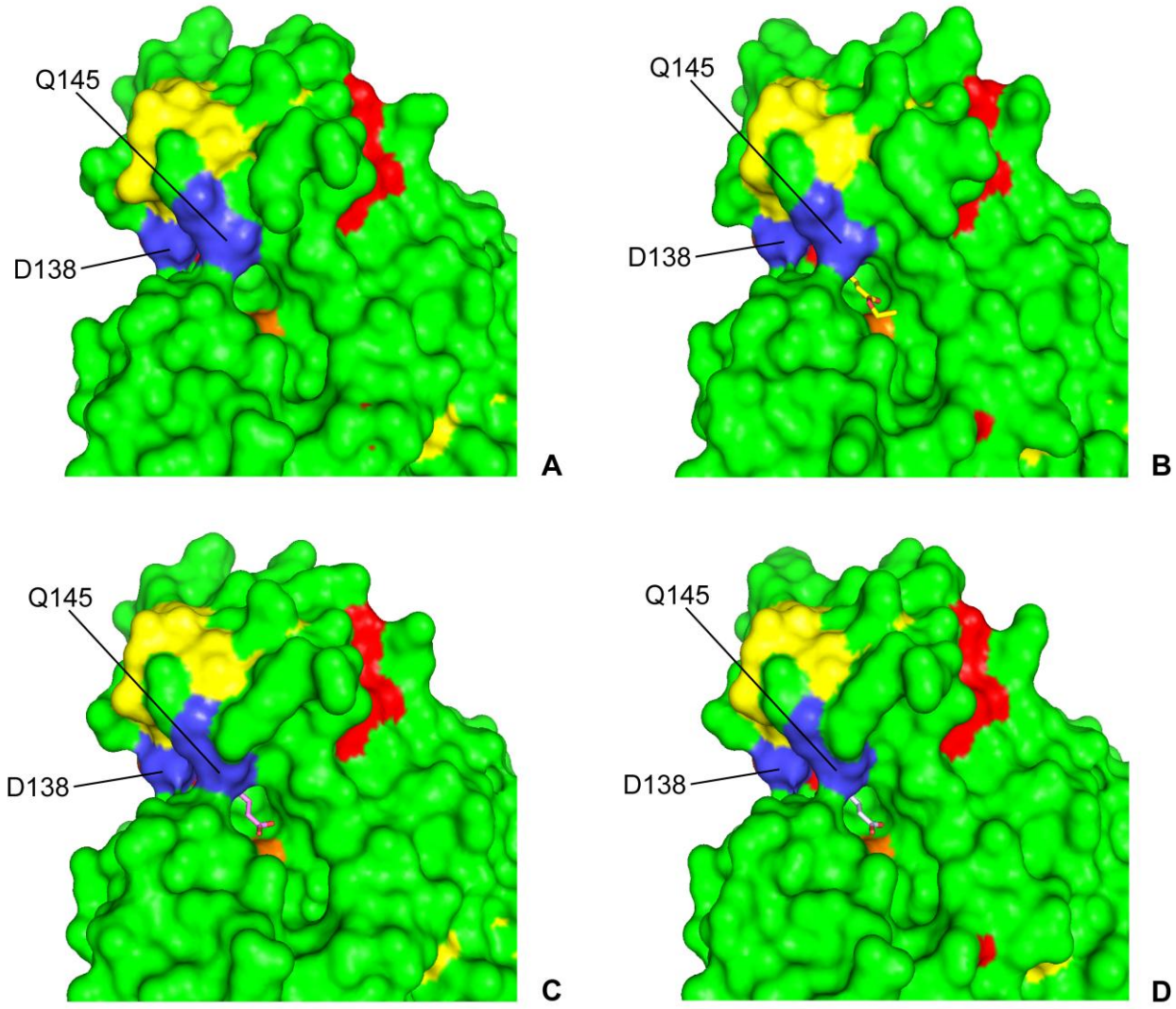

Figure 4-12. Surface representation of apo and co-crystallized structures of LJ0536 mutant S106A. (A) Apo S106A. (B) Mutant S106A co-crystallized with ethyl ferulate. (C) Mutant S106A co-crystallized with ferulic acid. (D) Mutant S106A co-crystallized with chlorogenic acid. Only caffeic acid is shown in the structure since the quinic acid adopted several positions and was not possible to create the model. The random positions adopted by quinic acid indicated minimal or no interactions with the protein surface. α-helices are colored red. β-sheets are colored yellow. Random coils are colored green. Residues involve in aromatic ring binding are colored blue. A106 is colored orange. Ligands are displayed in stick representation.

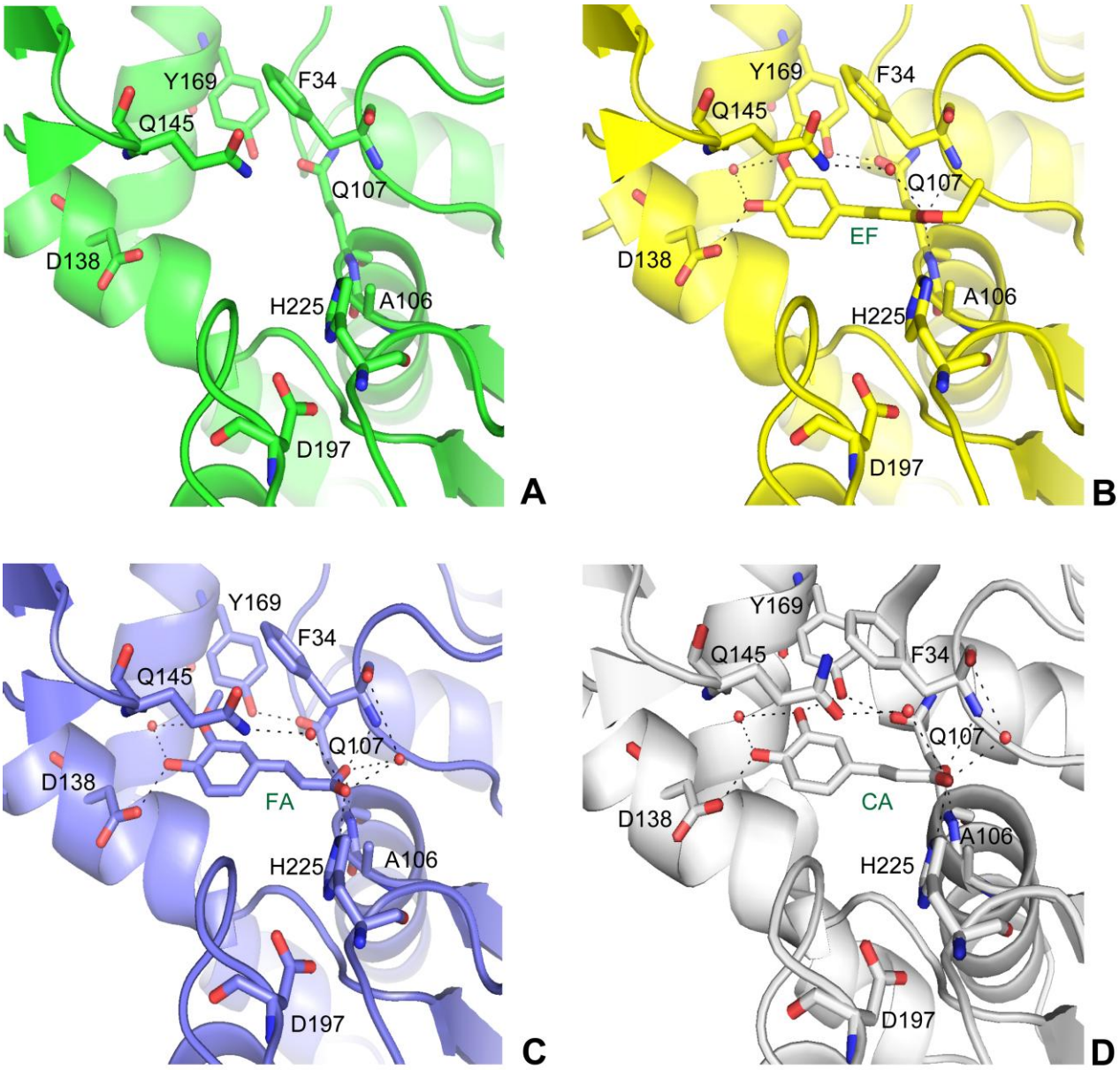

Figure 4-13. Enzyme-substrate interactions within binding cavity of LJ0536. D138 and Y169 form hydrogen bonds with the hydroxyl group of aromatic ring of phytophenols used. These bonds hold the substrates in the correct orientation for catalysis. (A) Apo structure of S106A. (B) Mutant S106A co-crystallized with ethyl ferulate (EF). (C) Mutant S106A co-crystallized with ferulic acid (FA). (D) Mutant S106A co-crystallized with chlorogenic acid. Only caffeic acid (CA) is shown in the diagram. The color of each structure is uniformed in one color for easy interpretation. Red spheres represent water molecules. Dash lines represent polar interactions.

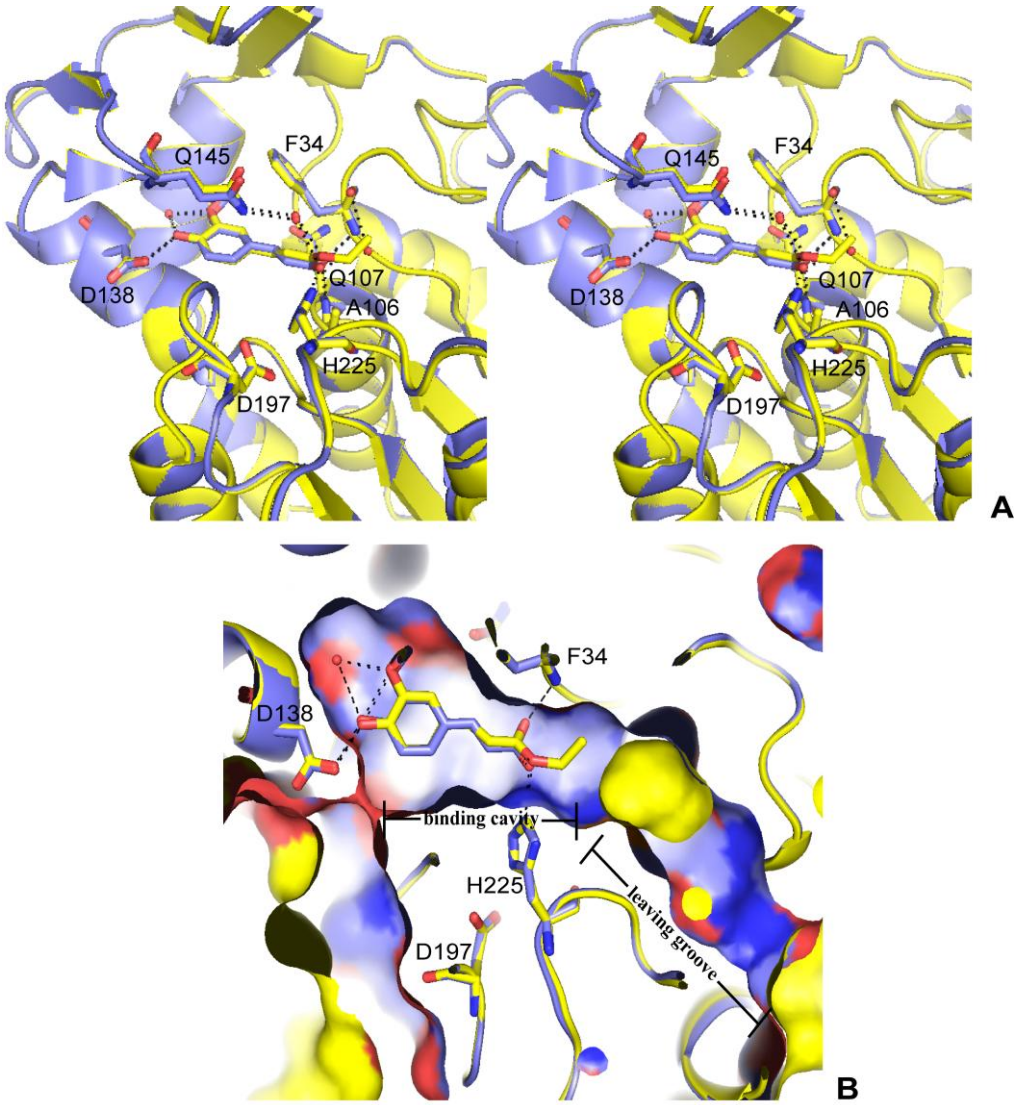

Figure 4-14. Structural superimposition of the mutant S106A co-crystallized with ethyl ferulate or ferulic acid. The mutant S106A co-crystallized with ethyl ferulate is colored yellow. The same protein co-crystallized with ferulic acid is colored blue. (A) The 4-hydroxyl group on the phenolic ring of ferulic acid and ethyl ferulate are hydrogen bonded with D138. These bondings hold the phenolic ring in the binding cavity. The additional polar interactions of 4-hydroxyl and 3-methoxy groups with water molecule further stabilize the binding of substrate. The residue Q145 coordinates a water molecule adjacent to the ester bond of substrate. This water molecule is a good candidate for activating S106 during hydrolysis. The oxyanion hole is formed by F34 and Q107. The structures are shown in stereo view to help the 3-dimensional visualization of the protein backbone. (B) Cutaway view of the mutant S106A surface representation. The image shows the phenolic ring, the binding cavity, and the leaving groove in details. Red spheres represent water molecules. Dash lines represent polar interactions.

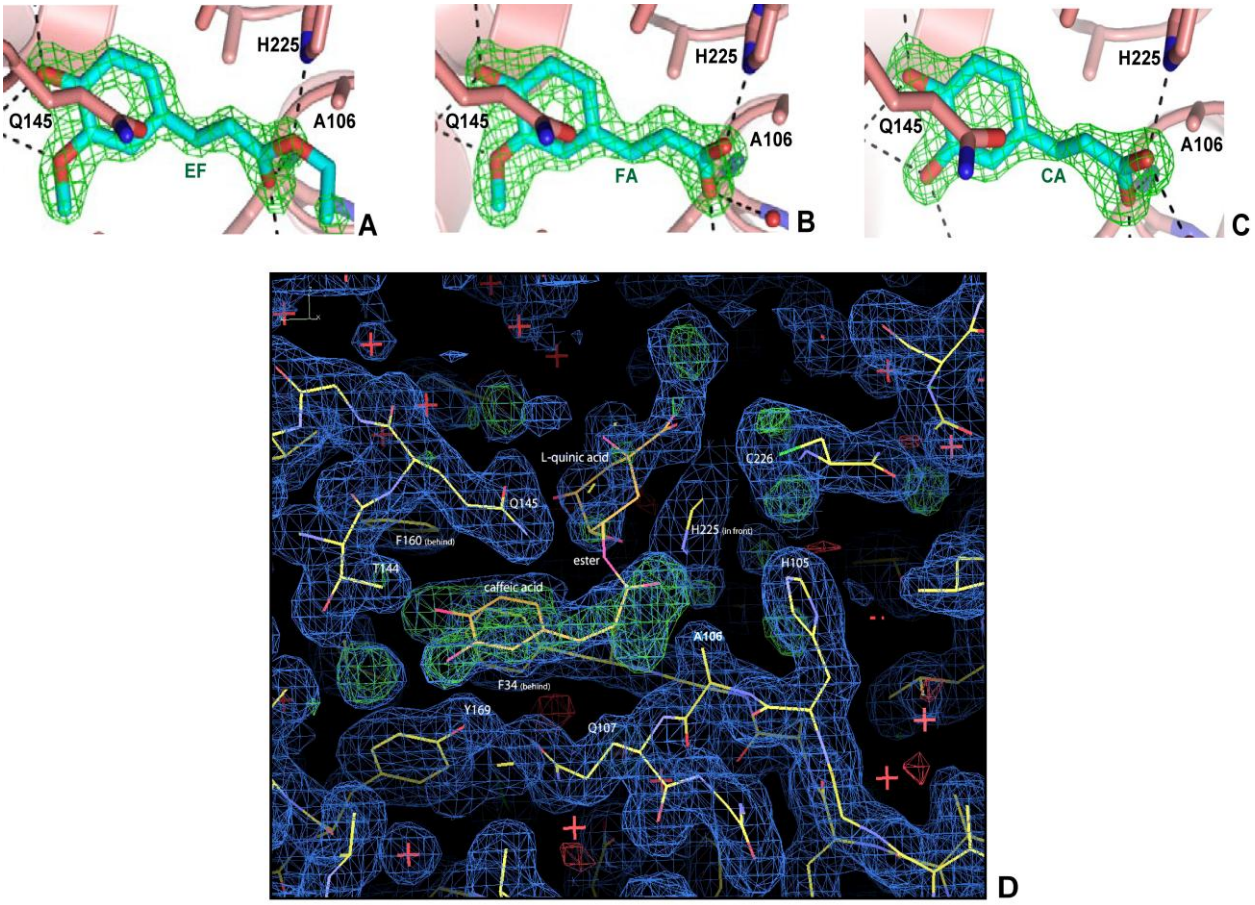

Figure 4-15. Electron density map of co-crystallized substrates. The moieties that are located next to the ester bond (the ethyl group of ethl ferulate, and the quinic acid of the chlorogenic acid) do not acquire full electron density, indicating the lack of interaction with the binding cavity. (A) Ethyl ferulate. (B) Ferulic acid. (C) Caffeic acid from chlorogenic acid. (D) Chlorogenic acid showing the full density of the caffeic acid with poor definition of the quinic acid.

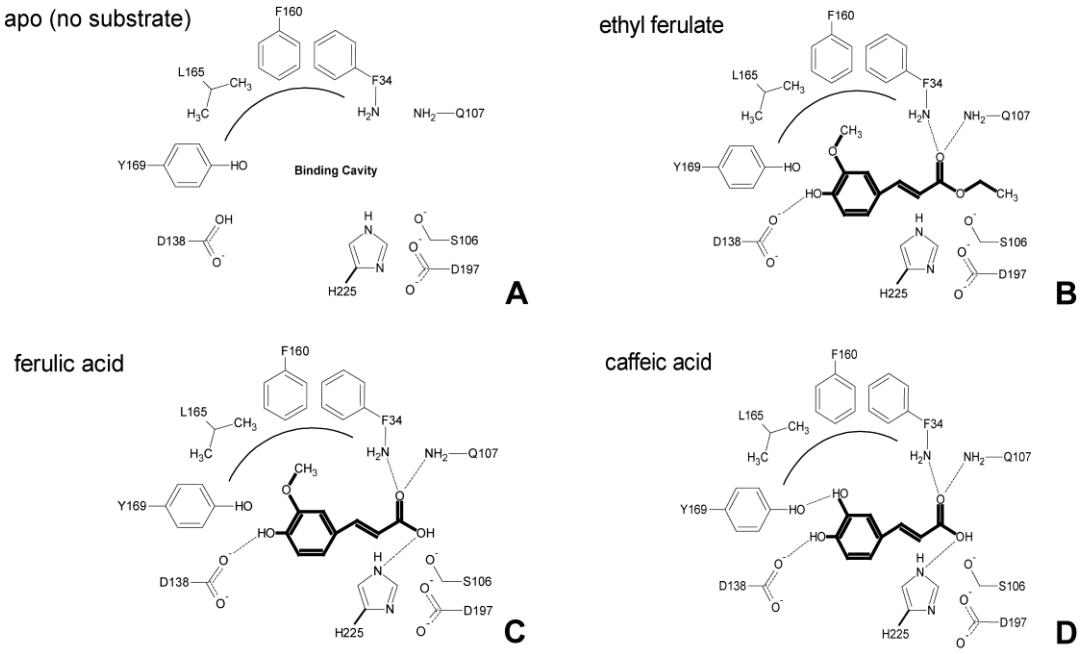

Figure 4-16. Schematic interpretation of the substrate interactions with LJ0536 binding cavity. (A) Apo structure without ligand. (B) Ethyl ferulate in the binding cavity. (C) Ferulic acid in the binding cavity. (D) Caffeic acid in the binding cavity. The substrates (ligands) are depicted in boldface. The dashed lines are used to represent the hydrogen bonds. The curved lines denote the hydrophobic region created by F34, F160, and L165. The 3-methoxy group (O-CH_3) of the ferulic ring is oriented towards the hydrophobic region in panels B and C. The D138 is hydrogen bonded with the 4-hydroxyl group of ferulic and caffeic acid ring. Y169 is hydrogen bonded only with the 3-hydroxyl group of the caffeic acid ring. The oxyanion hole is formed by the backbone of the nitrogen atoms of F34 and Q107.

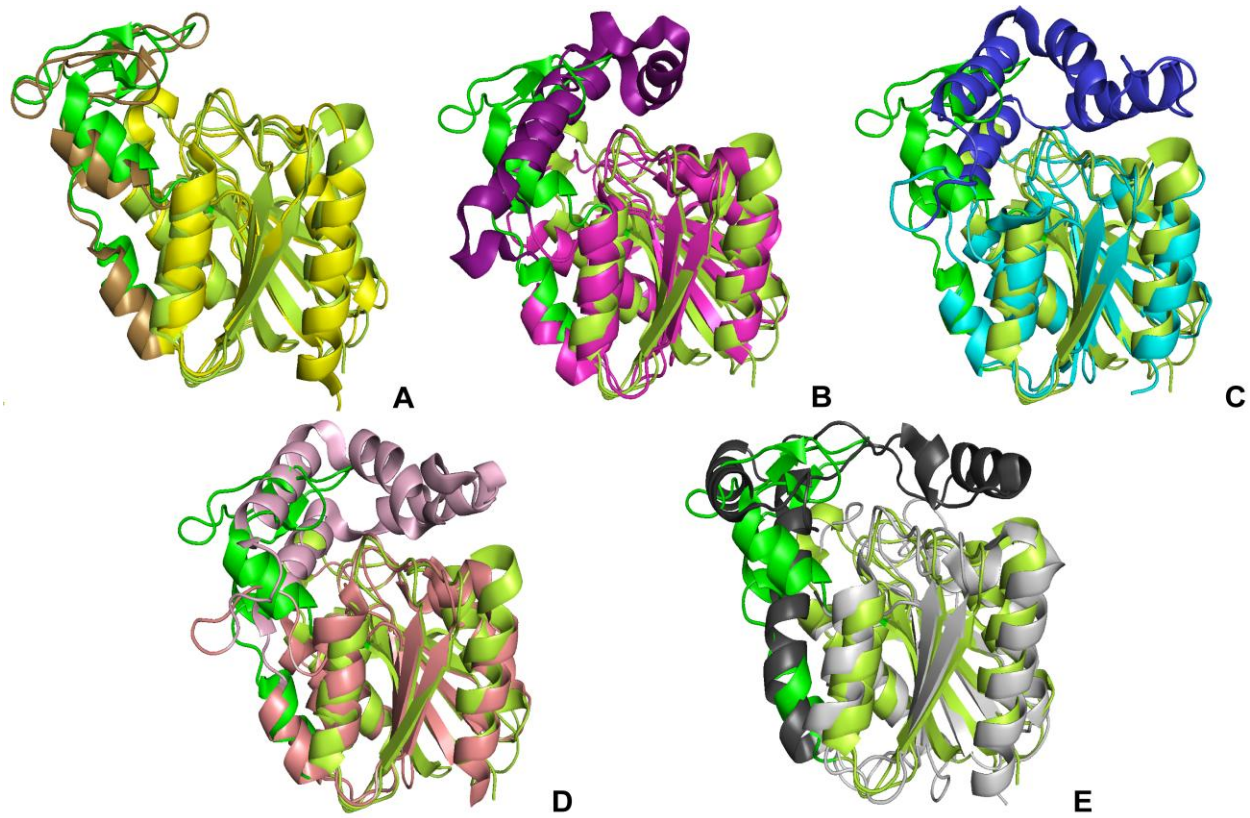

Figure 4-17. Structural comparison of LJ0536 and proteins with similar overall folding. Several enzymes involved in the catalysis of a variety of substrates display similar central core architecture. Interestingly, the major variations are observed in the inserted domains. In the following figures, LJ0536 (colored green) is superimposed with several structures retrieved from the database. (A) Est1E, (2WTM); (B) VACVase, (2OCG); (C) bromoperoxidase A1, (1A8Q); (D) aryl esterase, (3HI4); (E) human mono-glyceride lipase, (3JW8). The individual inserted domains of each protein are depicted in deeper colors. The PDB code for each protein is indicated between parentheses.

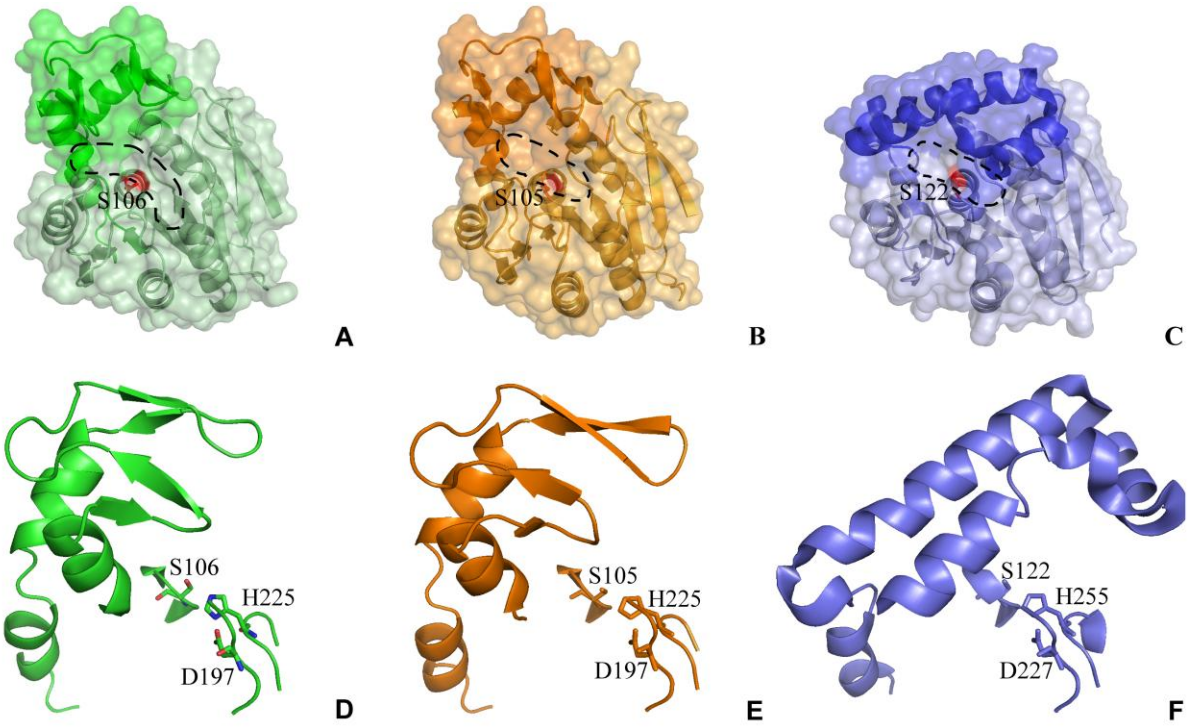

Figure 4-18. Structural comparison of (A) LJ0536 with (B) Est1E, and (C) VACVase. The semitransparent view is used in the figure to visualize the inserted domain in the context of overall protein structure. All enzymes share similar protein central core with a correct orientation of the catalytic triad. The catalytic serine was centered as a reference and colored in red. The binding cavity is circled with dash lines. The general architecture of the inserted domain of the bacterial enzymes LJ0536 and Est1E showed significant differences with VACVase. The inserted domains are shown in separate figures to better display the domain architecture. (D) LJ0536, (E) Est1E, and (F) VACVase. The catalytic triad was included as a reference.

CHAPTER 5
A NEW FACTOR CONTRIBUTES TO THE CLASSIFICATION OF FAES

Background

A recent review proposes a novel descriptor-based computational scheme for classification of FAEs (Udatha *et al*., 2011). The classification is based on a combination of several features such as enzymatic activity, sequence similarity, location of nucleophilic elbow, and the orientation of the catalytic triad. A weakness within the scheme is the absence of critical information relevant to bacterial FAEs. The classification scheme proposed relies largely on the characteristics of biochemically characterized proteins from fungal origin.

The recently proposed classification scheme is composed of twelve families. Neither LJ0536 or any of its homologs were included in any groups of the review (Udatha *et al*., 2011). Consequently, the sequences of LJ0536, LJ1228, and Est1E were analyzed by the sequence-derived descriptor. The results suggested that the important structural features, such as the architecture of the catalytic pocket, should be used to validate the classification system.

Result and Discussion

Structural Differences of Bacterial and Fungal FAEs

The structures of only two FAEs (AnFaeA of *A. niger* and Est1E of *B. proteoclasticus*) are available in the public database Protein Data Bank (Berman *et al*., 2000). The structure of LJ0536 was previously compared with bacterial FAE Est1E (Goldstone *et al*., 2010) in Chapter 4. Both enzymes showed high structural similarity. In order to investigate the conservation of the structures, bacterial FAEs and fungal FAEs were also compared.

The architecture of the catalytic pocket and the substrate binding mechanism are the major differences between LJ0536 and fungal FAE AnFaeA. The binding cavity of AnFaeA (pdb: 2BJH) (Hermoso *et al*., 2004) is a narrow, open cleft formed by a small lid domain composed of 23 amino acids (T68 to Q90). This lid domain contains a short α-helix, a short β-strand, and random coils (Figure 5-1A and B). The structure of AnFaeA lid domain is clearly different from the inserted α / β domain of LJ0536, which is composed of 54 amino acids (P131 to Q184) (Figure 5-1C and D). The binding cavity of AnFaeA is more hydrophobic than that of LJ0536. However, the stabilization of the substrate is similar to that of LJ0536. In both cases, the ferulic acid is stabilized in the binding cavity by hydrogen bonds. A hydrogen bond is formed between the hydroxyl group of the ferulic ring and the Y80 located on the lid domain of AnFaeA. In contrast, there is no amino acid residue similar to the Q145 of the enzyme LJ0536, which can coordinate a molecule of water on top of the catalytic serine and create a bridge-like structure on top of the binding cavity. The comparison of LJ0536 and AnFaeA is summarized in Table 5-1.

To confirm that the folding of fungal FAEs is different from LJ0536, the structures of other fungal FAEs were predicted. All predictions were done with SWISS MODEL (Arnold *et al.*, 2006). SWISS MODEL is a structure homology-modeling server, which allows users to predict the structure of a protein with a simple input of the peptide sequence. The modeling is generated based on existing protein structures. The quality of the modeling is estimated by the E-value, QMEAN Z-Score, and QMEANscore4 (Benkert *et al.*, 2011). The E-value is a parameter that describes the number of hits that you expect to find a protein by chance when searching a database. The lower the E-

value, the more structurally significant the hit is. The Q-MEAN Z-Score measures the absolute quality of a model. A strongly negative value indicates a model of low quality. The QMEANscore4 represents the probability that the input protein matches the predicted model. The value ranges between 0 and 1. The probability of matching is higher as the value gets closer to 1. The structures of the three biochemically characterized fungal FAEs used to design the classification scheme were predicted. NCR, a FAE from *Neurospora crassa*, was predicted to be similar to polyhydroxybutyrate depolymerase from *Penicillium funiculosum* (PDB: 2D81). PFU, a FAE from *Penicillium funiculosum*, was predicted to be similar to cellobiohydrolase from *Trichoderma reesei* (PDB: 1CBH). PEQ, a FAE from *Piromyces equi*, was predicted to match with a component of *P. equi* cellulosome (PDB: 2J4M). The results are summarized in Table 5-2.

The second round of prediction was done using LJ0536 as a template structure. The results are summarized in Table 5-3. Besides the improvement of E-value, both QMEAN Z-Score and QMEANscore4 had either no significant change or decreased dramatically. The results suggested that the structure of fungal FAEs does not have similarities with LJ0536.

Classification of LJ0536 and LJ1228

The Udatha classification scheme describes twelve FAE families. Since both LJ0536 and LJ1228 were not previously classified using this scheme, the sequences of LJ0536 and LJ1228 together with the recently crystallized *B. proteoclasticus* FAE Est1E were submitted to the descriptor for analysis. All three proteins were clustered in the subfamily 1B of Feruloyl Esterases Family 1 together with six hypothetical or putative bacterial proteins listed in Table 5-4 (Udatha *et al*., 2011). The descriptor was able to

identify the catalytic triad residues precisely. In order to investigate whether the substrate binding mechanism is conserved within the subfamily 1B, the structure of each protein was predicted using SWISS-MODEL (Arnold *et al*., 2006). The results are summarized in Table 5-4. Only LBI, a putative feruloyl esterase from *Leptospira biflexa* serovar Patoc strain, was predicted to be similar to Est1E (PDB: 2WTM). The hypothetical protein SLI was predicted to be similar to an esterase from *Pseudomonas fluorescens* (PDB: 3IA2). The remaining four proteins were predicted to be similar to FAE domain of cellulosomal xylanase Z (FAE-XynZ) from *Clostridium thermocellum* (PDB: 1JJF). The prediction done using LJ0536 chain B as template did not improve the quality of the models (Table 5-5). The quality of several models was even impaired. These predictions indicated that these proteins are not similar to LJ0536.

The protein structures within subfamily 1B are represented by two templates: LJ0536 and FAE-XynZ. The major differences between these two enzymes are the features of the substrate binding mechanism. The substrate binding mechanism of LJ0536 was described in Chapter 4. Specific amino acids of the inserted α / β domain interact directly with the phenolic ring of substrates. The interaction orients the aromatic acyl moiety of the substrate into the deepest part of the hydrophobic binding cavity. The leaving moiety remains exposed to the solvent (Figure 5-1C and D). In contrast, the FAE-XynZ displays a different substrate binding mechanism, although the overall folding of the enzymes and orientation of catalytic triad are highly similar (Figure 5-2 and 5-3). The inserted α / β fold domain is not present in FAE-XynZ to facilitate the binding of aromatic acyl moiety in the binding cavity. The structure suggested that the phenolic ring of the substrate does not interact with the protein. Only the water

molecules interact with the hydroxy and methoxy groups of the aromatic ring. The substrate is held in position by direct interactions with the catalytic residues (S172, H260, D230) and the oxanion hole (I90, M173). The substrate enzyme interaction is clearly demonstrated in the crystal structure of catalytic serine-deficient S172A FAE-XynZ mutant in complex with feruloyl arabinoxylan (PDB: 1JT2). Due to the absence of the inserted α / β domain in FAE-XynZ, the aromatic ring of ferulic acid is exposed to the solvent area in the binding cavity. Consequently, the subfamily 1B could be divided into two subgroups according to the presence or absence of the α / β fold inserted domain.

Structural Prediction of LJ0536 and LJ1228 Homologs

I hypothesized that the inserted α / β domain is conserved among LJ0536 and LJ1228 homologs and paralogs. To test this hypothesis, the structures of LJ0536 and LJ1228 homologs and paralogs, previously identified in Chapter 3, were predicted using the SWISS MODEL modeling tool (Arnold *et al*., 2006). The results found using an automatic template search are summarized in Table 5-6. All predictions provided good quality models except for the modeling of EVE, a hypothetical protein from *Eubacterium ventriosum* ATCC 27560. EVE has an E-Value of 1.40E-28, a QMEANscore4 of 0.477, and a QMEAN Z-Score of -4.276. BFI-1, a cinnamoyl ester hydrolase from *Butyrivibrio fibrisolvens* E14, has the best quality of model with an E-Value of 1.61E-91, a QMEANscore4 of 0.82, and a QMEAN Z-Score of 0.425. Among all 11 proteins, 9 were predicted to have similar folding to Est1E (Goldstone *et al*., 2010). The predictions were validated by including the sequences of LJ0536 and LJ1228 in the analysis.

The homologs, LBA-1 and BFI-2, do not have a similar Est1E folding. LBA-1 is annotated as α / β superfamily hydrolase in *L. acidophilus* NCFM. It was predicted to be

similar to lipase in *Burkholderia cepacia* (PDB: 1YS1). BFI-2 is annotated as cinnamoyl ester hydrolase in *B. fibrisolvens* E14. It was predicted to be similar to acetyl xylan esterase in *Bacillus pumilus* (PDB: 3FVR).

In order to prove that the folding of LJ0536 is conserved in LBA-1 and BFI-2, a second prediction was preformed using Est1E or LJ0536 as the template structure (Table 5-7). When Est1E was used as the template, the E-value of LBA-1 improved from 2.40E-08 to 2.70E-32. QMEAN Z-Score and QMEANscre4 decreased from -2.414 to -3.495 and from 0.556 to 0.527, respectively. When the prediction was done using LJ0536 as a template, the E-value improved to 1.2E-32, the QMEAN Z-Score decreased to -2.533, and the QMEANscre4 improved to 0.598. A similar scenario was observed when the protein BFI-2 was analyzed (the parameters obtained are summarized in Table 5-7). The results indicated that the folding of LJ0536 is conserved in LBA-1 and BFI-2.

The homologs and paralogs of LJ0536 and LJ1228 herein analyzed display similar structures. Thus, these proteins should be grouped together into the same subfamily under FEF1.

Among the homolog proteins, LRE (LREU1684 from *L. reuteri*) was previously cloned and purified in Chapter 3. Two other homologs, LBA-1 (LBA1350 from *L. acidophilus*) and LGA (LGAS1762 from *L. gasseri*), were also cloned and purified. These three enzymes showed FAE activity on MRS-EF screening plates, indicating that the activity and the structures are, indeed, conserved.

A PSI-BLAST search was used to detect distant evolutionary relationships of LJ0536. The sequences of five bacterial proteins annotated as cinnamoyl ester

hydrolase or feruloyl esterase were retrieved from the NCBI database. The protein structures were predicted using the same software (Arnold *et al*., 2006). The results are summarized in Table 5-8. Three out of five proteins were predicted to have similar folding using Est1E as a template (PDB: 2WTM). RAL is annotated as feruloyl esterase family protein from *Ruminococcus albus* 8 and predicted to be similar to *B. cepacia* lipase (PDB: 1YS1). When LJ0536 was used as a template to predict RAL structure, the E-value improved from 9.50E-13 to 2.40E-35, the QMEAN Z-Score increased from -4.437 to -3.427, and the QMEANscore4 improved from 0.341 to 0.536.

POR is annoated as feruloyl esterase from *Prevotella oris* F0302. It was predicted to be similar to a thiol–disulfide oxidoreductase, ResA, from *Bacillus subtilis* (PDB: 3C71). When LJ0536 was used as a template structure to predict POR, the E-value improved to from 1.8E-27 to 7.9E-38 (Table 5-9). However, The QMEAN Z-Score and QMEANscre4 decreased from -0.995 to -2.688 and from 0.704 to 0.587, respectively. Even though the values of QMEAN Z-Score and QMEANscore4 obtained using LJ0536 as a template are lower than the values obtained from automatic template search, the result sill indicated POR could have similar folding.

Altogether, the predicted folding of the putative bacterial FAEs identified using PSI-BLAST displayed similar folding to LJ0536.

Summary

Structural comparison of LJ0536 and AnfaeA indicates that the substrate binding mechanism of fungal enzymes is different from that of bacterial FAEs analyzed. The overall structure of the binding cavity is different and can be used to recognize the origin of the enzymes.

Even though both LJ0536 and FAE-XynZ are able to hydrolyze similar substrates, FAE-XynZ does not have an inserted domain. These specific protein structures are easily recognized and could be used to improve the current classification scheme.

The results herein analyzed allow us to extract conclusions limited to the subfamily 1B. There is not enough evidence in the database to expand the conclusion to other families within the classification scheme. The analysis of more structures is required to withdraw further conclusions.

Consequently, based on the mechanism of substrate binding and the architecture of the binding cavity, bacterial feruloyl estereases such as LJ0536, LJ1228, Est1E and their homologs should be clustered together as a new subfamily in the FEF1 group.

Table 5-1. Comparison of LJ0536 and AnFaeA

	LJ0536	AnFaeA
Size	249 amino acids	281 amino acids
Binding Cavity	hydrophobic, less open to solvent	Less hydrophobic, open to solvent
Catalytic Triad	S106, H225, D197	S133, H247, D194
Oxyanion Hole	F34, Q107	T68, L134
Binding Mechanism	D138: hydrogen bonds with hydroxyl group on aromatic ring. Q145: orients water molecule towards the binding cavity and creates a bridge-like structure to stabilize substrate binding	Y80: hydrogen bonds with hydroxyl group on aromatic ring
Lid / Inserted domain	54 amino acids, three α-helices and two hairpins	23 amino acids, one α-helix and one β-strand

Table 5-2. Structural prediction of fungal FAEs using SWISS-MODEL (automatic modeling)

Enzyme	Organism	Annotation	PDB match	Sequence Identity [%]	E-value	QMEAN Z-Score	QMEAN score4
NCR	*Neurospora crassa*	feruloyl esterase	2d81A (1.66 Å)	20.3	7.20E-15	-4.509	0.327
PFU	*Penicillium funiculosum*	feruloyl esterase	1cbhA [99.9 Å]	69.4	4.02E-05	-1.355	0.311
PEQ	*Piromyces equi*	feruloyl esterase	2j4mA [99.9 Å]	40.4	2.20E-07	-0.640	0.505

Numbers in round parentheses indicate X-ray resolution. Numbers in square parentheses indicate NMR resolution.

Table 5-3. Structural prediction of fungal FAEs using SWISS-MODEL (manual modeling)

Enzymes	Sequence Identity [%]	E-value	QMEAN Z-Score	QMEANscore4
NCR	9.1	5.00E-20	-5.765	0.371
PFU	10.3	2.80E-17	-6.620	0.299
PEQ	13.2	1.80E-12	-4.819	0.384

Template used: LJ0536 chain B

Table 5-4. Structural prediction of putative FAEs in subfamily 1B using SWISS-MODEL (automatic modeling)

Enzyme	Organism	Annotation	PDB match	Sequence Identity [%]	E-value	QMEAN Z-Score	QMEAN score4
LBI	*Leptospira biflexa* serovar Patoc strain	putative feruloyl esterase	2wtmC (1.60 Å)	22.0	1.40E-18	-3.943	0.437
PAE	*Paenibacillus sp*. W-61	putative feruloyl esterase	1jjfA (1.75 Å)	44.6	0.01E-01	-1.846	0.649
CCE	*Clostridium cellulovorans* 743B	putative esterase	1jjfA (1.75 Å)	40.3	3.10E-43	-3.196	0.552
GEO	*Geobacillus sp*. Y412MC10	putative esterase	1jjfA (1.75 Å)	44.1	1.40E-45	-2.213	0.622
SLI	*Spirosoma linguale* DSM 74	hypothetical protein SlinDRAFT_02770	3ia2A (1.65 Å)	22.0	6.80E-09	-4.790	0.304
ALG	*Algoriphagus sp*. PR1	Possible xylan degradation enzyme	1jjfA (1.75 Å)	49.0	0.01E-01	-1.502	0.674

Numbers in round parentheses indicate X-ray resolution.

Table 5-5. Structural prediction of putative FAEs in subfamily 1B using SWISS-MODEL (manual modeling)

Enzymes	Sequence Identity [%]	E-value	QMEAN Z-Score	QMEANscore4
LBI	17.0	2.30E-18	-4.215	0.413
PAE	12.0	1.10E-12	-5.337	0.396
CCE	c.n.d.	c.n.d.	c.n.d.	c.n.d.
GEO	c.n.d.	c.n.d.	c.n.d.	c.n.d.
SLI	12.8	5.70E-14	-5.514	0.269
ALG	13.9	9.30E-12	-5.972	0.347

c.n.d.: could not determine due to low similarity.
Template used: LJ0536 chain B.

Table 5-6. Structural prediction of LJ0536, LJ1228, and homologs / paralogs using SWISS-MODEL (automatic modeling)

Protein	Organism	Annotation	PDB match	Sequence Identity [%]	E-value	QMEAN Z-Score	QMEAN score4
LJO-1	*L. johnsonii* N6.2	cinnamoyl esterase	2wtmC (1.60 Å)	30.9	6.00E-42	-1.223	0.696
LJO-2	*L. johnsonii* N6.2	cinnamoyl esterase	2wtmC (1.60 Å)	31.3	4.70E-43	-1.844	0.651
LRE	*L. reuteri* DSM 20016	α / β fold family hydrolase-like protein	2wtmC (1.60 Å)	32.9	1.20E-43	-1.599	0.669
LBA-1	*L. acidophilus* NCFM	α / β superfamily hydrolase	1ys1X (1.10 Å)	24.6	2.40E-08	-2.414	0.556
LBA-2	*L. acidophilus* NCFM	α / β superfamily hydrolase	2wtmC (1.60 Å)	29.7	4.20E-41	-1.490	0.677
EVE	*Eubacterium ventriosum* ATCC 27560	hypothetical protein	2wtmC (1.60 Å)	25.6	1.40E-28	-4.276	0.477
TDE	*Treponema denticola*	cinnamoyl ester hydrolase	2wtmC (1.60 Å)	24.4	8.50E-38	-1.362	0.686
BFI-1	*Butyrivibrio fibrisolvens* E14	cinnamoyl ester hydrolase	2wtnA (2.10 Å)	64.6	1.64E-91	0.425	0.820
BFI-2	*Butyrivibrio fibrisolvens* E14	cinnamoyl ester hydrolase	3fvrC (2.50 Å)	20.1	1.70E-32	-3.380	0.539
LPL	*L. plantarum* WCSF1	putative esterase	2wtmC (1.60 Å)	29.7	3.60E-42	-0.949	0.717
LGA	*L. gasseri* ATCC 33323	α / β fold family hydrolase	2wtmC (1.60 Å)	30.9	1.20E-40	-1.046	0.710
LHV	*L. helveticus* DPC 4571	α / β fold family hydrolase	2wtmC (1.60 Å)	29.7	4.80E-42	-1.558	0.672
LAF	*L. fermentum* IFO 3956	hypothetical protein	2wtmC (1.60 Å)	32.0	3.60E-42	-1.819	0.653

Numbers in round parentheses indicate X-ray resolution.

Table 5-7. Structural prediction of LBA-1 and BFI-2 using SWISS-MODEL (manual modeling)

Protein	Template used: 2wtmA				Template used: LJ0536 Chain B			
	Sequence Identity [%]	E-value	QMEAN Z-Score	QMEAN score4	Sequence Identity [%]	E-value	QMEAN Z-Score	QMEAN score4
LBA-1	23.1	2.70E-32	-3.495	0.527	25.9	1.20E-32	-2.533	0.598
BFI-2	27.6	3.10E-37	-2.151	0.627	24.6	2.70E-38	-1.959	0.643

Table 5-8. Structural prediction of bacterial FAEs using SWISS-MODEL (automatic modeling)

Enzyme	Organism	Annotation	PDB match	Sequence Identity [%]	E-value	QMEAN Z-Score	QMEAN score4
TDE-2	*Treponema denticola* F0402	cinnamoyl ester hydrolase	2wtmC (1.60 Å)	24.8	1.50E-38	-1.992	0.639
SSA	*Streptococcus sanguinis* VMC66	cinnamoyl ester hydrolase	2wtmC (1.60 Å)	25.7	2.50E-35	-1.935	0.644
RAL	*Ruminococcus albus* 8	feruloyl esterase family protein	1ys1X (1.10 Å)	17.2	9.50E-13	-4.437	0.341
CRU	*Cellulosilyticum ruminicola*	feruloyl esterase III	2wtmC (1.60 Å)	27.4	3.60E-34	-2.870	0.575
POR	*Prevotella oris F0302*	feruloyl esterase	3c71A (1.90 Å)	29.7	1.80E-27	-0.995	0.704

Numbers in round parentheses indicate X-ray resolution.

Table 5-9. Structural prediction of bacterial FAEs using SWISS-MODEL (manual modeling)

Enzymes	Sequence Identity [%]	E-value	QMEAN Z-Score	QMEANscore4
RAL	24.0	2.4E-35	-3.427	0.536
POR	41.3	7.9E-38	-2.688	0.587

Template used: LJ0536 chain B

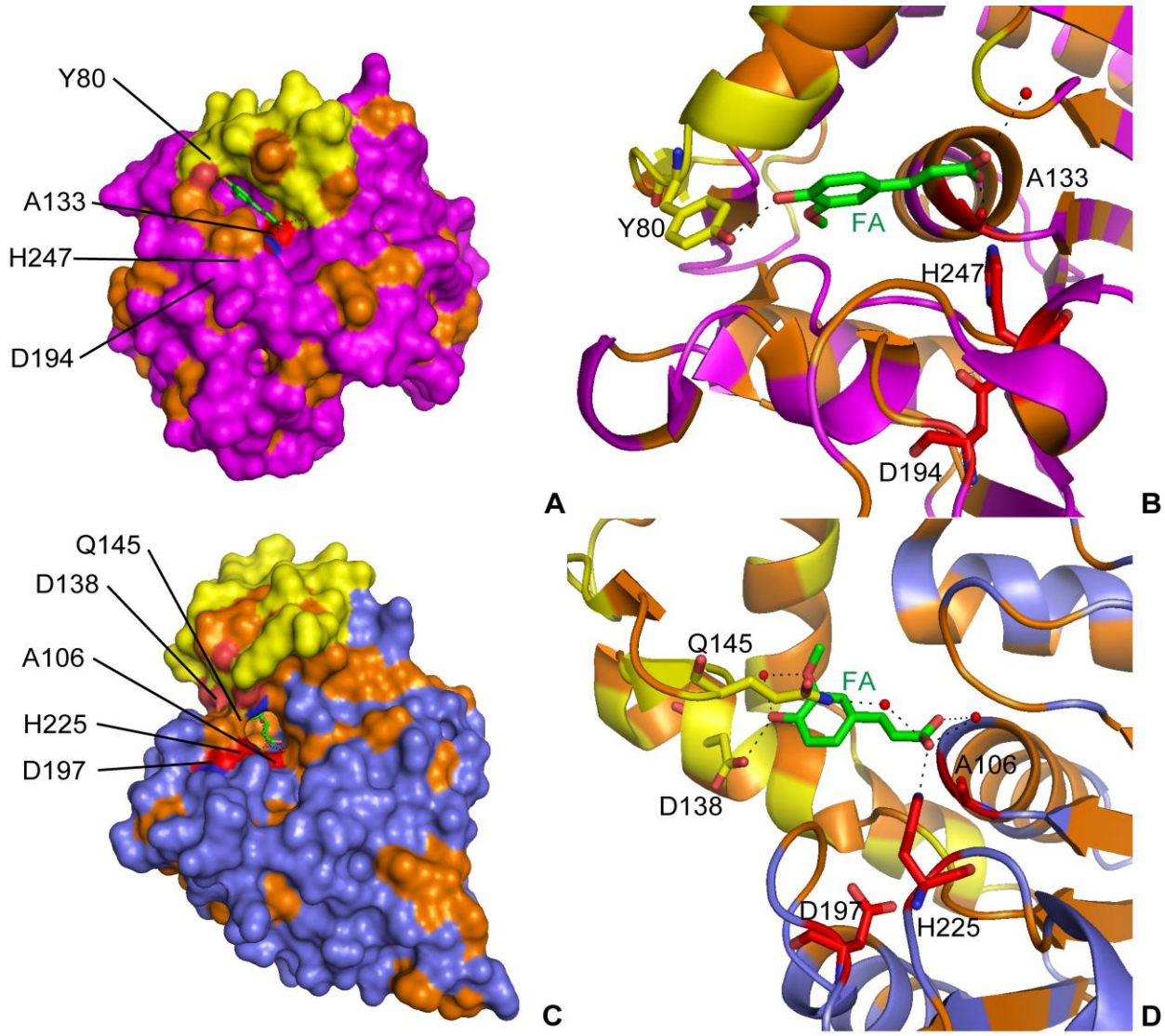

Figure 5-1. Structural comparison of LJ0536 and AnFaeA. (A) Surface and (B) ribbon representation of AnFaeA-S133A with ferulic acid in the binding cavity. (C) Surface and (D) ribbon representations of LJ0536-S106A with ferulic acid in the binding cavity. The insertion domains are colored yellow. The hydrophobic residues are colored orange. The amino acids of the catalytic triad are colored red. The ligands (ferulic acids) are depicted in green. The red spheres represent the water molecules observed in the crystal. The dashed lines represent the hydrogen bonds.

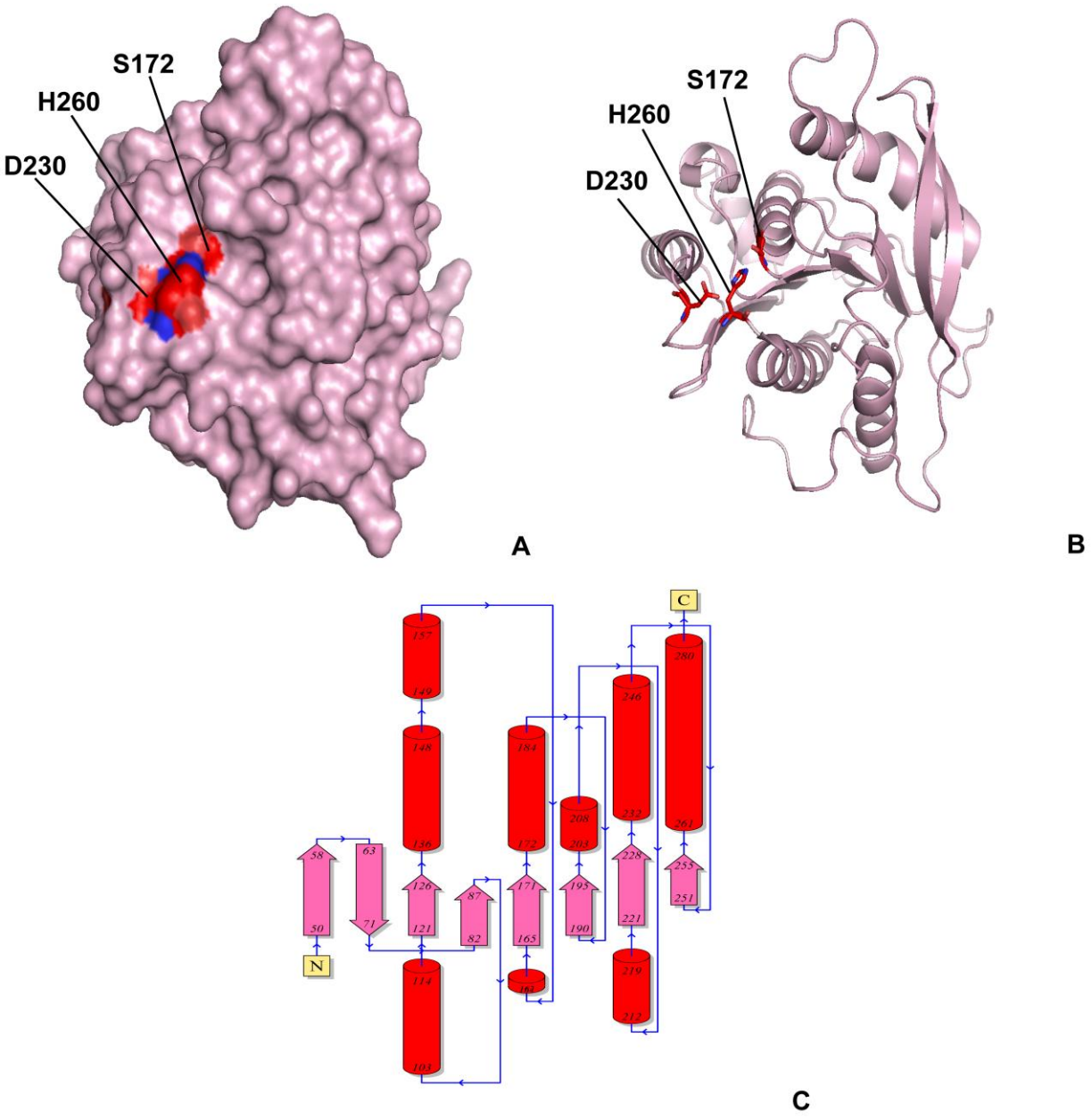

Figure 5-2. Structure of FAE-XynZ. (A) Surface representation, (B) ribbon representation, and (C) topology diagram. The catalytic triad S172, H260, and D230 are colored in red. The inserted domain is not present in FAE-XynZ.

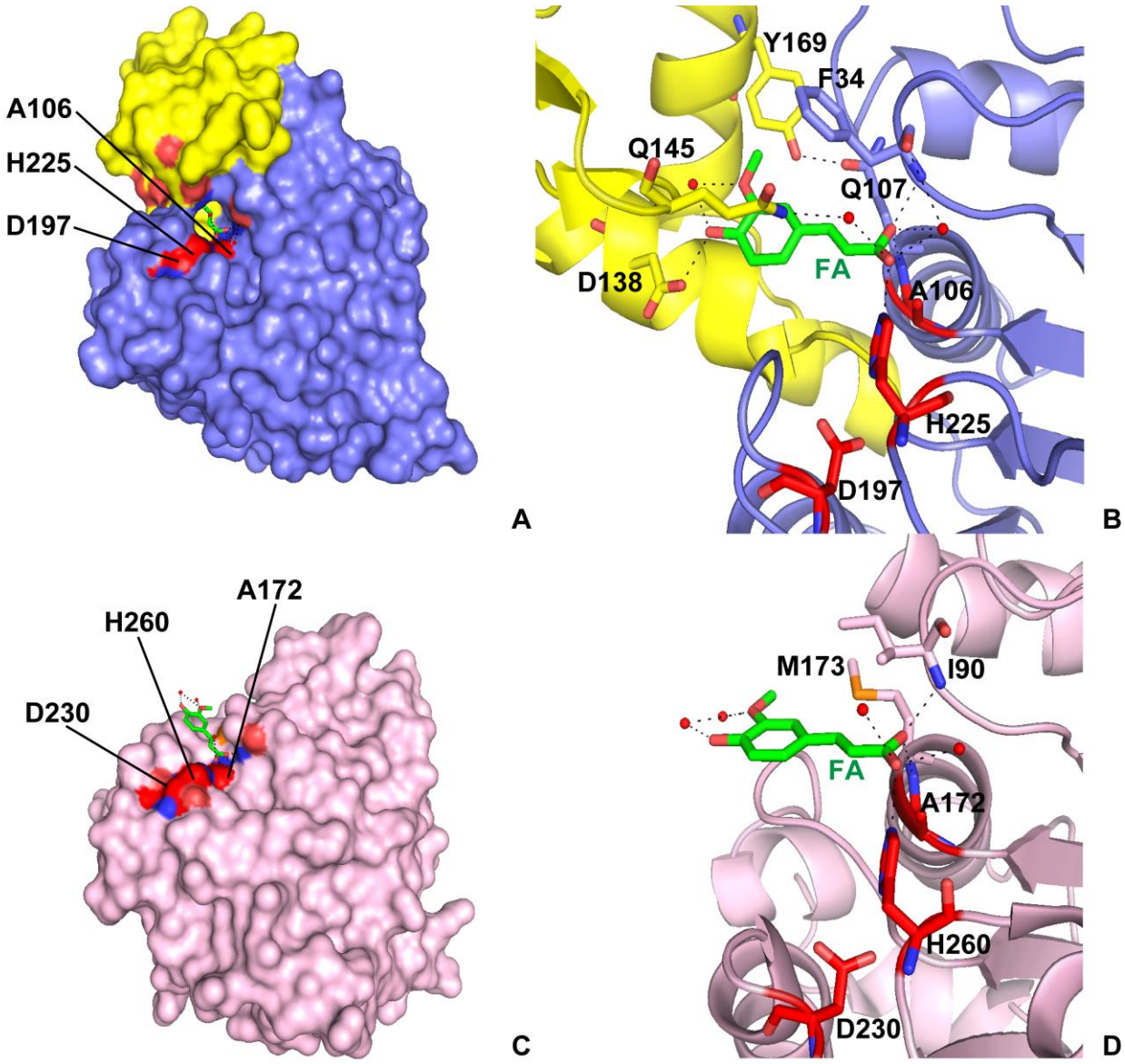

Figure 5-3. Structural comparison of LJ0536 and FAE-XynZ co-crystallized with their respective substrates. (A) Surface representation and (B) ribbon representation of LJ0536 S106A co-crystallized with ferulic acid. The catalytic triad is composed of S106, H225, and D197. The oxyanion hole is formed by the backbone nitrogen atoms of F34 and Q107. The D138 and Q145 of the inserted α / β domain participates in substrate binding. (C) Surface representation and (D) ribbon representations of FAE-XynZ S172A co-crystallized with feruloyl arabinoxylan. The catalytic triad is composed of S172, H260, and D230. The oxyanion hole is formed by the backbone nitrogen atoms of I90 and M173. The inserted domain is not present in FAE-XynZ. The catalytic triad is colored red. The inserted domain is colored yellow. The water molecules are represented by red spheres. The dashed lines were used to indicate the hydrogen bonds. The ligands (ferulic acid) are colored green.

CHAPTER 6
SUMMARY AND CONCLUSIONS

The overall goal of this work is to enhance the understanding of FAEs produced by intestinal gut microbiota. FAE application is one of the major fields of study for improving the bioavailability of phenolic acids in food components (phytophenols). The released phenolic acids from phytophenols by FAE activity are subjected to intestinal assimilation to provide beneficial functions to the host. To the best of today's knowledge, there is no study that describes the purification and characterization of FAEs from the intestinal gut microbiota. The first part of this study has successfully identified two FAEs, LJ0536 and LJ1228, from a commensal bacterium *L. johnsonii* N6.2. Both enzymes showed high substrate preferences towards aromatic esters that present in foods and the capability to tolerate harsh intestinal chemicals. Phylogenetic analysis indicates LJ0536 and LJ1228 homologs are widely distributed in lactobacilli. The findings disclose the potential utilization of probiotic bacterial FAEs to improve the bioavailability of phenolic acids.

The second part of this study provides the first crystal structure of a FAE of *L. johnsonii*. X-ray crystallization of LJ0536 identified specific features involved in ester hydrolysis. LJ0536 shows a typical α / β fold structure which is common in serine proteases. The catalytic triad is composed of S106, H225, and D197. Site directed mutagenesis and co-crystallization of S106A with aromatic esters allow us to pinpoint the binding mechanism of LJ0536. The substrate binding mechanism consists of a small hydrophobic cavity in a boomerang shape and an inserted α / β domain located on top of the binding cavity. An oxyanion hole is formed by the backbone nitrogen atoms of F34 and Q107. It assists ester hydrolysis by stabilizing the enzyme-ester intermediate

and orientating the ester bond near the catalytic serine residue. The inserted α / β domain is composed of 54 amino acids (P131 to Q184). Q145 of the inserted α / β domain forms a bridge-like structure on top of the binding cavity to protect the small hydrophobic region. It also assists in orientating a water molecule near the site of hydrolysis. Residues D138 and Y169 of the inserted α / β domain form hydrogen bonds with the hydroxyl groups of the aromatic ring of the substrate. The hydrogen bonding stabilizes the substrate within the binding cavity. The difference in secondary structure of inserted domains among homolog proteins determines substrate specificity. The features of the inserted α / β domain contribute to substrate discrimination.

The last part of this study involved bioinformatics and structural comparisons of LJ0536 with other biochemically characterized and putative FAEs of bacterial and fungal species. The current FAE classification scheme is primarily based on the enzyme activity and the primary sequence identity of fungal FAEs. For instance, the unique features of protein structure showed in the LJ0536 crystal, the inserted domain, could contribute as an extra element for the classification of FAEs in subfamily 1B. However, the insufficiency of FAE structures in the current public PDB database limits the feasiblility of applying the inserted domains as one of the features in the full classification scheme. Further exploration of FAE structures is required to provide insight on the use of inserted domains in the classification scheme.

REFERENCE LIST

Adams, P., P. Afonine, G. Bunkóczi, V. Chen, I. Davis, N. Echols, J. Headd, L. Hung, G. Kapral, R. Grosse-Kunstleve, A. McCoy, N. Moriarty, R. Oeffner, R. Read, D. Richardson, J. Richardson, T. Terwilliger & P. Zwart, (2010) PHENIX: a comprehensive Python-based system for macromolecular structure solution. *Acta Crystallogr D Biol Crystallogr* **66**: 213-221.

Adisakwattana, S., P. Moonsan & S. Yibchok-Anun, (2008) Insulin-releasing properties of a series of cinnamic acid derivatives in vitro and in vivo. *J Agric Food Chem* **56**: 7838-7844.

Akihisa, T., K. Yasukawa, M. Yamaura, M. Ukiya, Y. Kimura, N. Shimizu & K. Arai, (2000) Triterpene alcohol and sterol ferulates from rice bran and their anti-inflammatory effects. *J Agric Food Chem* **48**: 2313-2319.

Akin, D. E., (2008) Plant cell wall aromatics: influence on degradation of biomass. *Biofuel Bioprod Bior* **2**: 288-303.

Altermann, E., W. M. Russell, M. A. Azcarate-Peril, R. Barrangou, B. L. Buck, O. McAuliffe, N. Souther, A. Dobson, T. Duong, M. Callanan, S. Lick, A. Hamrick, R. Cano & T. R. Klaenhammer, (2005) Complete genome sequence of the probiotic lactic acid bacterium *Lactobacillus acidophilus* NCFM. *Proc Natl Acad Sci U S A* **102**: 3906-3912.

Altschul, S. F., T. L. Madden, A. A. Schäffer, J. Zhang, Z. Zhang, W. Miller & D. J. Lipman, (1997) Gapped BLAST and PSI-BLAST: a new generation of protein database search programs. *Nucleic Acids Res* **25**: 3389-3402.

Andreasen, M., P. Kroon, G. Williamson & M. Garcia-Conesa, (2001) Esterase activity able to hydrolyze dietary antioxidant hydroxycinnamates is distributed along the intestine of mammals. *J Agric Food Chem* **49**: 5679-5684.

Arnold, K., L. Bordoli, J. Kopp & T. Schwede, (2006) The SWISS-MODEL workspace: a web-based environment for protein structure homology modelling. *Bioinformatics* **22**: 195-201.

Asther, M., M. I. Estrada Alvarado, M. Haon, D. Navarro, M. Asther, L. Lesage-Meessen & E. Record, (2005) Purification and characterization of a chlorogenic acid hydrolase from *Aspergillus niger* catalysing the hydrolysis of chlorogenic acid. *Journal of Biotechnology* **115**: 47-56.

Athar, M., J. H. Back, L. Kopelovich, D. R. Bickers & A. L. Kim, (2009) Multiple molecular targets of resveratrol: Anti-carcinogenic mechanisms. *Arch Biochem Biophys* **486**: 95-102.

Baba, S., N. Osakabe, M. Natsume & J. Terao, (2004) Orally administered rosmarinic acid is present as the conjugated and/or methylated forms in plasma, and is degraded and metabolized to conjugated forms of caffeic acid, ferulic acid and m-coumaric acid. *Life Sci* **75**: 165-178.

Balasubashini, M., R. Rukkumani & V. P. Menon, (2003) Protective effects of ferulic acid on hyperlipidemic diabetic rats. *Acta Diabetol* **40**: 118-122.

Balasubashini, M., R. Rukkumani, P. Viswanathan & V. Menon, (2004) Ferulic acid alleviates lipid peroxidation in diabetic rats. *Phytother Res* **18**: 310-314.

Beckman, C. H., (2000) Phenolic-storing cells: keys to programmed cell death and periderm formation in wilt disease resistance and in general defence responses in plants? *Physiol Mol Plant Path* **57**: 101-110.

Benkert, P., M. Biasini & T. Schwede, (2011) Toward the estimation of the absolute quality of individual protein structure models. *Bioinformatics* **27**: 343-350.

Benoit, I., M. Asther, Y. Bourne, D. Navarro, S. Canaan, L. Lesage-Meessen, M. Herweijer, P. Coutinho & E. Record, (2007) Gene overexpression and biochemical characterization of the biotechnologically relevant chlorogenic acid hydrolase from *Aspergillus niger*. *Appl Environ Microbiol* **73**: 5624-5632.

Benoit, I., E. G. Danchin, R. J. Bleichrodt & R. P. de Vries, (2008) Biotechnological applications and potential of fungal feruloyl esterases based on prevalence, classification and biochemical diversity. *Biotechnol Lett* **30**: 387-396.

Benson, D. A., I. Karsch-Mizrachi, D. J. Lipman, J. Ostell & E. W. Sayers, (2011) GenBank. *Nucleic Acids Res* **39**: D32-D37.

Berman, H. M., J. Westbrook, Z. Feng, G. Gilliland, T. N. Bhat, H. Weissig, I. N. Shindyalov & P. E. Bourne (2000) The Protein Data Bank. In.: *Nucleic Acids Res*, pp. 235-242.

Bertrand, T., F. Augé, J. Houtmann, A. Rak, F. Vallée, V. Mikol, P. F. Berne, N. Michot, D. Cheuret, C. Hoornaert & M. Mathieu, (2010) Structural basis for human monoglyceride lipase inhibition. *J Mol Biol* **396**: 663-673.

Blanc, E., P. Roversi, C. Vonrhein, C. Flensburg, S. Lea & G. Bricogne, (2004) Refinement of severely incomplete structures with maximum likelihood in BUSTER-TNT. *Acta Crystallogr D Biol Crystallogr* **60**: 2210-2221.

Bornscheuer, U. T., (2002) Microbial carboxyl esterases: classification, properties and application in biocatalysis. *FEMS Microbiol Rev* **26**: 73-81.

Bradford, M. M., (1976) A rapid and sensitive method for the quantitation of microgram quantities of protein utilizing the principle of protein-dye binding. *Anal Biochem* **72**: 248-254.

Brenner, S., (1988) The molecular evolution of genes and proteins: a tale of two serines. *Nature* **334**: 528-530.

Cani, P., R. Bibiloni, C. Knauf, A. Waget, A. Neyrinck, N. Delzenne & R. Burcelin, (2008) Changes in gut microbiota control metabolic endotoxemia-induced inflammation in high-fat diet-induced obesity and diabetes in mice. *Diabetes* **57**: 1470-1481.

Cani, P., S. Possemiers, T. Van de Wiele, Y. Guiot, A. Everard, O. Rottier, L. Geurts, D. Naslain, A. Neyrinck, D. Lambert, G. Muccioli & N. Delzenne, (2009) Changes in gut microbiota control inflammation in obese mice through a mechanism involving GLP-2-driven improvement of gut permeability. *Gut* **58**: 1091-1103.

Chao, P., C. Hsu & M. Yin, (2009) Anti-inflammatory and anti-coagulatory activities of caffeic acid and ellagic acid in cardiac tissue of diabetic mice. *Nutr Metab (Lond)* **6**: 33.

Chen, M. H. & C. J. Bergman, (2005) A rapid procedure for analysing rice bran tocopherol, tocotrienol and γ-oryzanol contents. *J Food Comp Anal* **18**: 319-331.

Chen, V., W. r. Arendall, J. Headd, D. Keedy, R. Immormino, G. Kapral, L. Murray, J. Richardson & D. Richardson, (2010) MolProbity: all-atom structure validation for macromolecular crystallography. *Acta Crystallogr D Biol Crystallogr* **66**: 12-21.

Cheng, C., S. Su, N. Tang, T. Ho, S. Chiang & C. Hsieh, (2008) Ferulic acid provides neuroprotection against oxidative stress-related apoptosis after cerebral ischemia/reperfusion injury by inhibiting ICAM-1 mRNA expression in rats. *Brain Res* **1209**: 136-150.

Costabile, A., A. Klinder, F. Fava, A. Napolitano, V. Fogliano, C. Leonard, G. R. Gibson & K. M. Tuohy, (2008) Whole-grain wheat breakfast cereal has a prebiotic effect on the human gut microbiota: a double-blind, placebo-controlled, crossover study. *Br J Nutr* **99**: 110-120.

Couteau, D. & P. Mathaly, (1998) Fixed-bed purification of ferulic acid from sugar-beet pulp using activated carbon: Optimization studies. *Bioresource Technol* **64**: 17-25.

Couteau, D., A. McCartney, G. Gibson, G. Williamson & C. Faulds, (2001) Isolation and characterization of human colonic bacteria able to hydrolyse chlorogenic acid. *J Appl Microbiol* **90**: 873-881.

Crepin, V. F., C. B. Faulds & I. F. Connerton, (2004) Functional classification of the microbial feruloyl esterases. *Appl Microbiol Biotechnol* **63**: 647-652.

Crozier, A., I. Jaganath & M. Clifford, (2009) Dietary phenolics: chemistry, bioavailability and effects on health. *Nat Prod Rep* **26**: 1001-1043.

Cygler, M., J. Schrag, J. Sussman, M. Harel, I. Silman, M. Gentry & B. Doctor, (1993) Relationship between sequence conservation and three-dimensional structure in a large family of esterases, lipases, and related proteins. *Protein Sci* **2**: 366-382.

Dalrymple, B., Y. Swadling, D. Cybinski & G. Xue, (1996) Cloning of a gene encoding cinnamoyl ester hydrolase from the ruminal bacterium *Butyrivibrio fibrisolvens* E14 by a novel method. *FEMS Microbiol Lett* **143**: 115-120.

Davidsen, T., E. Beck, A. Ganapathy, R. Montgomery, N. Zafar, Q. Yang, R. Madupu, P. Goetz, K. Galinsky, O. White & G. Sutton, (2010) The comprehensive microbial resource. *Nucleic Acids Res* **38**: D340-345.

DeLano, W. L., (2002) The PyMOL Molecular Graphics System, version 1.00, Schrödinger, LLC.

Ding, X., B. F. Rasmussen, G. A. Petsko & D. Ringe, (1994) Direct structural observation of an acyl-enzyme intermediate in the hydrolysis of an ester substrate by elastase. *Biochemistry* **33**: 9285-9293.

Dodson, G. & A. Wlodawer, (1998) Catalytic triads and their relatives. *Trends Biochem Sci* **23**: 347-352.

Donaghy, J., P. F. Kelly & A. M. McKay, (1998) Detection of ferulic acid esterase production by Bacillus spp. and lactobacilli. *Appl Microbiol Biotechnol* **50**: 257-260.

Dong, A., X. Xu, A. M. Edwards, C. Chang, M. Chruszcz, M. Cuff, M. Cymborowski, R. Di Leo, O. Egorova, E. Evdokimova, E. Filippova, J. Gu, J. Guthrie, A. Ignatchenko, A. Joachimiak, N. Klostermann, Y. Kim, Y. Korniyenko, W. Minor, Q. Que, A. Savchenko, T. Skarina, K. Tan, A. Yakunin, A. Yee, V. Yim, R. Zhang, H. Zheng, M. Akutsu, C. Arrowsmith, G. V. Avvakumov, A. Bochkarev, L. G. Dahlgren, S. Dhe-Paganon, S. Dimov, L. Dombrovski, P. Finerty, S. Flodin, A. Flores, S. Gräslund, M. Hammerström, M. D. Herman, B. S. Hong, R. Hui, I. Johansson, Y. Liu, M. Nilsson, L. Nedyalkova, P. Nordlund, T. Nyman, J. Min, H. Ouyang, H. W. Park, C. Qi, W. Rabeh, L. Shen, Y. Shen, D. Sukumard, W. Tempel, Y. Tong, L. Tresagues, M. Vedadi, J. R. Walker, J. Weigelt, M. Welin, H. Wu, T. Xiao, H. Zeng, H. Zhu, M. C. f. S. Genomics & S. G. Consortium, (2007) In situ proteolysis for protein crystallization and structure determination. *Nat Methods* **4**: 1019-1021.

Emsley, P. & K. Cowtan, (2004) Coot: model-building tools for molecular graphics. *Acta Crystallogr D Biol Crystallogr* **60**: 2126-2132.

Faulds, C., R. Molina, R. Gonzalez, F. Husband, N. Juge, J. Sanz-Aparicio & J. Hermoso, (2005) Probing the determinants of substrate specificity of a feruloyl esterase, AnFaeA, from *Aspergillus niger*. *FEBS J* **272**: 4362-4371.

Fazary, A. & Y. Ju, (2007) Feruloyl esterases as biotechnological tools: current and future perspectives. *Acta Biochim Biophys Sin (Shanghai)* **39**: 811-828.

Fazary, A. E. & Y.-H. Ju, (2008) The large-scale use of feruloyl esterases in industry. *Biotechnol. Mol. Biol. Rev* **3**: 95-110.

Ferreres, F., R. Figueiredo, S. Bettencourt, I. Carqueijeiro, J. Oliveira, A. Gil-Izquierdo, D. M. Pereira, P. Valentão, P. B. Andrade, P. Duarte, A. R. Barceló & M. Sottomayor, (2011) Identification of phenolic compounds in isolated vacuoles of the medicinal plant Catharanthus roseus and their interaction with vacuolar class III peroxidase: an H2O2 affair? *J Exp Bot* **62**: 2841-2854.

Fujita, A., H. Sasaki, A. Doi, K. Okamoto, S. Matsuno, H. Furuta, M. Nishi, T. Nakao, T. Tsuno, H. Taniguchi & K. Nanjo, (2008) Ferulic acid prevents pathological and functional abnormalities of the kidney in Otsuka Long-Evans Tokushima Fatty diabetic rats. *Diabetes Res Clin Pract* **79**: 11-17.

Giuliani, S., C. Piana, L. Setti, A. Hochkoeppler, P. G. Pifferi, G. Williamson & C. B. Faulds, (2001) Synthesis of pentylferulate by a feruloyl esterase from *Aspergillus niger* using water-in-oil microemulsions. *Biotechnol. Lett.* **23**: 325-330-330.

Goldstone, D., S. Villas-Bôas, M. Till, W. Kelly, G. Attwood & V. Arcus, (2010) Structural and functional characterization of a promiscuous feruloyl esterase (Est1E) from the rumen bacterium *Butyrivibrio proteoclasticus*. *Proteins* **78**: 1457-1469.

Gonthier, M., C. Remesy, A. Scalbert, V. Cheynier, J. Souquet, K. Poutanen & A. Aura, (2006) Microbial metabolism of caffeic acid and its esters chlorogenic and caftaric acids by human faecal microbiota in vitro. *Biomed Pharmacother* **60**: 536-540.

Gonzalez, C., M. Proudfoot, G. Brown, Y. Korniyenko, H. Mori, A. Savchenko & A. Yakunin, (2006) Molecular basis of formaldehyde detoxification. Characterization of two S-formylglutathione hydrolases from *Escherichia coli*, FrmB and YeiG. *J Biol Chem* **281**: 14514-14522.

Graf, E., (1992) Antioxidant potential of ferulic acid. *Free Radic Biol Med* **13**: 435-448.

Granados-Principal, S., J. L. Quiles, C. L. Ramirez-Tortosa, P. Sanchez-Rovira & M. C. Ramirez-Tortosa, (2010) Hydroxytyrosol: from laboratory investigations to future clinical trials. *Nutr Rev* **68**: 191-206.

Grochulski, P., Y. Li, J. D. Schrag & M. Cygler, (1994) Two conformational states of *Candida rugosa* lipase. *Protein Sci* **3**: 82-91.

Guthrie, J., P. Loppnau, I. Kozieradzki, A. Savchenko & C. Arrowsmith, (2007) Expression vectors for high-throughput in-fusion cloning. *Unpublished*.

Han, L. Y., C. Z. Cai, Z. L. Ji, Z. W. Cao, J. Cui & Y. Z. Chen, (2004) Predicting functional family of novel enzymes irrespective of sequence similarity: a statistical learning approach. *Nucleic Acids Res* **32**: 6437-6444.

Hatzakis, N. S., D. Daphnomili & I. Smonou, (2003) Ferulic acid esterase from *Humicola Insolens* catalyzes enantioselective transesterification of secondary alcohols. *J. Mol. Catal. B: Enzym.* **21**: 309-311.

Hatzakis, N. S. & I. Smonou, (2005) Asymmetric transesterification of secondary alcohols catalyzed by feruloyl esterase from *Humicola insolens*. *Bioorg Chem* **33**: 325-337.

Hedstrom, L., (2002) Serine protease mechanism and specificity. *Chem Rev* **102**: 4501-4524.

Hermoso, J., J. Sanz-Aparicio, R. Molina, N. Juge, R. González & C. Faulds, (2004) The crystal structure of feruloyl esterase A from *Aspergillus niger* suggests evolutive functional convergence in feruloyl esterase family. *J Mol Biol* **338**: 495-506.

Hofmann, B., S. Tölzer, I. Pelletier, J. Altenbuchner, K. H. van Pée & H. J. Hecht, (1998) Structural investigation of the cofactor-free chloroperoxidases. *J Mol Biol* **279**: 889-900.

Holm, L. & P. Rosenström, (2010) Dali server: conservation mapping in 3D. *Nucleic Acids Res* **38**: W545-549.

Holmquist, M., (2000) Alpha/Beta-hydrolase fold enzymes: structures, functions and mechanisms. *Curr Protein Pept Sci* **1**: 209-235.

Hooper, L. V. & J. I. Gordon, (2001) Commensal host-bacterial relationships in the gut. *Science* **292**: 1115-1118.

Hope, H., (1988) Cryocrystallography of biological macromolecules: a generally applicable method. *Acta Crystallogr B* **44 (Pt 1)**: 22-26.

Huang, D., S. Shen & J. Wu, (2009) Effects of caffeic acid and cinnamic acid on glucose uptake in insulin-resistant mouse hepatocytes. *J Agric Food Chem* **57**: 7687-7692.

Huang, Z., B. Wang, D. H. Eaves, J. M. Shikany & R. D. Pace, (2007) Phenolic compound profile of selected vegetables frequently consumed by African Americans in the southeast United States. *Food Chem* **103**: 1395-1402.

Janes, L., C. Löwendahl & R. Kazlauskas, (1998) Quantitative Screening of Hydrolase Libraries Using pH Indicators: Identifying Active and Enantioselective Hydrolases. *Chem.–Eur. J.* **4**: 2324-2331.

Jensen, M. K., P. Koh-Banerjee, F. B. Hu, M. Franz, L. Sampson, M. Grønbaek & E. B. Rimm, (2004) Intakes of whole grains, bran, and germ and the risk of coronary heart disease in men. *Am J Clin Nutr* **80**: 1492-1499.

Jew, S., S. AbuMweis & P. Jones, (2009) Evolution of the human diet: linking our ancestral diet to modern functional foods as a means of chronic disease prevention. *J Med Food* **12**: 925-934.

Kim, H. Y., J. Park, K. H. Lee, D. U. Lee, J. H. Kwak, Y. S. Kim & S. M. Lee, (2011) Ferulic acid protects against carbon tetrachloride-induced liver injury in mice. *Toxicology* **282**: 104-111.

Kim, I., X. Chu, S. Kim, C. Provoda, K. Lee & G. Amidon, (2003) Identification of a human valacyclovirase: biphenyl hydrolase-like protein as valacyclovir hydrolase. *J Biol Chem* **278**: 25348-25356.

Kimber, M. S., F. Vallee, S. Houston, A. Necakov, T. Skarina, E. Evdokimova, S. Beasley, D. Christendat, A. Savchenko, C. H. Arrowsmith, M. Vedadi, M. Gerstein & A. M. Edwards, (2003) Data mining crystallization databases: knowledge-based approaches to optimize protein crystal screens. *Proteins* **51**: 562-568.

Konishi, Y. & S. Kobayashi, (2005) Transepithelial transport of rosmarinic acid in intestinal Caco-2 cell monolayers. *Biosci Biotechnol Biochem* **69**: 583-591.

Koshland, D. E., (1958) Application of a Theory of Enzyme Specificity to Protein Synthesis. *Proc Natl Acad Sci U S A* **44**: 98-104.

Krissinel, E. & K. Henrick, (2007) Inference of macromolecular assemblies from crystalline state. *J Mol Biol* **372**: 774-797.

Kroon, P. A., C. B. Faulds, P. Ryden, J. A. Robertson & G. Williamson, (1997) Release of Covalently Bound Ferulic Acid from Fiber in the Human Colon. *J. Agric. Food Chem.* **45**: 661-667.

Lai, K., G. Lorca & C. Gonzalez, (2009) Biochemical properties of two cinnamoyl esterases purified from a *Lactobacillus johnsonii* strain isolated from stool samples of diabetes-resistant rats. *Appl Environ Microbiol* **75**: 5018-5024.

Lai, L., Z. Xu, J. Zhou, K. Lee & G. Amidon, (2008) Molecular basis of prodrug activation by human valacyclovirase, an alpha-amino acid ester hydrolase. *J Biol Chem* **283**: 9318-9327.

Lam, B. Y., A. C. Lo, X. Sun, H. W. Luo, S. K. Chung & N. J. Sucher, (2003) Neuroprotective effects of tanshinones in transient focal cerebral ischemia in mice. *Phytomedicine* **10**: 286-291.

Landete, J., H. Rodríguez, J. Curiel, B. de las Rivas, J. Mancheño & R. Muñoz, (2010) Gene cloning, expression, and characterization of phenolic acid decarboxylase from *Lactobacillus brevis* RM84. *J Ind Microbiol Biotechnol* **37**: 617-624.

Larkin, M. A., G. Blackshields, N. P. Brown, R. Chenna, P. A. McGettigan, H. McWilliam, F. Valentin, I. M. Wallace, A. Wilm, R. Lopez, J. D. Thompson, T. J. Gibson & D. G. Higgins, (2007) Clustal W and Clustal X version 2.0. *Bioinformatics* **23**: 2947-2948.

Laskowski, R. A., (2009) PDBsum new things. *Nucleic Acids Res* **37**: D355-359.

Laskowski, R. A., M. W. MacArthur, D. S. Moss & J. M. Thornton, (1993) PROCHECK: a program to check the stereochemical quality of protein structures. *J Appl Crystallogr* **26**: 283-291.

Levasseur, A., D. Navarro, P. J. Punt, J. P. Belaïch, M. Asther & E. Record, (2005) Construction of engineered bifunctional enzymes and their overproduction in *Aspergillus niger* for improved enzymatic tools to degrade agricultural by-products. *Appl Environ Microbiol* **71**: 8132-8140.

Li, M. H., J. M. Chen, Y. Peng, Q. Wu & P. G. Xiao, (2008) Investigation of Danshen and related medicinal plants in China. *J Ethnopharmacol* **120**: 419-426.

Lilitchan, S., C. Tangprawat, K. Aryusuk, S. Krisnangkura, S. Chokmoh & K. Krisnangkura, (2008) Partial extraction method for the rapid analysis of total lipids and γ-oryzanol contents in rice bran. *Food Chem* **106**: 752-759.

Liu, A. M. F., N. A. Somers, R. J. Kazlauskas, T. S. Brush, F. Zocher, M. M. Enzelberger, U. T. Bornscheuer, G. P. Horsman, A. Mezzetti, C. Schmidt-Dannert & R. D. Schmid, (2001) Mapping the substrate selectivity of new hydrolases using colorimetric screening: lipases from *Bacillus thermocatenulatus* and *Ophiostoma piliferum*, esterases from *Pseudomonas fluorescens* and *Streptomyces diastatochromogenes*. *Tetrahedron: Asymmetry* **12**: 545-556.

Lorca, G., A. Ezersky, V. Lunin, J. Walker, S. Altamentova, E. Evdokimova, M. Vedadi, A. Bochkarev & A. Savchenko, (2007a) Glyoxylate and pyruvate are antagonistic effectors of the *Escherichia coli* IclR transcriptional regulator. *J Biol Chem* **282**: 16476-16491.

Lorca, G. L., R. D. Barabote, V. Zlotopolski, C. Tran, B. Winnen, R. N. Hvorup, A. J. Stonestrom, E. Nguyen, L. W. Huang, D. S. Kim & M. H. Saier, (2007b) Transport capabilities of eleven gram-positive bacteria: comparative genomic analyses. *Biochim Biophys Acta* **1768**: 1342-1366.

Maillard, M.-N. & C. Berset, (1995) Evolution of Antioxidant Activity during Kilning: Role of Insoluble Bound Phenolic Acids of Barley and Malt. *J Agric Food Chem* **43**: 1789-1793.

Mangel, W. F., P. T. Singer, D. M. Cyr, T. C. Umland, D. L. Toledo, R. M. Stroud, J. W. Pflugrath & R. M. Sweet, (1990) Structure of an acyl-enzyme intermediate during catalysis: (guanidinobenzoyl)trypsin. *Biochemistry* **29**: 8351-8357.

Mastihuba, V., L. Kremnický, M. Mastihubová, J. Willett & G. Côté, (2002) A spectrophotometric assay for feruloyl esterases. *Anal Biochem* **309**: 96-101.

Matsuzaki, T., Y. Nagata, S. Kado, K. Uchida, S. Hashimoto & T. Yokokura, (1997a) Effect of oral administration of *Lactobacillus casei* on alloxan-induced diabetes in mice. *APMIS* **105**: 637-642.

Matsuzaki, T., Y. Nagata, S. Kado, K. Uchida, I. Kato, S. Hashimoto & T. Yokokura, (1997b) Prevention of onset in an insulin-dependent diabetes mellitus model, NOD mice, by oral feeding of *Lactobacillus casei*. *APMIS* **105**: 643-649.

Matsuzaki, T., R. Yamazaki, S. Hashimoto & T. Yokokura, (1997c) Antidiabetic effects of an oral administration of *Lactobacillus casei* in a non-insulin-dependent diabetes mellitus (NIDDM) model using KK-Ay mice. *Endocr J* **44**: 357-365.

Maurya, D. K. & T. P. Devasagayam, (2010) Antioxidant and prooxidant nature of hydroxycinnamic acid derivatives ferulic and caffeic acids. *Food Chem Toxicol* **48**: 3369-3373.

McCoy, A., R. Grosse-Kunstleve, P. Adams, M. Winn, L. Storoni & R. Read, (2007) Phaser crystallographic software. *J Appl Crystallogr* **40**: 658-674.

Murakami, A., Y. Nakamura, K. Koshimizu, D. Takahashi, K. Matsumoto, K. Hagihara, H. Taniguchi, E. Nomura, A. Hosoda, T. Tsuno, Y. Maruta, H. Kim, K. Kawabata & H. Ohigashi, (2002) FA15, a hydrophobic derivative of ferulic acid, suppresses inflammatory responses and skin tumor promotion: comparison with ferulic acid. *Cancer Lett* **180**: 121-129.

Murshudov, G., A. Vagin & E. Dodson, (1997) Refinement of macromolecular structures by the maximum-likelihood method. *Acta Crystallogr D Biol Crystallogr* **53**: 240-255.

Musso, G., R. Gambino & M. Cassader, (2011) Interactions between gut microbiota and host metabolism predisposing to obesity and diabetes. *Annu Rev Med* **62**: 361-380.

Nardini, M. & B. W. Dijkstra, (1999) α/β Hydrolase fold enzymes: the family keeps growing. *Curr Opin Struct Biol* **9**: 732-737.

Negri, E., S. Franceschi, M. Parpinel & C. La Vecchia, (1998) Fiber intake and risk of colorectal cancer. *Cancer Epidemiol Biomarkers Prev* **7**: 667-671.

Ollis, D. L., E. Cheah, M. Cygler, B. Dijkstra, F. Frolow, S. M. Franken, M. Harel, S. J. Remington, I. Silman & J. Schrag, (1992) The alpha/beta hydrolase fold. *Protein Eng* **5**: 197-211.

Omar, S. H., (2010) Oleuropein in Olive and its Pharmacological Effects. *Sci Pharm* **78**: 133-154.

OriginLab, OriginLab, Northampton, MA.

Otwinowski, Z. & W. Minor, (1997) [20] Processing of X-ray diffraction data collected in oscillation mode. In: *Methods Enzymol.* Charles W. Carter, Jr. (ed). Academic Press, pp. 307-326.

Ou, S. & K.-C. Kwok, (2004) Ferulic acid: pharmaceutical functions, preparation and applications in foods. *J Sci Food Agric* **84**: 1261-1269.

Page, R. D., (1996) TreeView: an application to display phylogenetic trees on personal computers. *Comput Appl Biosci* **12**: 357-358.

Painter, J. & E. A. Merritt, (2006) Optimal description of a protein structure in terms of multiple groups undergoing TLS motion. *Acta Crystallogr D Biol Crystallogr* **62**: 439-450.

Panda, T. & B. S. Gowrishankar, (2005) Production and applications of esterases. *Appl Microbiol Biotechnol* **67**: 160-169.

Pervaiz, S. & A. L. Holme, (2009) Resveratrol: its biologic targets and functional activity. *Antioxid Redox Signal* **11**: 2851-2897.

Pindel, E. V., N. Y. Kedishvili, T. L. Abraham, M. R. Brzezinski, J. Zhang, R. A. Dean & W. F. Bosron, (1997) Purification and cloning of a broad substrate specificity human liver carboxylesterase that catalyzes the hydrolysis of cocaine and heroin. *J Biol Chem* **272**: 14769-14775.

Plumb, G. W., M. T. Garcia-Conesa, P. A. Kroon, M. Rhodes, S. Ridley & G. Williamson, (1999) Metabolism of chlorogenic acid by human plasma, liver, intestine and gut microflora. *J. Sci. Food Agr.* **79**: 390-392.

Priefert, H., J. Rabenhorst & A. Steinbüchel, (2001) Biotechnological production of vanillin. *Appl Microbiol Biotechnol* **56**: 296-314.

Puupponen-Pimiä, R., L. Nohynek, S. Hartmann-Schmidlin, M. Kähkönen, M. Heinonen, K. Määttä-Riihinen & K. Oksman-Caldentey, (2005) Berry phenolics selectively inhibit the growth of intestinal pathogens. *J Appl Microbiol* **98**: 991-1000.

Rajendra Prasad, N., A. Karthikeyan, S. Karthikeyan & B. V. Reddy, (2011) Inhibitory effect of caffeic acid on cancer cell proliferation by oxidative mechanism in human HT-1080 fibrosarcoma cell line. *Mol Cell Biochem* **349**: 11-19.

Record, E., M. Asther, C. Sigoillot, S. Pagès, P. J. Punt, M. Delattre, M. Haon, C. A. van den Hondel, J. C. Sigoillot & L. Lesage-Meessen, (2003) Overproduction of the *Aspergillus niger* feruloyl esterase for pulp bleaching application. *Appl Microbiol Biotechnol* **62**: 349-355.

Richelle, M., I. Tavazzi & E. Offord, (2001) Comparison of the antioxidant activity of commonly consumed polyphenolic beverages (coffee, cocoa, and tea) prepared per cup serving. *J Agric Food Chem* **49**: 3438-3442.

Rodríguez, H., I. Angulo, B. de Las Rivas, N. Campillo, J. Páez, R. Muñoz & J. Mancheño, (2010) p-Coumaric acid decarboxylase from *Lactobacillus plantarum*: structural insights into the active site and decarboxylation catalytic mechanism. *Proteins* **78**: 1662-1676.

Rodríguez, H., J. Curiel, J. Landete, B. de las Rivas, F. López de Felipe, C. Gómez-Cordovés, J. Mancheño & R. Muñoz, (2009) Food phenolics and lactic acid bacteria. *Int J Food Microbiol* **132**: 79-90.

Roesch, L., G. Lorca, G. Casella, A. Giongo, A. Naranjo, A. Pionzio, N. Li, V. Mai, C. Wasserfall, D. Schatz, M. Atkinson, J. Neu & E. Triplett, (2009) Culture-independent identification of gut bacteria correlated with the onset of diabetes in a rat model. *ISME J* **3**: 536-548.

Rogosa, M., J. Mitchell & R. Wiseman, (1951) A selective medium for the isolation and enumeration of oral lactobacilli. *J Dent Res* **30**: 682-689.

Sansbury, L. B., K. Wanke, P. S. Albert, L. Kahle, A. Schatzkin, E. Lanza & P. P. T. S. Group, (2009) The effect of strict adherence to a high-fiber, high-fruit and -vegetable, and low-fat eating pattern on adenoma recurrence. *Am J Epidemiol* **170**: 576-584.

Sato, Y., S. Itagaki, T. Kurokawa, J. Ogura, M. Kobayashi, T. Hirano, M. Sugawara & K. Iseki, (2011) In vitro and in vivo antioxidant properties of chlorogenic acid and caffeic acid. *Int J Pharm* **403**: 136-138.

Scheer, M., A. Grote, A. Chang, I. Schomburg, C. Munaretto, M. Rother, C. Söhngen, M. Stelzer, J. Thiele & D. Schomburg, (2011) BRENDA, the enzyme information system in 2011. *Nucleic Acids Res* **39**: D670-676.

Schmidt, K., J. Schölmerich, H. Ritter & J. Schmitt, (1982) In vitro studies on the interaction between bile salts and key enzymes of the liver. *Klin Wochenschr* **60**: 237-242.

Schubot, F. D., I. A. Kataeva, D. L. Blum, A. K. Shah, L. G. Ljungdahl, J. P. Rose & B. C. Wang, (2001) Structural basis for the substrate specificity of the feruloyl esterase domain of the cellulosomal xylanase Z from *Clostridium thermocellum*. *Biochemistry* **40**: 12524-12532.

Schüttelkopf, A. & D. van Aalten, (2004) PRODRG: a tool for high-throughput crystallography of protein-ligand complexes. *Acta Crystallogr D Biol Crystallogr* **60**: 1355-1363.

Selma, M., J. Espín & F. Tomás-Barberán, (2009) Interaction between phenolics and gut microbiota: role in human health. *J Agric Food Chem* **57**: 6485-6501.

Sigoillot, C., S. Camarero, T. Vidal, E. Record, M. Asther, M. Pérez-Boada, M. J. Martínez, J. C. Sigoillot, J. F. Colom & A. T. Martínez, (2005) Comparison of different fungal enzymes for bleaching high-quality paper pulps. *J Biotechnol* **115**: 333-343.

Slavin, J., (2008) Position of the American Dietetic Association: health implications of dietary fiber. *J Am Diet Assoc* **108**: 1716-1731.

Spencer, J. P., M. M. Abd El Mohsen, A. M. Minihane & J. C. Mathers, (2008) Biomarkers of the intake of dietary polyphenols: strengths, limitations and application in nutrition research. *Br J Nutr* **99**: 12-22.

Srinivasan, M., A. Sudheer & V. Menon, (2007) Ferulic Acid: therapeutic potential through its antioxidant property. *J Clin Biochem Nutr* **40**: 92-100.

Tada, H., Y. Murakami, T. Omoto, K. Shimomura & K. Ishimaru, (1996) Rosmarinic acid and related phenolics in hairy root cultures of *Ocimum basilicum*. *Phytochemistry* **42**: 431-434.

Tanida, M., T. Yamano, K. Maeda, N. Okumura, Y. Fukushima & K. Nagai, (2005) Effects of intraduodenal injection of *Lactobacillus johnsonii* La1 on renal sympathetic nerve activity and blood pressure in urethane-anesthetized rats. *Neurosci Lett* **389**: 109-114.

Topakas, E., H. Stamatis, P. Biely, D. Kekos, B. J. Macris & P. Christakopoulos, (2003) Purification and characterization of a feruloyl esterase from *Fusarium oxysporum* catalyzing esterification of phenolic acids in ternary water-organic solvent mixtures. *J Biotechnol* **102**: 33-44.

Topakas, E., C. Vafiadi & P. Christakopoulos, (2007) Microbial production, characterization and applications of feruloyl esterases. *Process Biochemistry* **42**: 497-509.

Udatha, D. B., I. Kouskoumvekaki, L. Olsson & G. Panagiotou, (2011) The interplay of descriptor-based computational analysis with pharmacophore modeling builds the basis for a novel classification scheme for feruloyl esterases. *Biotechnol Adv* **29**: 94-110.

Vaarala, O., M. Atkinson & J. Neu, (2008) The "perfect storm" for type 1 diabetes: the complex interplay between intestinal microbiota, gut permeability, and mucosal immunity. *Diabetes* **57**: 2555-2562.

Vafiadi, C., E. Topakas, P. Christakopoulos & C. B. Faulds, (2006) The feruloyl esterase system of *Talaromyces stipitatus*: determining the hydrolytic and synthetic specificity of TsFaeC. *J Biotechnol* **125**: 210-221.

Valladares, R., D. Sankar, N. Li, E. Williams, K. Lai, A. Abdelgeliel, C. Gonzalez, C. Wasserfall, J. Larkin, D. Schatz, M. Atkinson, E. Triplett, J. Neu & G. Lorca, (2010) *Lactobacillus johnsonii* N6.2 mitigates the development of type 1 diabetes in BB-DP rats. *PLoS One* **5**: e10507.

Walter, J., (2008) Ecological role of lactobacilli in the gastrointestinal tract: implications for fundamental and biomedical research. *Appl Environ Microbiol* **74**: 4985-4996.

Wang, H., G. J. Provan & K. Helliwell, (2004a) Determination of rosmarinic acid and caffeic acid in aromatic herbs by HPLC. *Food Chem* **87**: 307-311.

Wang, X., X. Geng, Y. Egashira & H. Sanada, (2004b) Purification and characterization of a feruloyl esterase from the intestinal bacterium *Lactobacillus acidophilus*. *Appl Environ Microbiol* **70**: 2367-2372.

Williamson, G., A. Day, G. Plumb & D. Couteau, (2000) Human metabolic pathways of dietary flavonoids and cinnamates. *Biochem Soc Trans* **28**: 16-22.

Xing, H. C., L. J. Li, K. J. Xu, T. Shen, Y. B. Chen, Y. Chen, S. Z. Fu, J. F. Sheng, C. L. Chen, J. G. Wang, D. Yan, F. W. Dai & X. Y. Sha, (2005) Effects of *Salvia miltiorrhiza* on intestinal microflora in rats with ischemia/reperfusion liver injury. *Hepatobiliary Pancreat Dis Int* **4**: 274-280.

Yamano, T., M. Tanida, A. Niijima, K. Maeda, N. Okumura, Y. Fukushima & K. Nagai, (2006) Effects of the probiotic strain *Lactobacillus johnsonii* strain La1 on autonomic nerves and blood glucose in rats. *Life Sci* **79**: 1963-1967.

Yi, W., J. Fischer, G. Krewer & C. C. Akoh, (2005) Phenolic compounds from blueberries can inhibit colon cancer cell proliferation and induce apoptosis. *J Agric Food Chem* **53**: 7320-7329.

Yin, d. L., P. Bernhardt, K. L. Morley, Y. Jiang, J. D. Cheeseman, V. Purpero, J. D. Schrag & R. J. Kazlauskas, (2010) Switching catalysis from hydrolysis to perhydrolysis in *Pseudomonas fluorescens* esterase. *Biochemistry* **49**: 1931-1942.

Yu, H. P., T. L. Hwang, C. H. Yen & Y. T. Lau, (2010) Resveratrol prevents endothelial dysfunction and aortic superoxide production after trauma hemorrhage through estrogen receptor-dependent hemeoxygenase-1 pathway. *Crit Care Med* **38**: 1147-1154.

BIOGRAPHICAL SKETCH

Kin-Kwan Lai was born in Hong Kong, 1982. He attended secondary school from 1993 to 1999 and moved to the United States in 2000. During his first few years in the U.S., he held a part-time job for two years and eventually attended Broward Community College from 2001 to 2004. He obtained his Associate of Arts Degree with the highest honor. Kin-Kwan then transferred to the University of Florida in January 2005, graduating cum laude with a Bachelors of Science in Microbiology in December 2006.

After gaining U.S. citizenship in 2006, Kin-Kwan continued with his interest in microbiology by applying to the University of Florida graduate program in August of 2007 under the guidance of Dr. Claudio Gonzalez. As a graduate student, he has attended symposiums such as the Florida Genetics Institute Research Symposium (2008) and the American Society of Microbiology (ASM) Branch and General Meetings (2009, 2010, and 2011). In 2010, Kin-Kwan received the ASM Beneficial Microbes Travel Grant. In addition, he has served as a mentor for two undergraduates, Clara Vu and Sara Molloy, and even assisted with the 2011 Undergraduate Microbiology Research Symposium as the graduate student representative. His work presented in this document generated two publications in peer-reviewed journals.

Kin-Kwan is currently pursuing a career in microbiology with the government or a biotechnology company.